December 2024
Report No. 24-064

Post-Fire Damage Inspection of Concrete Structures Phase III – In-Situ Experimental Phase

Principal Investigator (s)
Tom Toscano
Dr. Simos Gerasimidis
Dr. Scott Civjan

University of Massachusetts Amherst

Research and Technology Transfer Section
MassDOT Office of Transportation Planning

U.S. Department of Transportation
Federal Highway Administration

[This blank, unnumbered page will be the back of your front cover]

Technical Report Document Page

1. Report No. 24-064	2. Government Accession No.	3. Recipient's Catalog No.
4. Title and Subtitle Post-Fire Damage Inspection of Concrete Structures Phase III – In-Situ Experimental Phase		5. Report Date October 2024
		6. Performing Organization Code 24-064
7. Author(s) T. Toscano, S. Islam, S. Civjan, S. Gerasimidis		8. Performing Organization Report No.
9. Performing Organization Name and Address University of Massachusetts Amherst, UMass Transportation Center, 130 Natural Resources Way, Amherst, MA 01003 Massachusetts Institute of Technology		10. Work Unit No. (TRAIS)
		11. Contract or Grant No.
12. Sponsoring Agency Name and Address Massachusetts Department of Transportation Office of Transportation Planning Ten Park Plaza, Suite 4150, Boston, MA 02116		13. Type of Report and Period Covered Final Report October 2024 (Sept. 2024 - December 2024)
		14. Sponsoring Agency Code n/a

15. Supplementary Notes

Project Champion - John Czach - MassDOT

16. Abstract

Cementitious fireproofing has become an essential technique for safeguarding tunnel infrastructure against fire-induced damage, principally by providing a thermal barrier between flexural members and a fire event. Although fireproofing is extensively employed across different sectors, its specific utilization and efficacy in tunnel scenarios is inadequately explored. This research examines the thermal performance of cementitious fireproofing applied to steel beams within tunnels under intense fire conditions, as specified by ASTM E119 standards. The study indicates that beams with fireproofing exhibit substantial temperature reductions, achieving up to a 50% decrease compared to unprotected beams, thus delaying thermal degradation effectively. The results highlight the significance of fireproofing in prolonging the time prior to reaching critical temperatures, consequently mitigating structural damage during fire exposure. Furthermore, partial fireproofing demonstrated to offer significant protection, underlining its utility in situations where complete coverage may not be practical. The study underscores the critical role of cementitious fireproofing in enhancing the fire resilience of tunnel structures and its significance in protecting vital infrastructure during fire incidents.

17. Key Word Cementitious Fireproofing, Thermal Insulation in Tunnels, Fire-Induced Structural Damage, High-Temperature Performance, Fire Resistance of Steel Structures, Tunnel Infrastructure Protection, Heat Transfer Mechanisms	18. Distribution Statement

19. Security Classif. (of this report) unclassified	20. Security Classif. (of this page) unclassified	21. No. of Pages 104	22. Price n/a

Form DOT F 1700.7 (8-72) Reproduction of completed page authorized

This page left blank intentionally.

Post-Fire Damage Inspection of Concrete Structures
Phase III – In-Situ Experimental Phase

Final Report

Prepared By:

Thomas N. Toscano II
Undergraduate Student, UMass Amherst

Shahrukh Islam
PhD Candidate, UMass Amherst

Scott A. Civjan
Associate Dean & Professor, UMass Amherst

Simos Gerasimidis
Associate Professor, UMass Amherst

Prepared For:
Massachusetts Department of Transportation Office of Transportation Planning
Ten Park Plaza, Suite 4150 Boston, MA 02116

Project Champion/Technical Representative
David P. Kent, State Tunnel Inspection Engineer
MassDOT
10 Park Plaza
Boston, MA 02116

October 2024

This page left blank intentionally.

Acknowledgments

Prepared in cooperation with the Massachusetts Department of Transportation, Office of Transportation Planning, and the United States Department of Transportation, Federal Highway Administration.

The Project Team would like to acknowledge the efforts of Catherine-Hong Chen for her efforts to support the project and Mark Gauthier for his continuous lab support throughout the project.

Disclaimer

This page left blank intentionally.

Executive Summary

This study of Post-Fire Damage Inspection of Concrete Structures Phase III – In-Situ Experimental Phase, was undertaken as part of the Massachusetts Department of Transportation Research Program. This program is funded with Federal Highway Administration (FHWA) State Planning and Research (SPR) funds. Through this program, applied research is conducted on topics of importance to the Commonwealth of Massachusetts transportation agencies.

The primary focus of this research was to evaluate the effectiveness of fireproofing in protecting steel beams under severe fire conditions, specifically in the context of tunnel environments exemplified by the case study in Boston, Massachusetts. Given the potential for high-temperature fire events from fuel-related incidents, it is vital to ensure the structural integrity of steel beams, which form key load-bearing components in tunnel infrastructure.

The investigation analyzed four distinct fireproofing configurations in conjunction with a control case lacking any fireproofing to evaluate their influence on heat transmission and structural integrity. Both comprehensive and partial fireproofing configurations were designed to simulate practical tunnel contexts, wherein varying levels of protection may be implemented, or damage may reduce the coverage of fireproofing. The fire tests adhered to the ASTM E119 fire curve, thereby exposing the beams to elevated temperatures for a duration of three hours. Temperature measurements were recorded at crucial locations such as the bottom flange, mid-web, and top flange. The findings indicated that beams with complete fireproofing experienced considerable reductions in temperature as opposed to their unprotected counterparts, achieving temperature decreases of up to 50%. For example, the bottom flange of the fully fireproofed beam exhibited a peak temperature of 250°C, markedly lower than the 499°C observed in the unprotected control beam. Although partial fireproofing proved to be less effective than full coverage, it nonetheless facilitated significant reductions in temperature, as long as pathways for heat transfer were limited.

Finite-element analysis (FEA) was performed in conjunction with experimental testing to simulate the thermal response of beams under fire conditions. FEA replicated the experimental temperature behavior, corroborating the non-linear heat transfer observed in both fireproofed and unprotected beams. The analysis demonstrates that fireproofing effectively decelerates the temperature increase, thereby preserving the structural integrity of the steel. The findings underscore the critical importance of comprehensive fireproofing in high-risk areas to delay structural failure, thus providing emergency services with additional response time and enhancing the safety of tunnel users.

This research elucidates the imperative role of fireproofing in shielding tunnel infrastructure from fire damage. Comprehensive fireproofing is highly recommended for principal load-bearing components, particularly in regions susceptible to fires involving fuel. The outcomes underscore the significance of routine inspection and maintenance to guarantee the enduring efficacy of fireproofing materials. This report provides comprehensive guidance on augmenting fire safety within essential tunnel infrastructure.

This page left blank intentionally.

Table of Contents

This page left blank intentionally.

List of Tables

List of Figures

List of Acronyms

Acronym	Expansion
ACI	American Concrete Institute
ASCE	American Society of Civil Engineers
ASTM	American Society for Testing and Materials
CEN	Eurocode
CIA	Cooled in Air
CIB	Cooled in Blanket
CIW	Cooled in Water
DOT	Department of Transportation
EN	European Norm (Eurocode)
E_s	Modulus of Elasticity at Room Temperature
$E_{s,T}$	Modulus of Elasticity at Temperature 'T'
FEA	Finite-element analysis
FEM	Finite Element Modeling
FHWA	Federal Highway Administration
FRM	Fire-Resistant Materials
f_{uT}	Ultimate Strength at Temperature 'T'
f_u	Ultimate Strength at Room Temperature
$F_{y,T}$	Yield Strength at Temperature 'T'
F_y	Yield Strength at Room Temperature
f_{yT}	Residual Yield Strength at Temperature 'T'
f_y	Residual Yield Strength at Room Temperature
HSC	High Strength Concrete
IR	Infrared
NA	Not Available
NSC	Normal Strength Concrete
RWS	Rijkswaterstaat (a Dutch Fire Curve)
SPR	State Planning and Research

This page left blank intentionally.

1.0 Introduction

1.1 Overview of the Work

This study of Post-Fire Damage Inspection of Concrete Structures Phase III – In-Situ Experimental Phase was undertaken as part of the Massachusetts Department of Transportation (MassDOT) Research Program. This program is funded with Federal Highway Administration (FHWA) State Planning and Research (SPR) funds. Through this program, applied research is conducted on topics of importance to the Commonwealth of Massachusetts transportation agencies.

Tunnels are a vital part of Massachusetts infrastructure, most notably in Boston. Following the Central Artery/Tunnel Project, Interstate 93 runs through the downtown of Boston underground, beneath high-rise buildings and densely populated areas. Tunnel structures are subject to high-temperature fire events that can result from fuel ignition in a collision, presenting a risk to existing infrastructure. This concern must be investigated, as alternative fuels such as hydrogen, which burns significantly hotter than gasoline, are being considered for vehicles in the United States. The focus is on a tunnel that uses cementitious fireproofing on steel beams to resist damage in fire events. Conditions within tunnels are especially challenging for fireproofing materials because beams are frequently struck by vehicles. Maintaining the fireproofing is difficult due to the high volume of daily traffic passing through the tunnel.

The research effort will focus on the following objectives:

1. Evaluate the effectiveness of cementitious fireproofing in reducing the temperatures of steel beams during a fire event.
2. Examine the durability of cementitious fireproofing after a major fire event.
3. Research the reduction in strength of a steel beam after a fire event with and without fireproofing.
4. Determine the ease of application for cementitious fireproofing and assess whether it can be used to quickly repair damage from truck strikes.
5. Perform a finite-element analysis of a steel beam under the ASTM E119 fire curve and compare it with laboratory results.

1.2 Background

To understand the risks associated with tunnel fires, the impacts of high temperatures on popular structural materials must be evaluated. The two most common structural materials used in Boston tunnels are concrete and steel. Like other common building materials, under high temperatures, steel and concrete lose their strength and stiffness [1]. To properly understand the risks a fire event poses to the structural integrity of Massachusetts tunnels, changes in material properties and residual strength during and after a fire event must be determined for both materials.

Fire resistance is defined as the “ability of an element of building construction to fulfill its defined function for a period of time in the event of a fire” [2]. Research on fire resistance is mainly focused on fire resistance design, which is categorized by three approaches: fire testing, prescriptive methods, and performance-based methods [3].

Fire testing involves the exposure of structural elements to high temperatures in accordance with the design fire curves. The temperature at the interface between the structural element and the airspace is typically used as the test temperature.

Prescriptive methods for fire design typically involve design recommendations to limit the impacts of high temperatures. Examples include concrete clear cover to reinforcement for design fires and requirements of maximum temperatures within certain elements for a design fire [3]. Performance-based methods for fire design use calculations and finite-element analysis to demonstrate that structures can withstand fire requirements [3]. Table 1-1 reprints a non-exhaustive list of some popular standards [3].

Table 1-1: Fire resistance and design standards/codes

Organization	**Country/ Region**	**Document Name**	**Document Type**	**Publication Date**
Fire Safety Journal/CIB W14	N/A	*The Repairability of Fire-Damaged Structures*	Journal Article/Technical Report	1990
American Society of Civil Engineers (ASCE)	USA	*Structural Fire Protection*	Standard	1992
Eurocode (CEN)	EU	*EN 1992 1-2, EN 1993 1-2, EN 1994 1-2*	Building Code	2004, 2005
Concrete Society	Britain	*Assessment, Design, and Repair of Fire-Damaged Structures*	Technical Report	2008
International Federation for Structural Concrete (fib)	EU	*Fire Design of Concrete Structures – Structural Behavior and Assessment*	Technical Report	2008
Institution of Structural Engineers (ISE)	Britain	*Appraisal of Existing Structures*	Technical Report	2010
American Concrete Institute (ACI)	USA	*Code Requirements for Determining Dire Resistance of Concrete and Masonry Construction Assemblies*	Building Code	2019

Before delving into the behavior of steel and concrete under heat loading, it is important to distinguish between tests at elevated temperatures and tests of residual strength. Tests at elevated temperatures aim to highlight the strength reduction of structural materials during a significant fire event, while tests for residual strength are used to assess long-term damage to structural materials. In this report, tests at elevated temperatures are used in the context of evaluating the safety of structural elements during a significant fire event, and residual tests are used to determine whether replacement of structural elements is necessary following a significant fire event.

1.2.1 Steel Response to Heat

The impact of high-temperature events on steel can be attributed to changes in the microstructure and chemical composition of the steel [4]. Manufacturing methods for different types of steel can have a significant effect on the behavior at elevated temperatures and the residual behavior. Thermal exposure results in different effects in steel depending on the type of metal. Hot rolled structural steel, reinforcing steel, heat treated/cold worked or work hardened steel, and prestressing steel all behave differently during a fire event. This report will focus on structural steel, which is commonly used for beams in tunnels. Structural steel is generally the least susceptible to the effects of thermal exposure.

The specific response of structural steel members to high temperatures is governed by the thermal, mechanical, and deformation properties of the material. The thermal properties determine the temperature profile, and the mechanical properties determine the extent of deformations in steel [1]. Knowledge of the thermal properties of structural members at high temperatures is important for the structural integrity of a tunnel because thermal conductivity and specific heat influence the spread of high temperatures throughout a structural system. Limited research has been conducted on the thermal conductivity and specific heat of steel at high temperatures, but existing data suggest a nearly linear decrease in thermal conductivity with increases in temperature up to 1,000°C (Figure 1-1) [1,5,6,7,8,9,10,11].

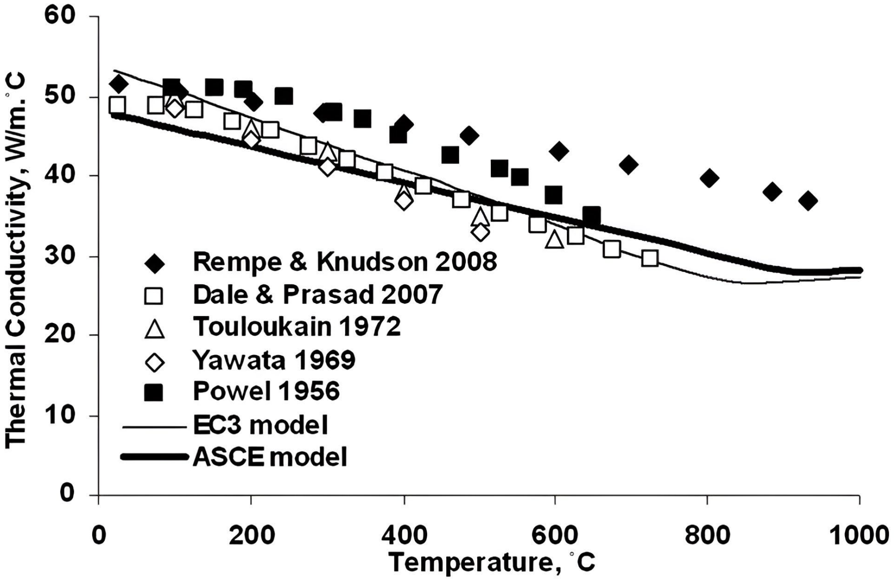

Figure 1-1: Thermal conductivity vs. temperature for structural steel

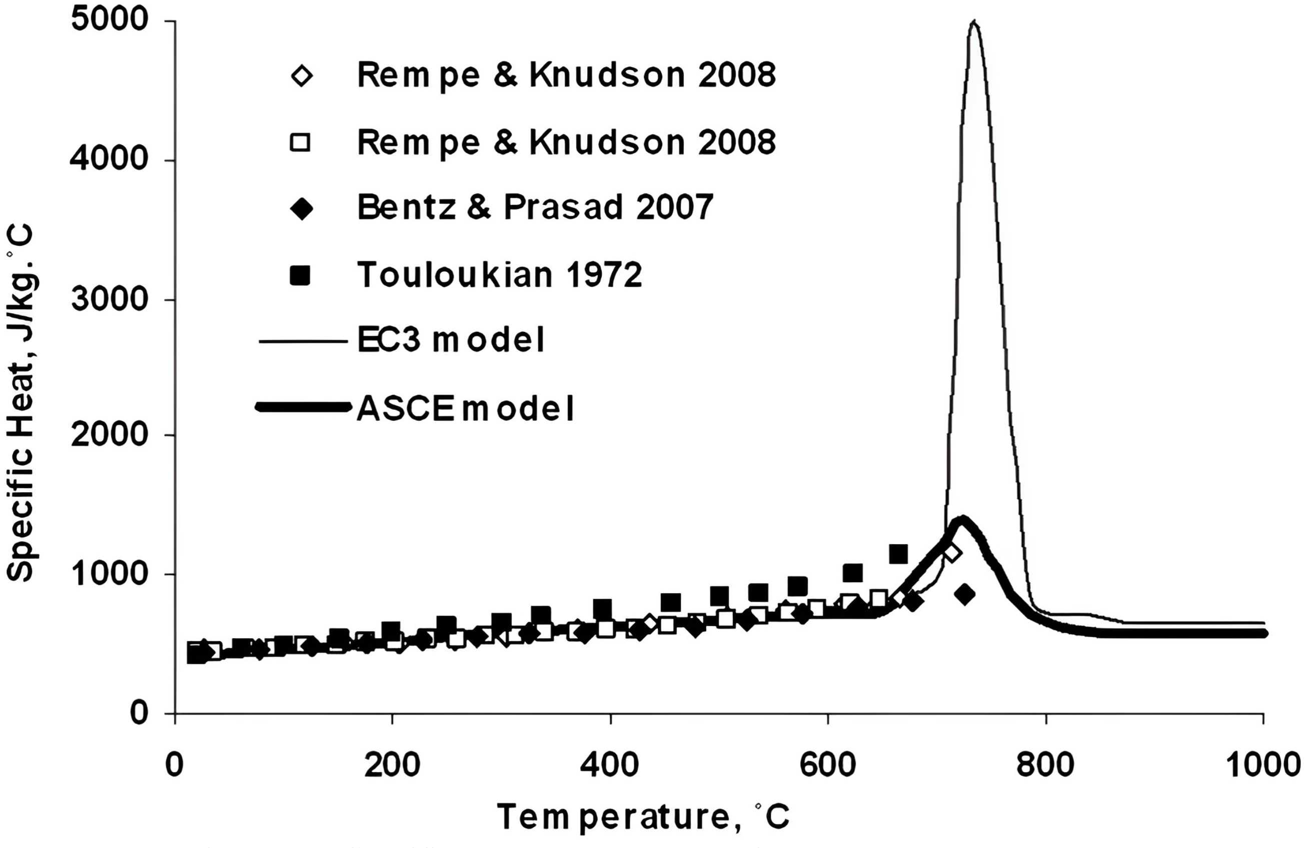

Figure 1-2: Specific heat vs. temperature for structural steel

The ASCE and Eurocode models for the specific heat capacity of steel indicate a nearly linear increase from ambient temperature up to 700°C, succeeded by a significant rise [1,5,6]. This considerable rise can be attributed to the increased separation of individual atoms [1]. This phenomenon is depicted in Figure 1-2 [1].

In addition to thermal characteristics, alterations in mechanical properties are of significant interest. The modulus of elasticity and yield strength are of paramount concern due to their role in controlling the stiffness and strength of structural components. Both the yield strength and the modulus of elasticity diminish as the temperature rises from ambient conditions to 1,000°C [1,12,13,14,15]. EN 1993 1-2 offers equations and graphs that depict the reduction in strength for structural steel. The reduction factors per EN 1993 are illustrated in Figure 1-3 [11].

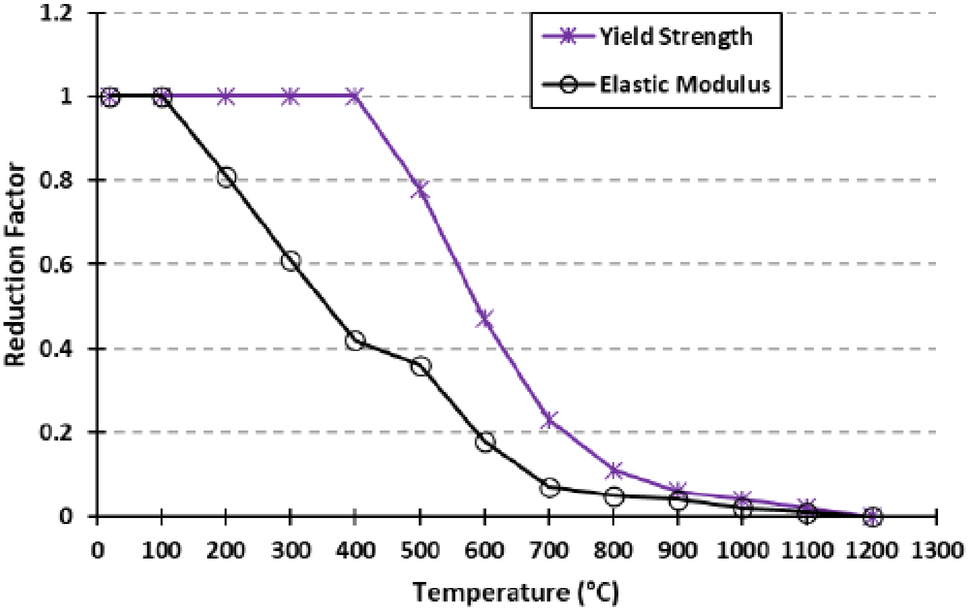

Figure 1-3: Strength and stiffness reduction factors for structural steel

In addition to examining design standards, experimental data should also be evaluated. A 2015 study [1] compiled the results of five studies on reduction in yield strength and six studies on reduction in modulus of elasticity and compared them with data from ASCE Structural Fire Protection Standard and the Eurocode model. These results are presented in Figures 1-4 and 1-5. Both figures are reprinted from [1].

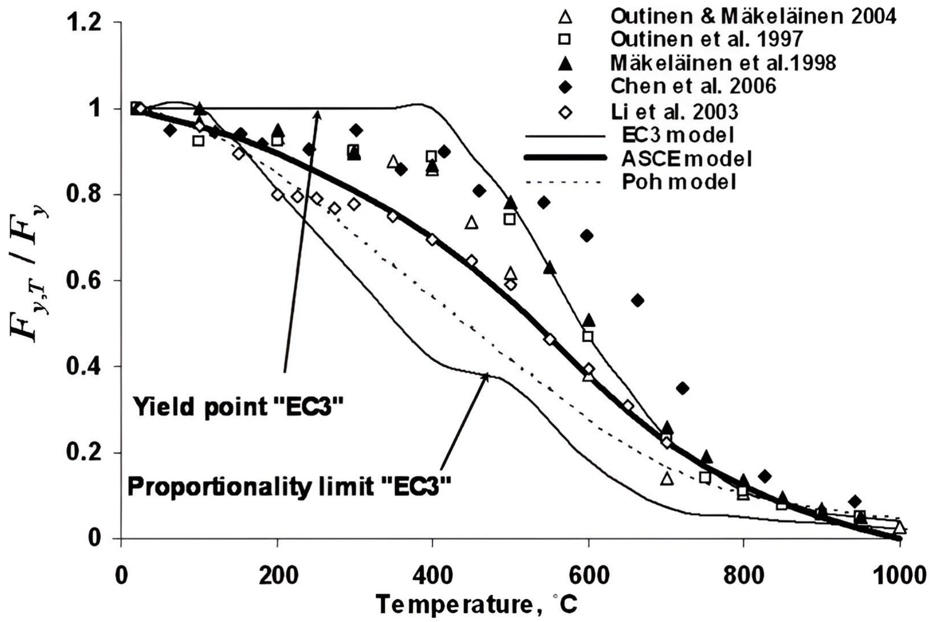

Figure 1-4: Ratio yield strength: temperature T vs. room temperature

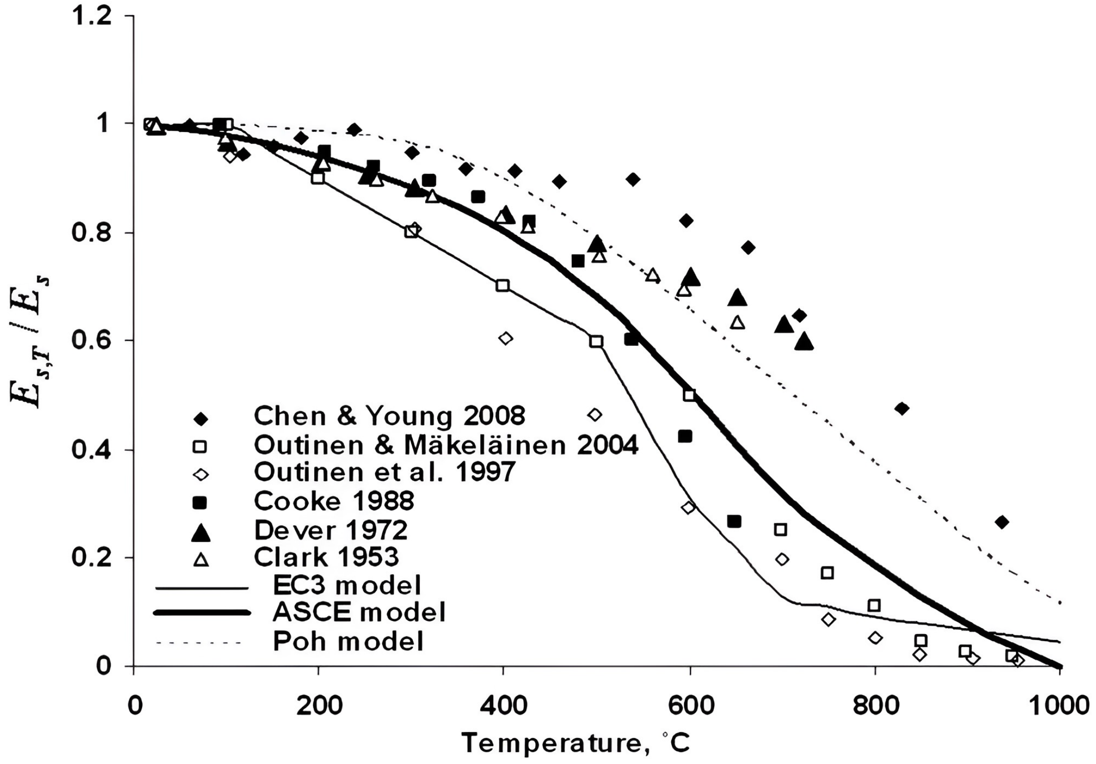

Figure 1-5: Ratio of modulus of elasticity: temperature T vs. room temperature

The experimental data and the ASCE model both predict a reduction in yield strength at temperatures as low as 200°C, although a minor one. This contradicts the Eurocode presented in Figure 1-3. The aggressive reduction in yield strength exhibited by experimental data indicates that even at relatively low temperatures, the reduction in strength of a steel component may pose a significant hazard. At 300°C, a steel beam will lose approximately 20% of its overall strength [1, 12, 13, 14, 15]. The reduction in modulus of elasticity is not as severe, with an approximate reduction of 15% at 300°C. This could lead to excessive deflections in structural components that present the risk of a serviceability failure.

Additionally, the experimental data show less reduction in elastic modulus than the Eurocode model does, with the exception of a study by Outinen et al. [12]. The reduction for modulus of elasticity is a considerably smaller reduction than comparison to yield strength [16].

Another meta-analysis of eight studies on residual properties of structural steel including stress-strain curves, yield strength, ultimate strength, and modulus of elasticity was conducted in 2013. The residual yield and ultimate strength as a function of temperature are displayed in Figures 1-6 and 1-7, respectively. The line in each graph is the best-fit line for the data. Both figures are reprinted from [17].

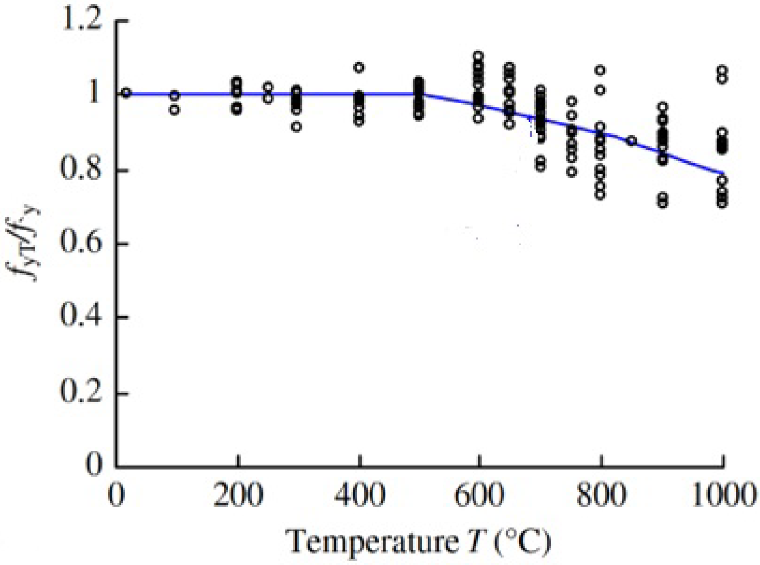

Figure 1-6: Yield stress with increasing temperature

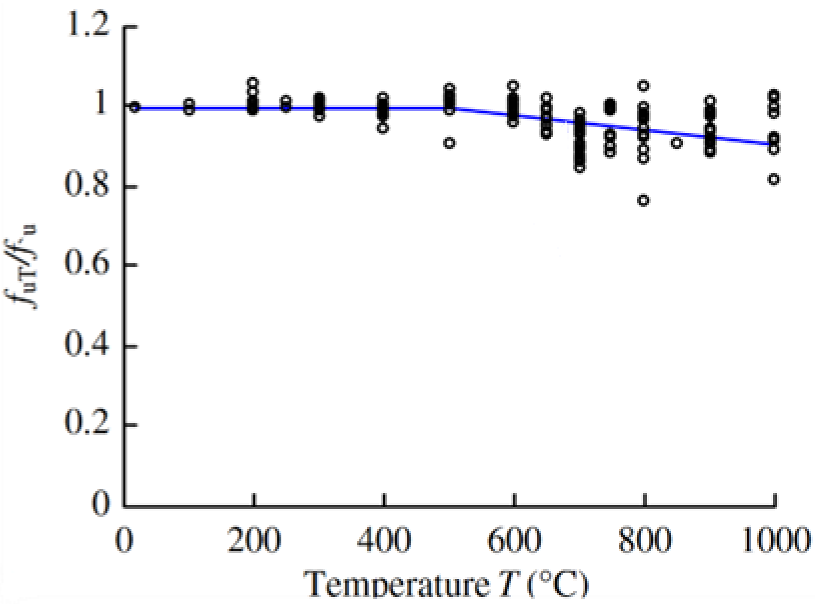

Figure 1-7: Ultimate stress with increasing temperature

The residual yield and ultimate strength for structural steel are not affected by temperatures up to 500°C. The ultimate strength is less affected by high heat events than yield strength and exhibits a minimal reduction in residual strength when heated to temperatures upward of 1,000°C. The residual strength and behavior of steel following a significant fire event are vital to determining whether there is a significant permanent loss of strength or changes in material behavior following a fire event. Figure 1-8 shows the stress strain curves for fire-damaged steel at room temperature after heating to 300, 500, 800, and 1,000°C. [17; data from 18].

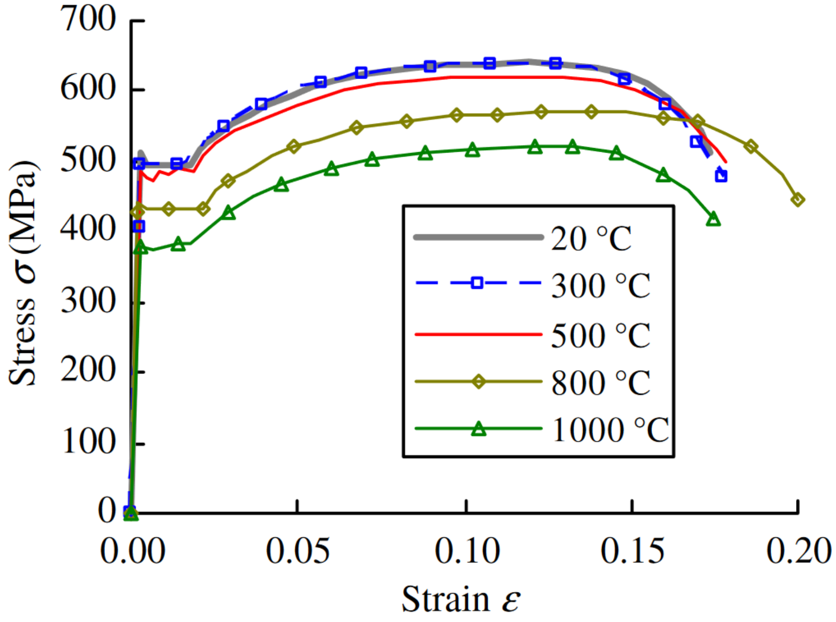

Figure 1-8: Residual stress strain behavior of fire-damaged steel

A study indicates that there are no permanent changes in ductility, yield strength, or ultimate strength for steel heated to 300°C [18]. In fact, some research suggests that heating to 250°C provides a slight increase in the yield strength of the steel [16]. There is a slight reduction in residual strength and a change in behavior for steel heated to 500°C, but the reduction in yield strength is minimal. Once heated to 800°C and above, there is a significant reduction in strength. This provides a standard for our laboratory testing. The magnitude of the strength reduction is also worth noting. Structural steel experienced a 12.2% and 21% reduction in residual yield strength when heated to 800 and 1,000°C, respectively [16].

Despite the reduction in strength, the shape of the stress-strain curve remains the same after heating and cooling [16,17,18]. This is important because it indicates that the steel remains ductile. High-ductility failures are desirable, particularly in infrastructure because they provide a warning before a failure occurs. Ductility is also desirable because it increases the ability of a structural component to resist dynamic loads and redistribute forces and stresses.

As with yield strength, modulus of elasticity does not experience a permanent reduction until it is heated above 500°C. There is a slight modulus of elasticity decline above 500°C, which follows a linear decline. A 6.5% decline in Young's Modulus was observed at 1,000°C [16].

The steels examined in references 17 and 18 are less common in the United States, so an evaluation of a study involving ASTM A992 steel (which was used in the experiments for this report) is necessary. Jinwoo et al. [19] conducted a study evaluating the effect of different cooling methods, including cooled under blanket (CIB), cooled in air (CIA) and cooled in water (CIW). The residual stress strain curves for steel heated to 200°C, 500°C, 700°C, and 1,000°C and cooled by the three different methods are shown in Figures 1-9 and 1-10. Both figures are reprinted from [19].

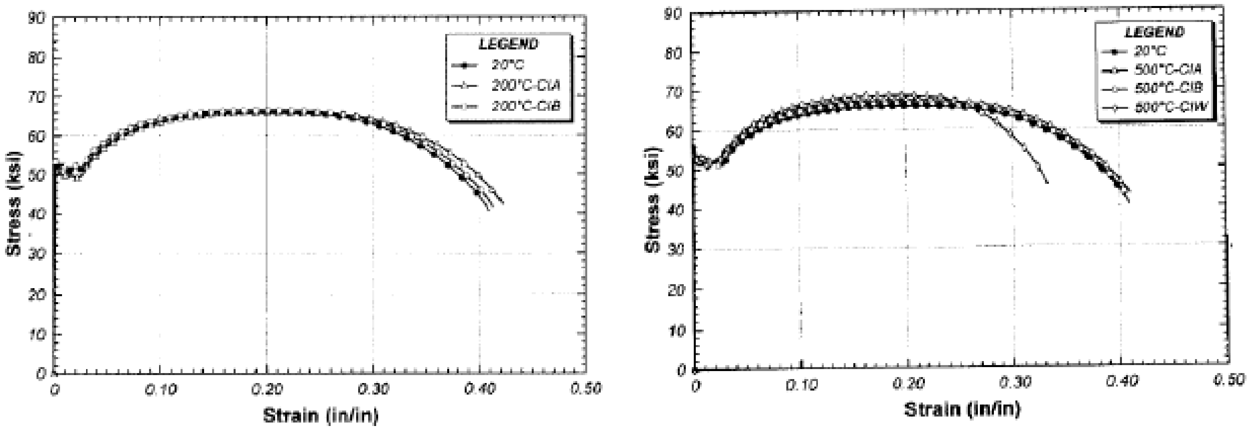

Figure 1-9: Residual stress strain curves after heating to 200°C and 500°C

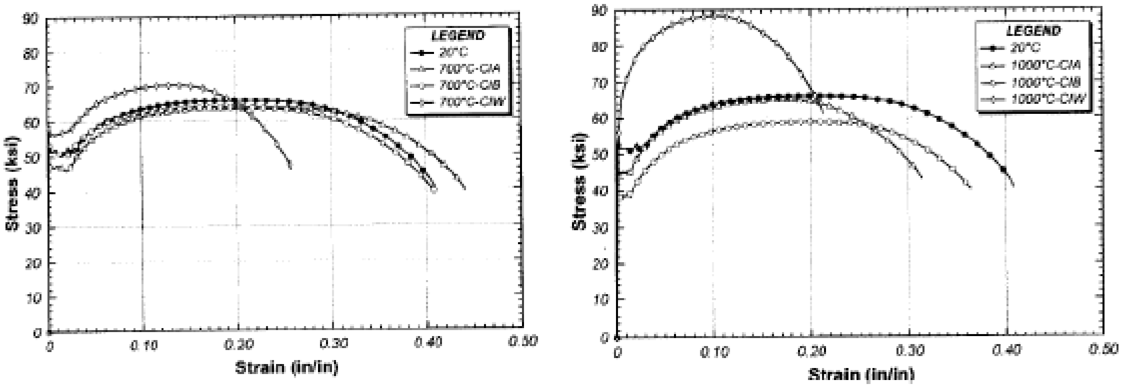

Figure 1-10: Residual stress strain curves after heating to 700°C and 1,000°C

The data in Figures 1-9 and 1-10 show good agreement with Figure 1-8. The method of cooling following a fire event is significant for this study. Knowledge of the impact of cooling method on residual strength is important for tunnel structures after a fire event because some methods may allow steel to recover strength and prevent full replacement of a damaged material. This data suggests that the method cooling has limited impact on the residual strength of the steel for members heated to 500°C, with the exception of cooling in water from 500°C. Steel that was heated to 500°C and then cooled in water showed significantly lower residual strength than that cooled in air or by blanket methods. The steel heated up to 1,000°C and then cooled in water shows a strength increase. This is supported by other research, which indicates that cooling steel in water or using a water jet results in a strength recovery for coupons heated above 600°C [16].

The deformation properties that influence the fire response of steel are thermal strain and high temperature creep. The thermal strain increases with temperature nearly linearly from room temperature to 750°C, at which point it becomes constant due to a phase change. Above 800°C, thermal strain continues to increase [1,12,20,21,22]. Thermal strain is significant in structural systems because it can lead to over-confinement and result in extreme stresses in vital components like beams and columns.

Another important deformation property is creep, which does not occur in steel at room temperatures. Creep is defined as an increasing deformation of a structural material despite no changes in the loading conditions. Creep becomes noticeable at 400°C under normal conditions and 300°C under high stress conditions [23]. Very little data is available on the effect of high temperature creep on the structural response of steel.

1.2.2 Concrete Response to Heat

Concrete is the most used structural material in tunnel structures because it is incombustible and has a low thermal diffusivity [24]. Fire damage to concrete structural elements manifests itself in the form of strength loss, stiffness decrease, and most devastatingly, spalling.

When evaluating the effect of fire damage on a concrete structural element, the maximum temperature reached by the concrete is the most important parameter because it relates to the mechanical response of heat exposure [25]. Concrete behavior under heat is more complex than most materials because it is a composite material made up of a diverse group of constituents. The different parts of concrete react to changes in temperature in different ways. This makes establishing theoretical models for concrete strength at elevated temperatures and residual strength difficult. Consequently, most existing models for concrete strength before and after heating are based on experimental studies.

Portland cement acts as a binder between aggregates in concrete. Physical and chemical changes to cement paste and aggregate, differential thermal strains between aggregate and cement paste, and pore pressure build up from moisture contribute to concrete damage under heat [2]. Cement paste experiences degradation reactions during heating. When heated above room temperature, dehydration and water expulsion reactions are followed by changes in chemical composition up to 1,000°C [25]. The ultimate compressive strength and modulus of elasticity of cement paste under heat (varying temperatures) is presented in Figure 1-11 (graph from [26]).

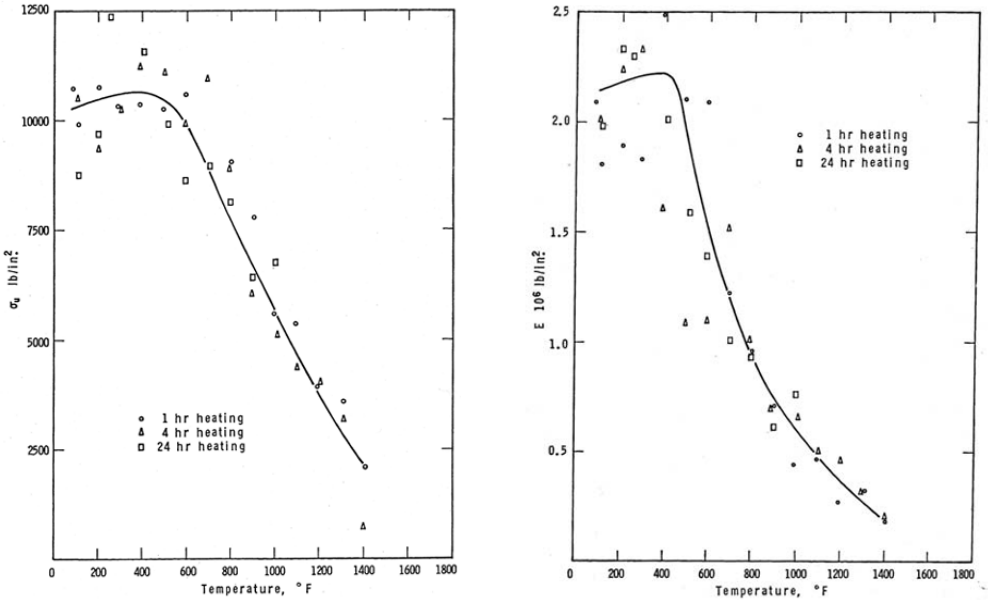

Figure 1-11: Compressive stress and elastic modulus of cement paste

The chemical changes that occur in cement paste after heating result in significant reductions in both compressive strength and elastic modulus for concrete [2].

Aggregate is the main ingredient in concrete that provides the high compressive strength necessary for most structural applications. Thermal conductivity and expansion, chemical stability at temperature, and thermal stability are important physical properties of aggregate that influence the behavior of concrete at high temperatures. Thermal stability is defined as the ability of a material to withstand changes in structure and performance under high heat. Commonly used aggregate materials are thermally stable up to 300–350°C [25]. When heated to 500–650°C aggregate expands during a process called crystallization, which leads to volume changes in concrete [25]. Certain types of aggregates that are commonly used in concrete, such as calcareous, magnesite, and dolomite dissociate into an oxide and CO_2 at temperatures higher than 600°C. Other aggregates, such as igneous rocks show degassing and expansion at extremely high temperatures (1,200–1,300°C).

The interaction between aggregate and cement paste at high temperatures contributes to concrete strength reduction. Cement paste will physically expand when being heated up to 150-200°C, but then contracts at higher temperatures. Aggregates continuously expand with increasing temperature, creating differential thermal strains that weaken concrete [27]. When under load, differential thermal strain effects are reduced during heating because of load-induced thermal strain, which causes the relaxation and redistribution of thermal stresses in concrete [2]. The effects of high temperatures on concrete as a whole are summarized in Table 1-2 [28].

Table 1-2: Effects of increased temperatures on concrete

Heating Temperature (°C)	Mineralogical changes caused by heating	Strength changes caused by heating
70–80	Dissociation of ettringite	Minor loss of strength (<10%)
105	Loss of physically bound water in aggregate and cement matrix, increasing capillary porosity	Minor loss of strength (<10%)
120–163	Decomposition of gypsum	Minor loss of strength (<10%)
250–350	Oxidation of iron compounds causing pink/red discoloration of aggregate. Loss of bound water in cement matrix and associated degradation becomes more prominent	Significant loss of strength starts at 300°C
450–500	Dehydroxylation of portlandite. Aggregate calcines, changing color to white/grey	Significant loss of strength starts at 300°C
573	5% increase in volume of quartz (α- to β-quartz transition) causing radial cracking around quartz grains in aggregate	Concrete not structurally useful after heating in temperatures over 500–600°C
600–800	Release of carbon dioxide from carbonates, causing considerable contraction of concrete with severe micro-cracking of the cement matrix	Concrete not structurally useful after heating in temperatures over 500–600°C
800–1,200	Dissociation and extreme thermal stress cause complete disintegration of calcareous constituents, resulting in whitish-grey concrete color and severe micro-cracking	Concrete not structurally useful after heating in temperatures over 500–600°C
1,200	Concrete starts to melt	
1,300–1,400	Concrete completely melted	

In addition to the constituents of concrete itself, the behavior of the reinforcing steel in concrete under high temperatures is extremely important to consider. Because concrete is such a poor conductor of heat, the temperature of the concrete cross section does not rise as quickly as it does for steel [25]. This creates a lag in the temperatures experienced by the reinforcing steel in comparison to the concrete, which helps preserve strength in a fire event.

The spalling of concrete poses a great risk to the reinforcing steel because it may expose the steel to the harsh surrounding environment and lead to corrosion. This must be considered when inspecting tunnel structures following a fire environment. Any exposed rebar must be patched and covered after major damage. Causes of spalling will be covered later in this section.

The effects of these changes on the chemical and physical properties of concrete components must be understood in the context of how the overall performance of concrete is affected. Concrete strength decreases at high temperatures because of the chemical degredation of its constitutents. The main factors that affect the strength of concrete during and after thermal exposure are the compressive strength of the original concrete and the type of aggregate [29 and 30].

Empirical models will be used to examine the reduction in stength and stiffness of concrete at elevated temperatures. Reduction factors for the stiffness and strength of concrete at elevated temperatures are included in both the ACI and Eurocode (CEN) standards. The CEN standard reduction factors are displayed in Figure 1-12 (reprinted from [27], data from [29]).

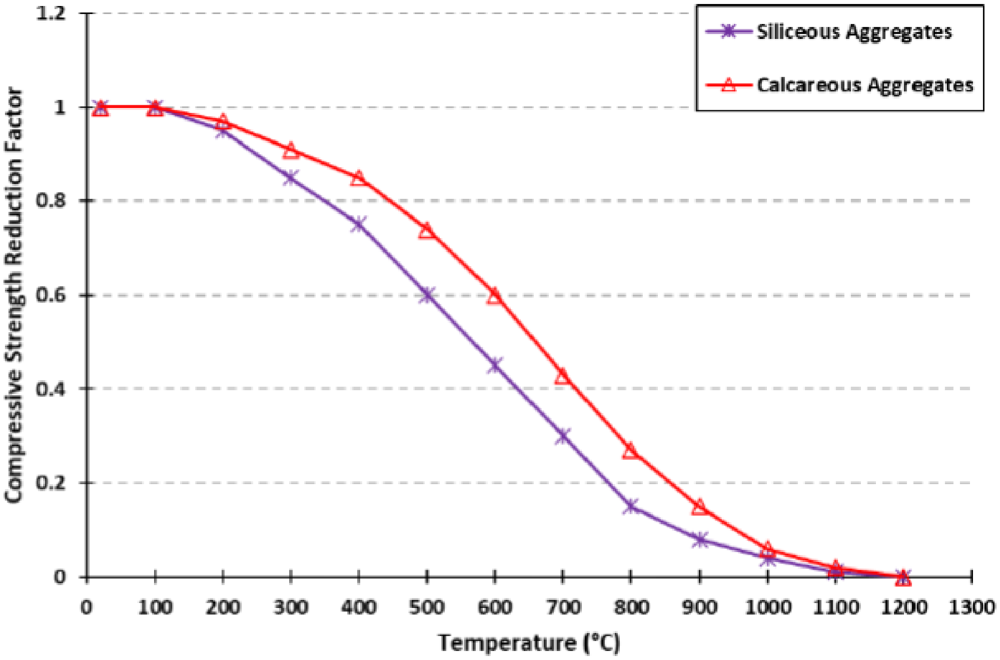

Figure 1-12: Compressive strength reduction factor vs. temperature

The reduction in concrete strength depends on the aggregate used. Calcareous aggregate performs better than Siliceous aggregate under identical fire exposures. Despite this, both concretes made of calcareous and siliceous aggregate experience major losses in compressive strength beginning at temperatures higher than 200°C. The stress strain behavior of concrete at high temperatures per EN 1992 1-2 is shown in Figure 1-13 (reprinted from [27], data from [29]).

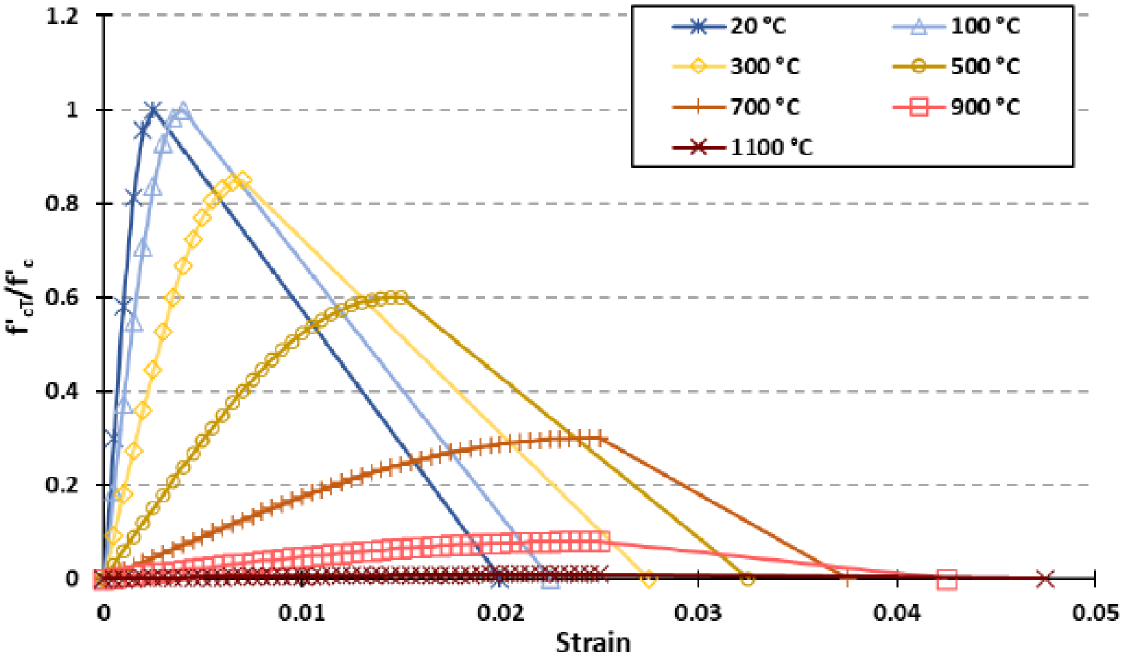

Figure 1-13: Compressive stress strain behavior of concrete at high temperatures

In addition to losing a significant portion of its compressive strength, the stiffness of the material also decreases with increased temperatures, as evidenced by the decreased slope in the stress strain curves of Figure 1-13.

Both Figures 1-12 and 1-13 are adapted from Eurocode, which provides a wealth of information on concrete behavior at high temperatures. Despite this, it is important to note that this code was developed based on construction practices and common materials in Europe, which may differ from the United States. Models from the ACI are provided in Figures 1-14 and 1-15 for comparison [31]. There are separate curves for stressed and unstressed concrete strength. The stressed test involves applying a preload of 25–55% of axial compressive strength while heating, and the unstressed condition involves no preloading. Figures 1-14 and 1.15 include stressed, unstressed, and unstressed residual tests, and both figures are reprinted from [31].

The ACI standard produces a strength reduction that is similar but not identical to Eurocode. The ACI standard predicts a 20% decrease in compressive strength for siliceous aggregate concrete at 800°F (426°C), while Eurocode predicts a 20% reduction at 400°C (752°F).

The experimental data collected in Reference 32 was used to evaluate the strength and stiffness losses of concrete. Data are separated based on the type of concrete aggregate (siliceous, calcareous, lightweight) and the strength of the concrete [normal strength (NSC) or high strength (HSC)]. The residual strength is compared to the stressed and unstressed conditions of concrete under heat (room temperature to 871°C). Residual, stressed, and unstressed data are presented in Figure 1-16(a–c) [32]. All compiled data are compared against the ACI 216 standard.

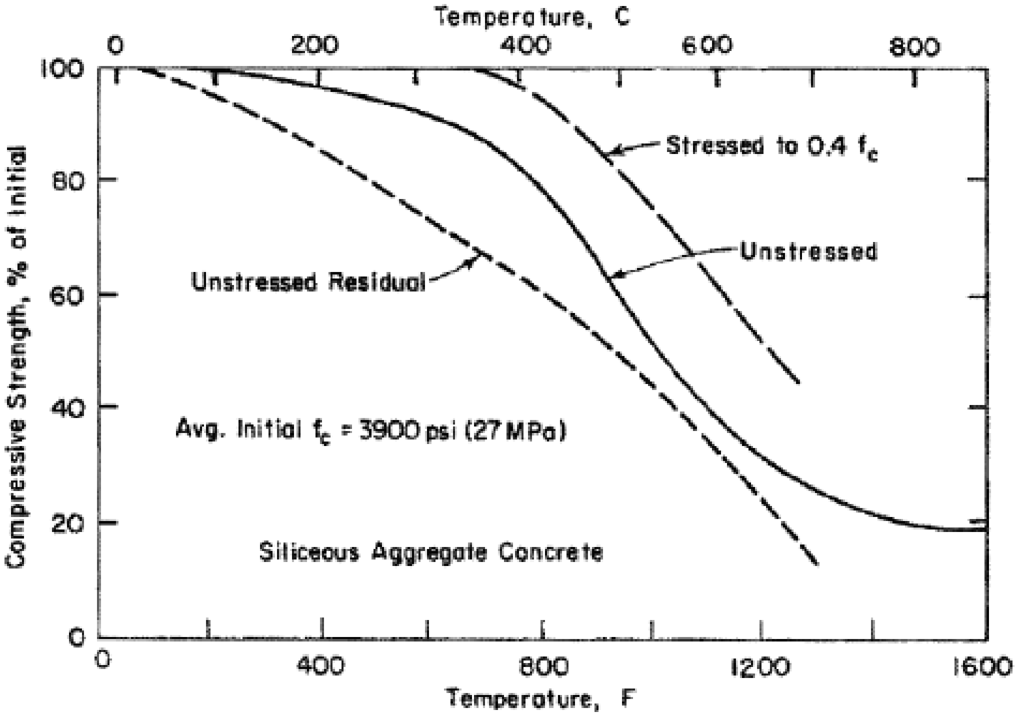

Figure 1-14: Strength reduction curves for siliceous aggregate-based concrete

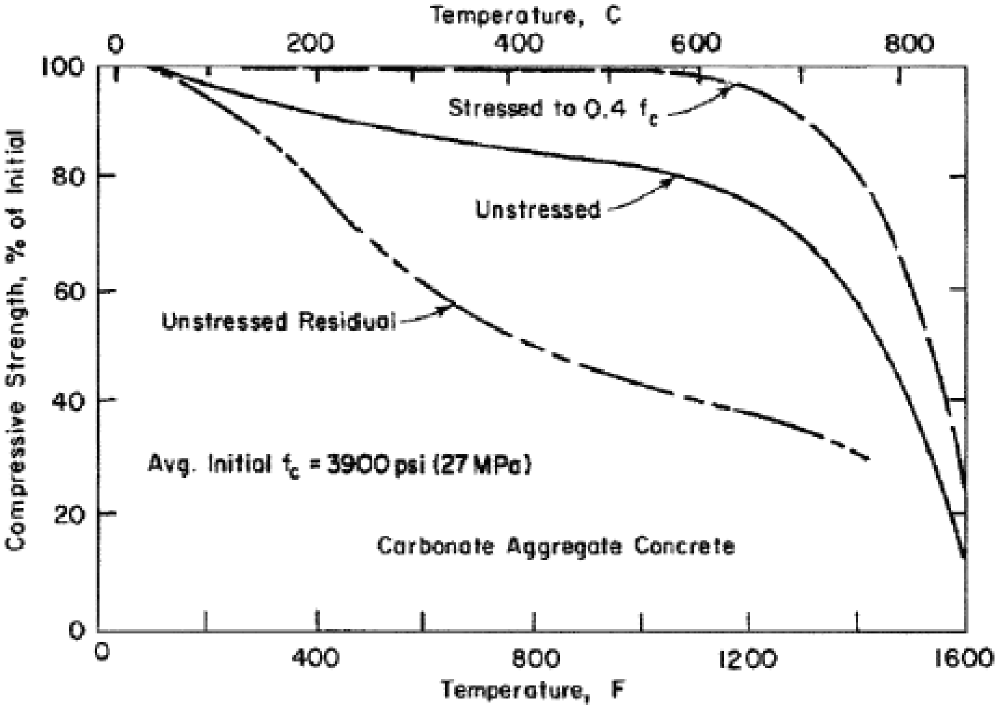

Figure 1-15: Strength reduction curves for calcareous aggregate-based concrete

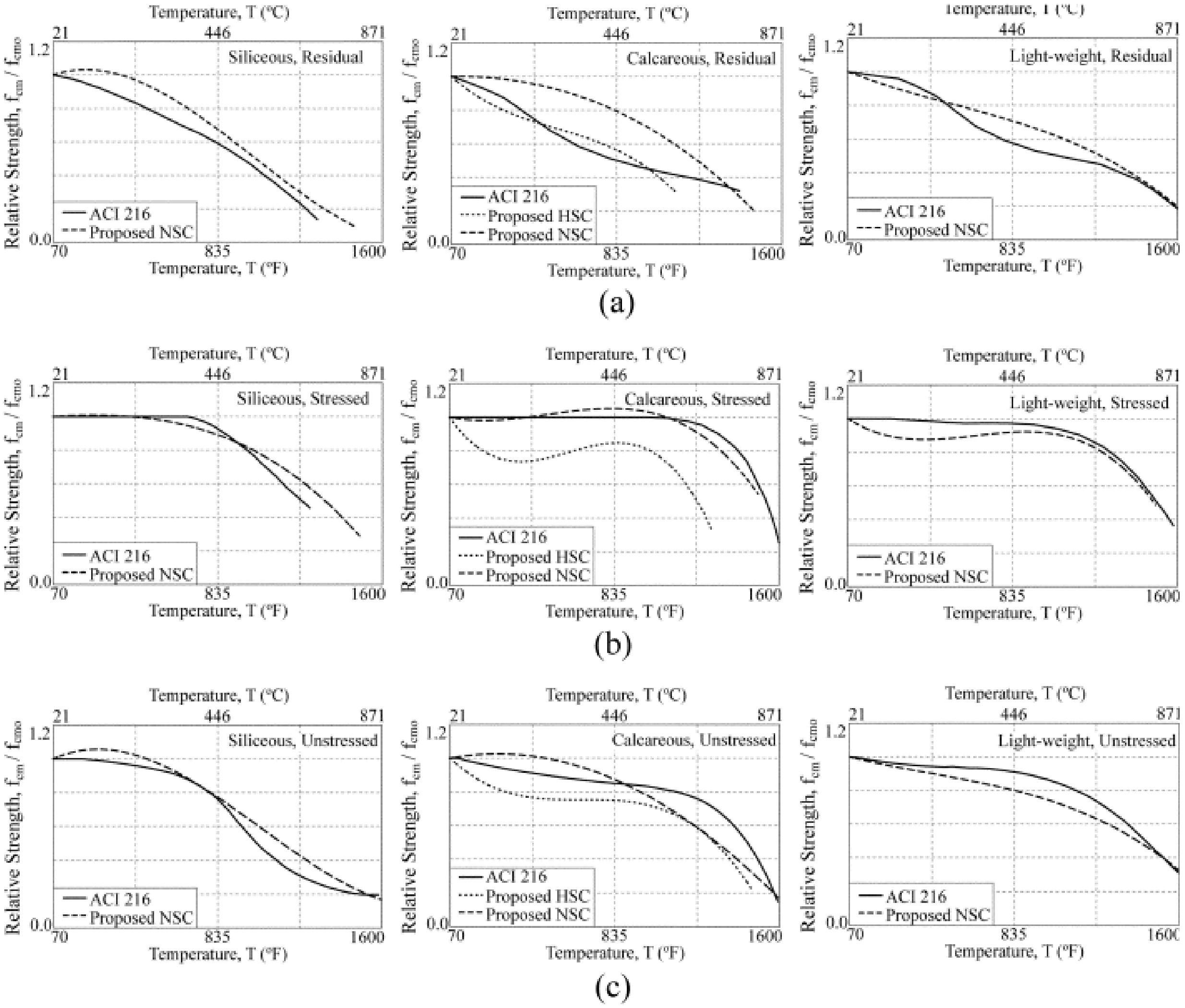

Figure 1-16: Residual (a), stressed (b), and unstressed (c) strength of concrete

Experimental data [32] show a good correlation with the ACI 216 standard, particularly for normal strength concrete. As predicted by the Eurocode, the concrete strength drops significantly above 100°C (212°F). In particular, the residual strength of the concrete is lower than that of the stressed and unstressed test. This indicates that concrete loses strength as it cools down. The stressed tests exhibited the lowest reduction in strength.

Furthermore, high-strength concrete performs worse than normal-strength concrete. This issue poses a concern for tunnel structures, which, at times, incorporate the use of high-strength concrete. Further research confirms this issue. A recent study [33] conducted a meta-analysis of 54 studies that examined the residual strength of high-strength concrete, which was characterized as having a compressive strength higher than 6 ksi. The experimental data is presented in Figure 1-17, which is reprinted from [33].

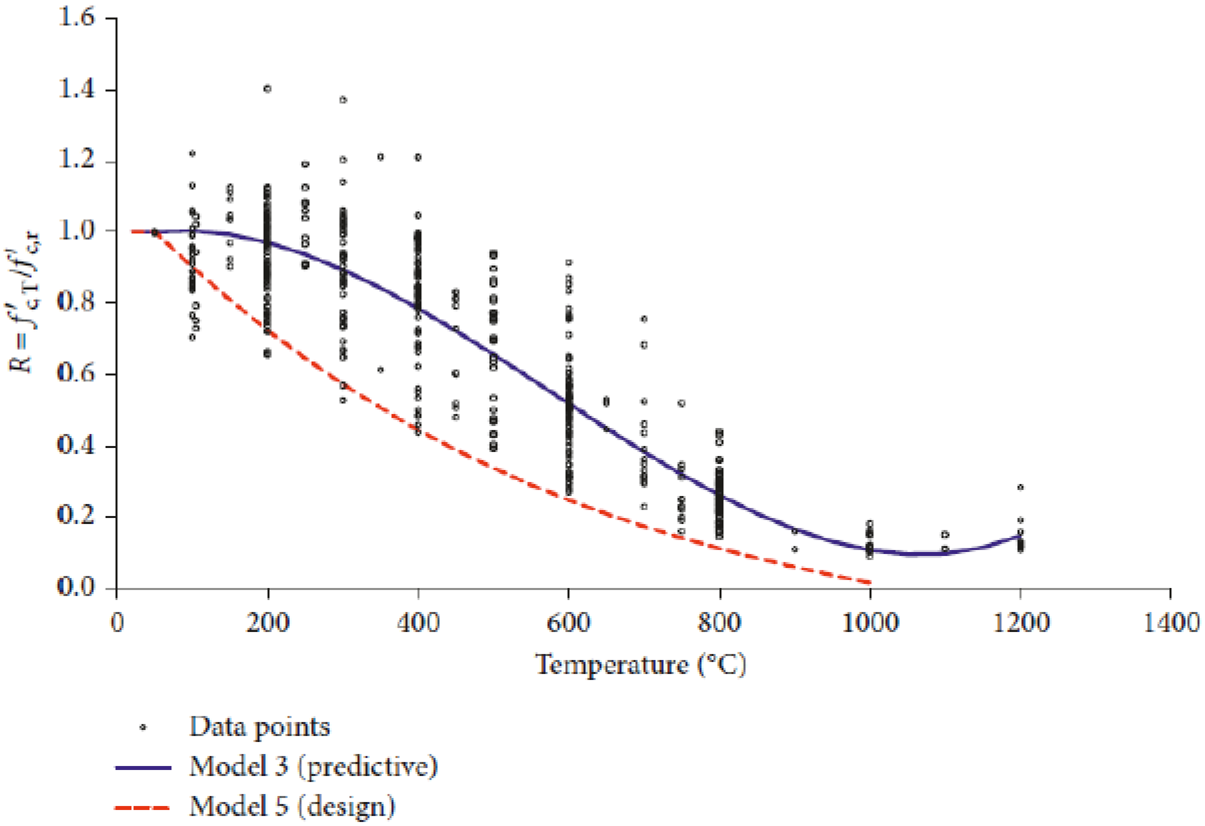

Figure 1-17: Residual strength for compressive strength of high strength concrete

The blue (solid) line represents the line of best fit for the data and the red (dashed) line represents a conservative design curve [33]. These data are in alignment with reference 32 and predict a 50% reduction in concrete strength at 600°C. This data does not distinguish between aggregate type or admixtures.

The strength reduction curve in Figure 1-17 shows that high strength concrete may have a higher residual strength than normal strength concrete. This contrasts with [32], which predicts worse residual strength for high-strength concrete compared to normal-strength concrete.

In addition to reduction in strength at elevated temperatures, concrete also loses stiffness during a significant fire event. Research on this topic is somewhat limited, but a well-known study [31] compiled the results of several studies to display the relationship between modulus of elasticity and maximum temperature for normal weight high-strength concrete, normal-strength concrete, and lightweight high-strength concrete. Only data for the unstressed and unstressed residual tests are available. In Figures 1-18 and 1-19, each line shows a different study, and these figures are reprinted from [33].

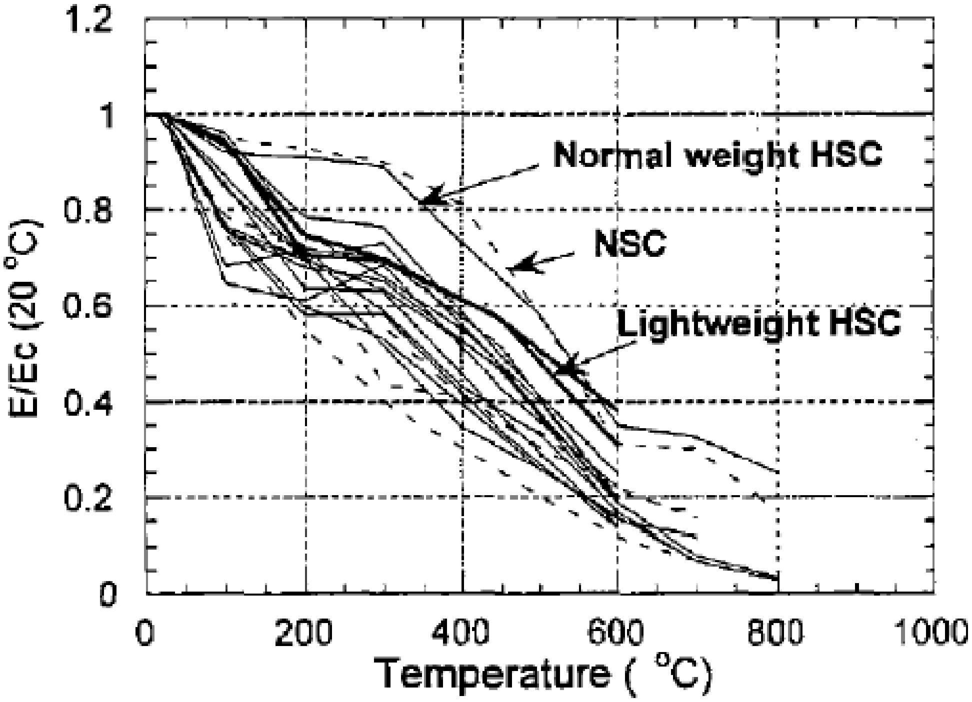

Figure 1-18: Modulus of elasticity reduction of concrete for the unstressed test type

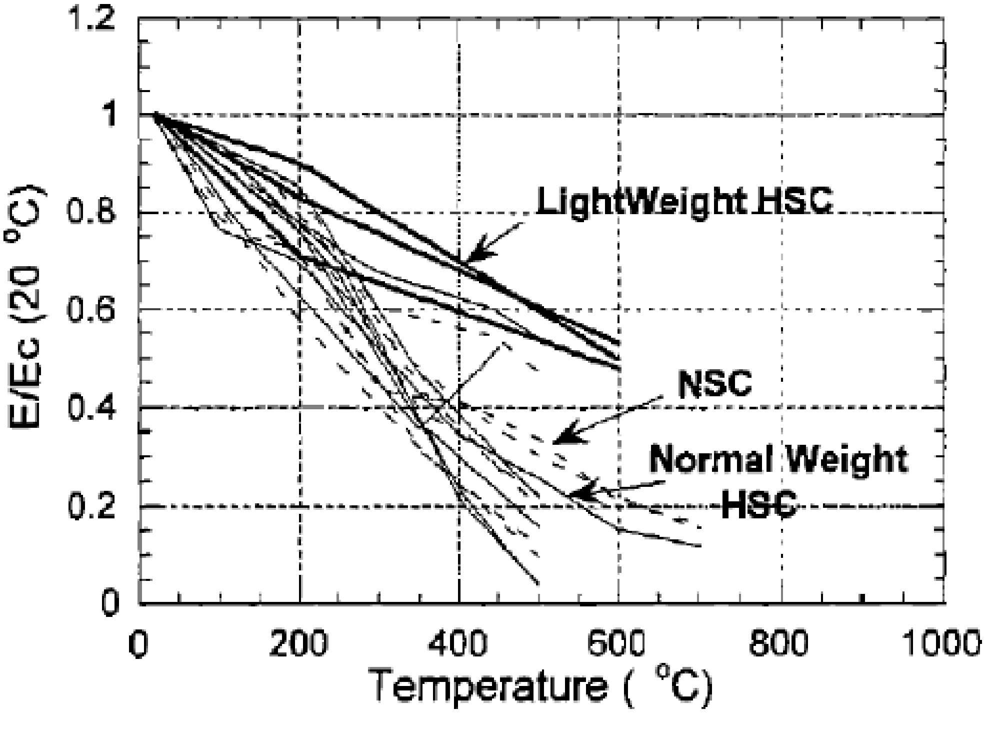

Figure 1-19: Residual modulus of elasticity reduction tests for unstressed condition

As with strength, the stiffness of concrete decreases significantly with increasing temperatures. This presents serviceability issues in structural elements and could lead to cracking of the pavement and elements of the road above.

The thermal spalling of concrete is another possible negative effect of heating concrete. The structural impacts of spalling vary between a post-fire scenario and during a fire event. Spalling reduces the cross-sectional area of members, which can reduce the compressive strength of the section or expose reinforcing steel to high temperatures and weaken the bond between the concrete and rebar [34].

There are four types of spalling observed in concrete. Explosive spalling is recognized as the most severe type, and results in an explosion that removes a layer of concrete with dimensions in the 100-300 mm range in length or width and 15–20 mm in depth. Explosive spalling typically occurs within the first 7–30 minutes of a fire in the temperature range of 150°C–450°C [34, 35]. There is no consensus as to what causes explosive spalling, but it is agreed that high-strength concrete has a higher probability of experiencing it than normal-strength concrete [35].

Another form of spalling in concrete is surface spalling that is recognized as a subset of explosive spalling. It is generally less severe than explosive spalling [35].

Corner spalling is a type of spalling that occurs after chemical processes such as a reduced bond between the aggregate and the cement occur. This gradually removes concrete layers at the edges of beams and columns [36, 37].

Aggregate spalling is the last type of concrete spalling, and it is not considered to have a significant effect on the structural capacity of the members. It is the result of water retained by aggregates such as flint or sandstone, which creates high vapor pressures and causes the aggregate to burst out of the concrete [38, 39].

1.2.3 Heat Transfer and Thermal Modeling of Structures in Fire Scenarios

The finite-element modeling (FEM) approaches for thermal analysis in fire simulations are well documented across various studies, each employing distinct methodologies to capture the temperature distribution and its effects on structural behavior. Neupane [40] begins with a 2D thermal analysis in Abaqus [41], focusing on heat transfer mechanisms such as conduction, convection, and radiation. Using temperature-dependent material properties, such as thermal conductivity, specific heat, and density according to EN 1994-1-2 standards, the analysis models convection and radiation through boundary conditions. Fourier's law is used to iteratively solve the temperature distribution, which is then mapped onto 3D structural models for mechanical analysis. This stepwise process ensures a comprehensive understanding of how temperature gradients affect steel structures during fire exposure.

Based on the importance of temperature-dependent properties, Kodur et al. [42] adopt a similar approach, but focus specifically on high-temperature material degradation for fire resistance analysis. Their FEM methodology incorporates the reduction of the yield strength and elastic modulus as temperatures rise. They also simulate the interaction of conductive and radiative heat transfer, creating a temperature history that helps predict structural failure under fire conditions. By comparing their results to real-world fire test data, Kodur et al. validated their model, emphasizing the critical need for accurate modeling of material behavior under fire exposure.

Expanding the application of FEM to steel members with claddings, Ma et al. [43] use LS-DYNA to conduct thermal simulations. The process starts with a 2D thermal analysis to determine thermal gradients across steel sections, assigning different convection coefficients for exposed and unexposed surfaces. Heat transfer mechanisms, including convection and radiation (modeled using Stefan-Boltzmann law), are captured to create thermal loads that are later used for structural analysis. Their model successfully predicts local buckling and lateral-torsional buckling during fire exposure, with experimental validation confirming the model's accuracy.

Ma et al. [44] further extend the application of FEM by focusing on steel structures protected by intumescent paint. Their simulations account for the expansion and thermal insulation properties of the intumescent coating, using a temperature-dependent thermal conductivity model to reflect how the coating delays heat penetration. Radiative heat transfer is modeled using Stefan-Boltzmann's law, while convection is based on empirical data. By comparing temperature rises in protected and unprotected sections, the model effectively predicts when steel reaches failure temperatures under fire conditions, validated against experimental data.

Usmani et al. [45] approach thermal simulations by exploring the complex thermal and structural behavior of composite steel frames under fire. Their simulations apply heat flux to replicate fire exposure, generating critical temperature gradients across steel sections. These gradients are essential for capturing thermal expansion and bowing, which are modeled to show how differential heating leads to axial compressive forces and bending moments, driving structural instability. Their analysis provides insight into the role of restraint conditions in determining the extent of thermal deformation and failure.

Huang et al. [46] continue the discussion of FEM by focusing on thermomechanical coupling and fire resistance in tunnel joints. Using Abaqus, their simulation process involves a sequential coupling of thermal and mechanical analyses. First, a heat transfer analysis calculates the temperature distribution across tunnel joints exposed to fire. This is followed by a thermomechanical analysis that evaluates the structural response based on the thermal results. The simulation incorporates heat transfer brick elements and reduced integral elements to accurately reflect temperature distribution and structural performance under fire, accounting for boundary conditions like friction and rigid body constraints.

Similarly, Bentz and Prasad [47] use FEM to simulate the thermal performance of fire-resistant materials (FRM) with a one-dimensional heat transfer model based on the NIST slug calorimeter setup. The model evaluates temperature changes in a stainless-steel slug coated with FRM during controlled heating and cooling cycles. By incorporating temperature-dependent thermophysical properties, such as thermal conductivity and specific heat, the model predicts the thermal response of the material under fire exposure, with applications in standardized fire tests such as ASTM E119.

Finally, Jeffers [48] addresses the modeling of 3D thermal responses in non-uniformly heated plates and shells. His approach uses Abaqus to discretize the temperature field into 2D layers, simplifying the 3D problem. This method, which combines finite elements and control volume techniques, captures heat transfer between layers via finite difference approximations. Boundary conditions such as convection, radiation, and heat flux are applied to ensure accurate thermal representation. The layered formulation maintains computational efficiency while producing accurate temperature distributions, verified against traditional 3D finite element models.

2.0 Research Methodology

In this chapter, the research methodology for evaluating the effect of a fire event on a tunnel is presented. First, the test setup and the rationale behind the test procedures will be discussed. Schematics of the setup will be provided, along with pictures of the steel beams and the fireproofing process, to demonstrate the feasibility of using such materials in tunnel applications.

2.1 Heating Setup

The heating process employed three Watlow Ceramic 2030 Style Heaters (Figure 2-1), capable of reaching temperatures up to 1,100°C (2,012°F). The Watlow F4T (Figure 2-3) provided power, facilitated temperature monitoring, and enabled the recording of test data. Type K thermocouples were utilized for temperature measurement (Figure 2-2; reprinted from [49]).

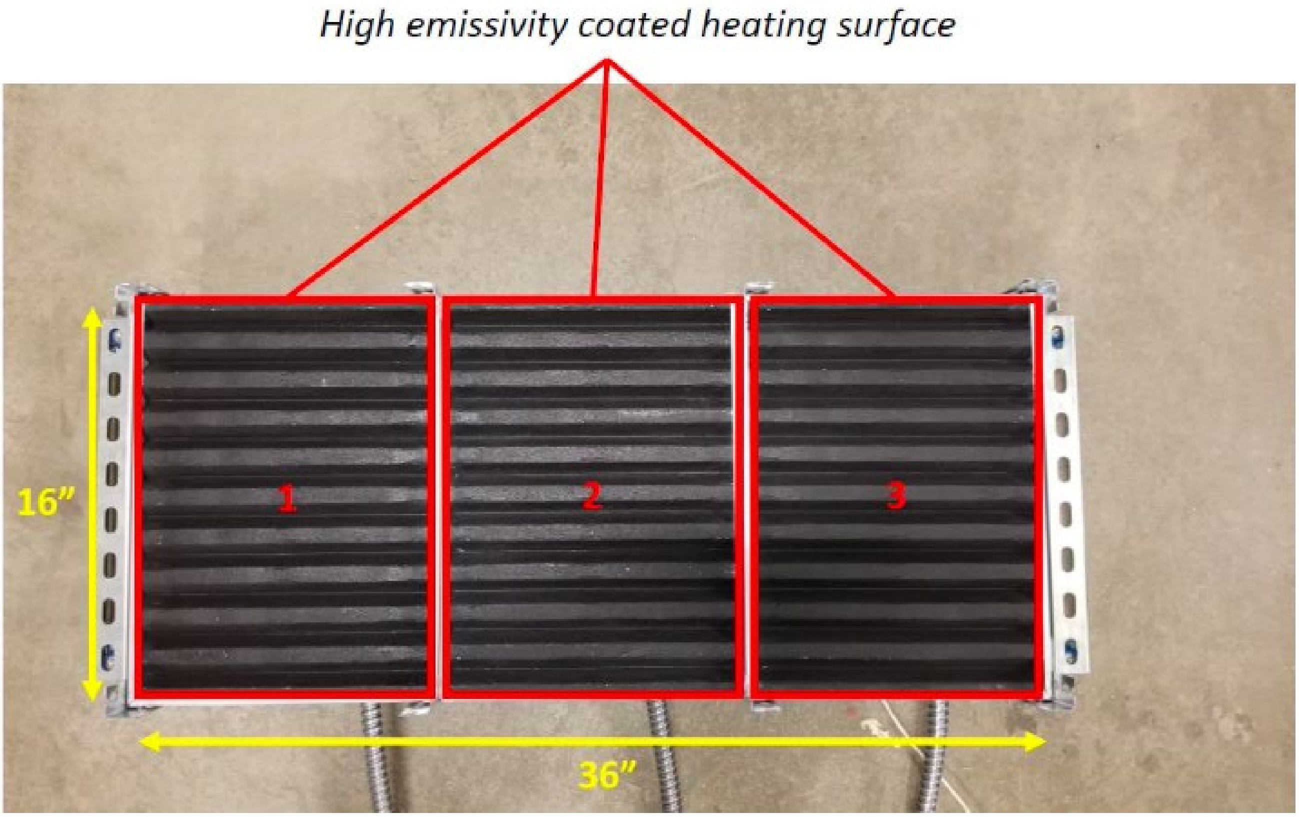

Figure 2-1: Watlow ceramic 2030 style heaters

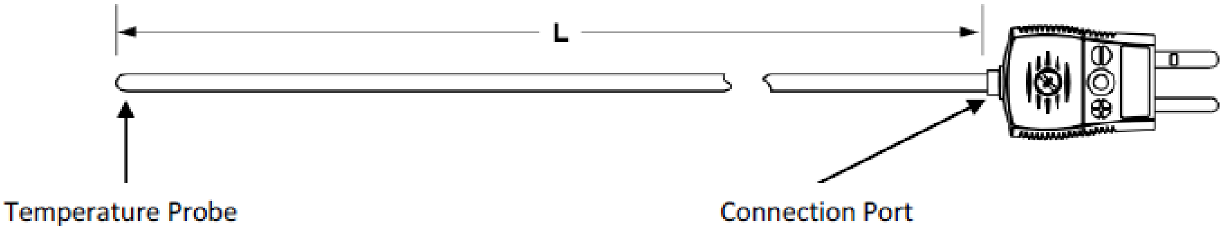

Figure 2-2: Thermocouple schematic

Figure 2-3: F4T terminal attached to the heaters

The heaters were affixed to a forklift mount and subsequently lowered into the experimental setup (Figure 2-4). Firebricks were employed to construct an enclosed area. Following the lowering of the heaters onto the firebricks, the setup was enveloped in ceramic fiber insulation (Figure 2-5). The complete assembly was positioned on a layer of ceramic fiber insulation overlaying a wooden platform. This wooden platform was reinforced by galvanized steel beams.

Figure 2-4: Firebricks, heaters, and insulation setup

Figure 2-5: Ceramic fiber insulation wrapped around the firebricks and heater setup

The configuration comprising the firebrick and Watlow heater established an interior space measuring 2.5 ft in length, 13 in. in width, and 22 in. in height for testing purposes. The dimensions of the beam were chosen accordingly.

2.2 Selection of Steel Beams

The selection of the beams for this study was based on considerations from a tunnel in the case study area. The smallest beams used in the tunnel were W21 × 163; however, due to the difficulty in sourcing this size, W21 × 147 beams were selected for testing (Figure 2-6). Each beam was fabricated to a length of two feet to fit within the constraints of the available heater space. All steel used was grade A992, with a yield strength of 55 ksi, ensuring that the material properties closely aligned with the structural elements typically used in the tunnel.

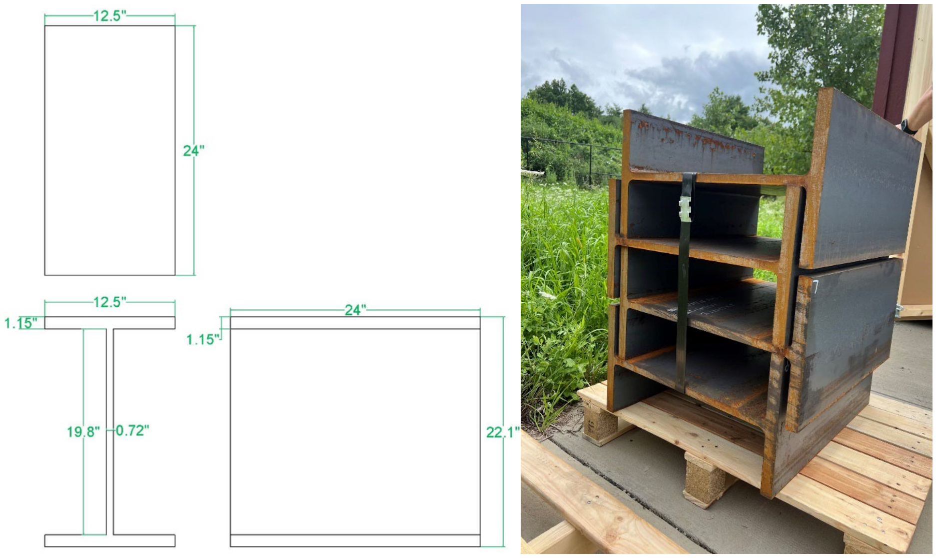

Figure 2-6: W21 × 147 beam dimensions used in testing; delivered beams

2.3 Testing Setup

The testing setup was designed to reflect the conditions in situ as accurately as possible. The case study tunnel uses 1.5 in. steel decking that connects each roof girder (Figure 2-7). The roof girders support a concrete roof slab.

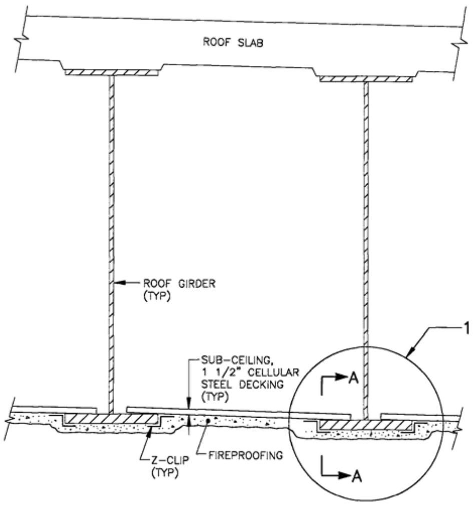

Figure 2-7: Typical girder section in the case study tunnel

To emulate this in our testing, galvanized steel L-channels were attached to the top flange of each beam using self-drilling screws (Figure 2-8). Unlike in situ conditions, the steel decking on the test beams is installed on the exposed surface of the flange. This adjustment was necessitated by geometrical limitations of our testing setup, which prevented the beam from fitting in with the heater configuration with the decking installed on the non-exposed surface. Additionally, while in situ conditions include potential composite action between the steel deck and concrete slab, this behavior was not replicated in the lab setup. However, this simplification does not impact the validity of the thermal response results, as the focus of the study is on the beam's thermal behavior during fire exposure.

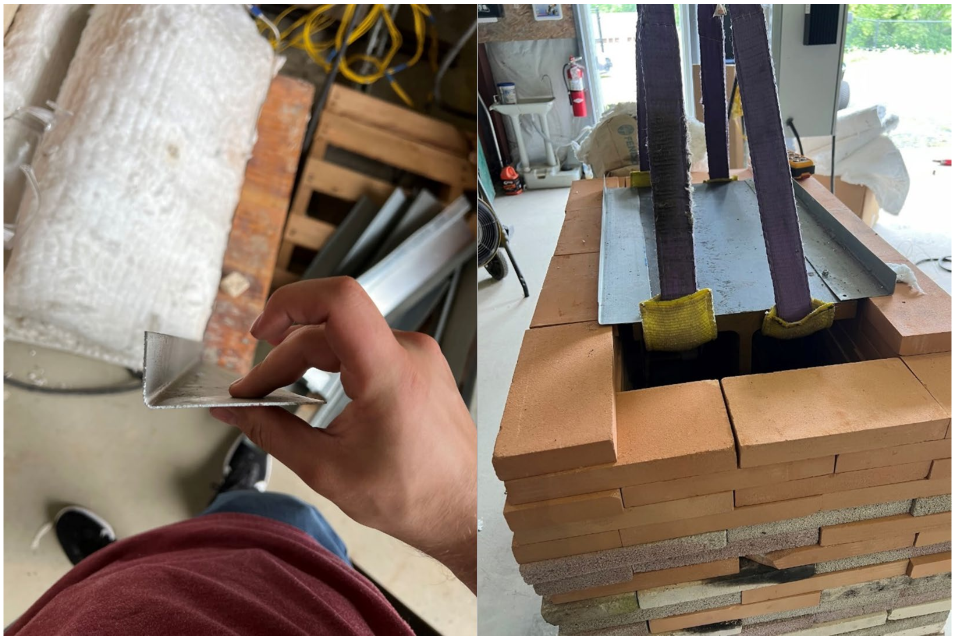

Figure 2-8: Steel used to emulate the 1.5 in. decking

Significant fire events in situ predominantly affect the exposed surface of the beam, as it is the sole surface directly interacting with the fire. In our laboratory testing configuration, this is represented by the top surface of the top flange. A thermocouple was positioned on the non-exposed surface of the top flange to capture the temperature gradient and validate heat transfer assumptions. Furthermore, thermocouples were placed in the middle of the web and at the bottom flange to monitor heat propagation throughout the beam's cross-section.

In situ conditions, such as shear connectors and composite action, significantly influence heat transfer during fire exposure. Shear connectors, like studs or bolts, create a thermal pathway, allowing rapid heat conduction from the exposed steel beam to the concrete slab. This interaction may alter the slab's thermal and structural behavior, potentially leading to spalling or degradation of the concrete. Composite action, while enhancing stiffness and capacity under normal conditions, introduces complex thermal interactions during fires. Differential thermal expansion between steel and concrete can induce stresses at the interface, causing cracking or delamination. Understanding these coupled thermal and structural behaviors is crucial for evaluating the performance of composite systems under fire conditions and addressing potential vulnerabilities in their design.

While these aspects were not explicitly modeled in our laboratory testing, understanding their effects is crucial for extrapolating the findings to in situ conditions. The comprehensive heating setup, including thermocouples, can be observed in Figure 2-9.

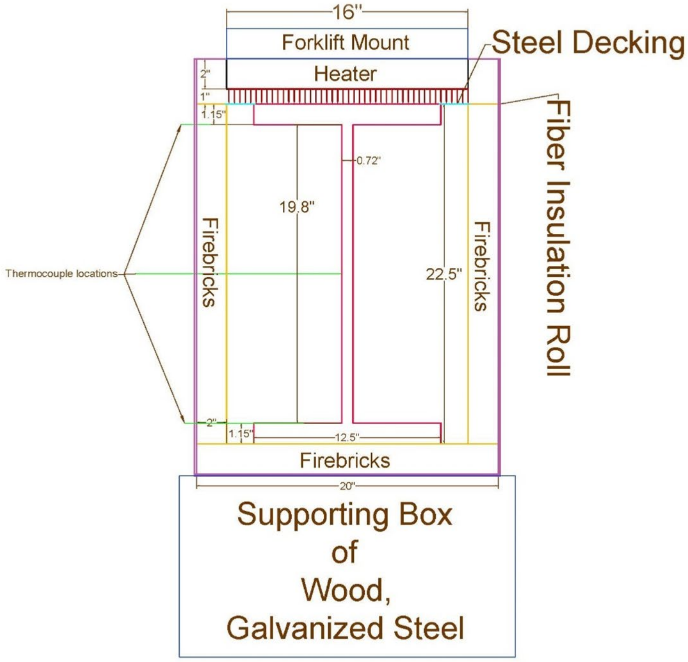

Figure 2-9: Heater testing schematic and dimensions

2.4 Fireproofing Setup

The roof girders within the case study tunnel are protected with cementitious fireproofing on their exposed surfaces. This study seeks to replicate this condition by utilizing a readily available cementitious fireproofing material. This fireproofing can be applied either by spraying or with a trowel. Particular emphasis was directed toward identifying a material that requires minimal maintenance and is straightforward to apply. Consequently, the fireproofing chosen for laboratory testing was applied with a trowel and necessitated only water for both mixing and cleaning.

In real-world applications, fire protection is exposed to harsh conditions, including frequent truck strikes that can damage or strip fireproofing from beams. To replicate these field conditions in our tests, multiple fireproofing scenarios were developed. These scenarios were created in collaboration with MassDOT, reflecting typical configurations encountered in practice. Four distinct fireproofing scenarios were selected for testing, along with a control test using a non-fireproofed beam. In total, five tests were conducted, and the details of each fireproofing scenario are illustrated in Figures 2-10 through 2-13. In each figure, the thicker (green) lines represent fireproofing, and the thinner (red) lines represent no fireproofing (thickness of fireproofing layer = ¾ in.).

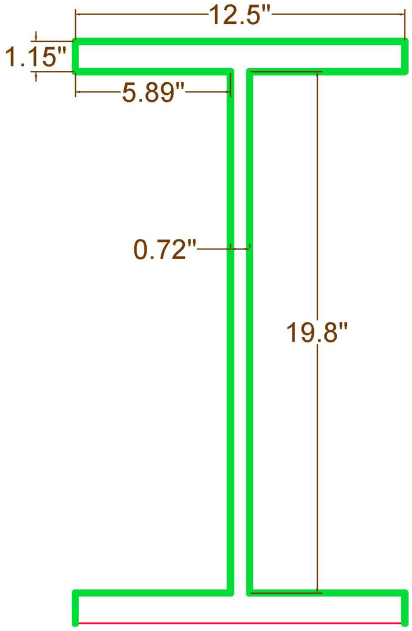

Figure 2-10: Scenario 1 fireproofing configuration

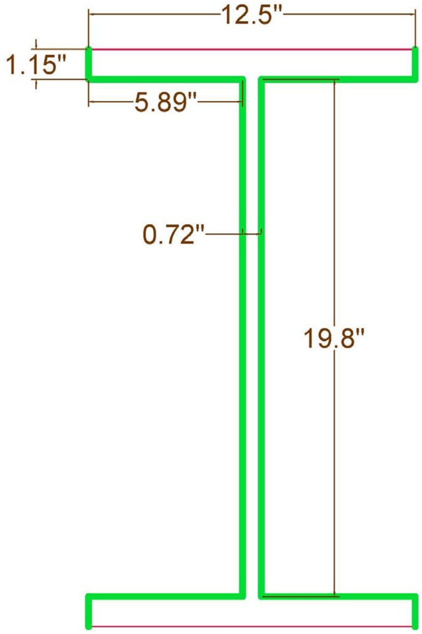

Figure 2-11: Fireproofing scenario 2

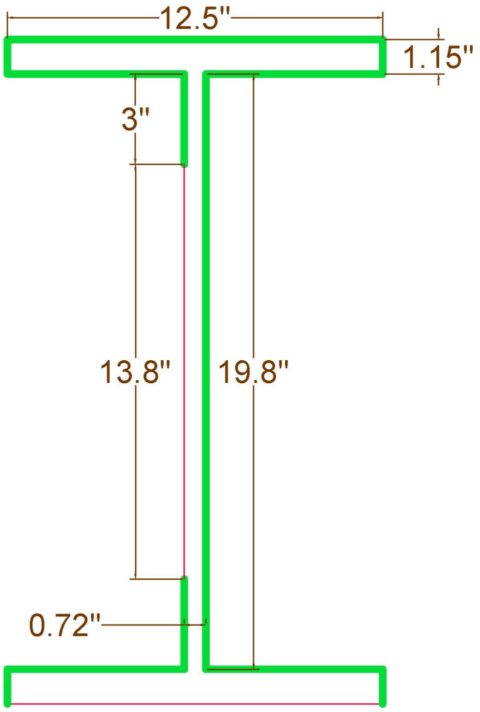

Figure 2-12: Fireproofing scenario 3

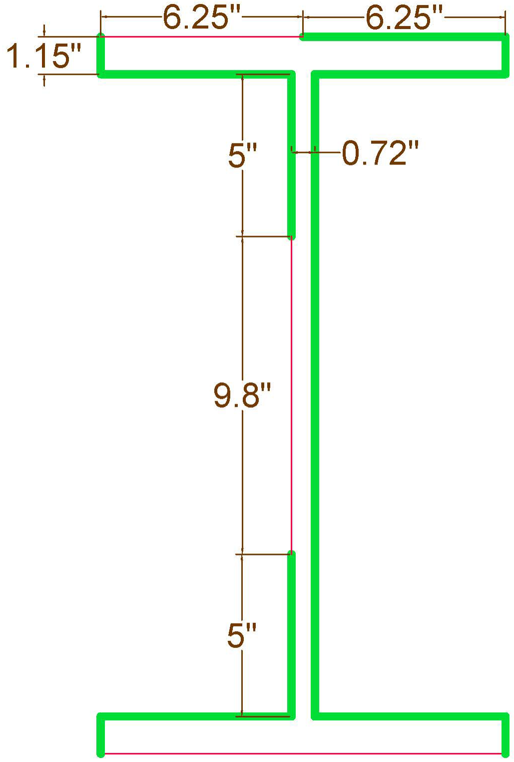

Figure 2-13: Fireproofing scenario 4

The only surface preparation done to the beams prior to fireproofing was wire brushing. This was done to eliminate dirt and debris that can interfere with the bond between steel and fireproofing. Pictures of the fireproofing process beams can be seen in Figure 2-14.

Figure 2-14: Fireproofing process

The thickness of the fire protection was selected based on the UL BXUV X790 standard [50]. Based on a 3-hour fire exposure in accordance with ASTM E119, a thickness of 13/16 in. was recommended. The more conservative value of ¾ in. was selected based on recommendation from MassDOT to simulate the harsh conditions of the tunnel and potential issues with the application process. This thickness was achieved on the top flange of the beams, but it was difficult to maintain a consistent thickness on the webs of these beams because the fireproofing was resistant to adhering to the bare steel. This issue was addressed for the third and fourth beams by orienting them laterally and applying the fireproofing in stages. However, achieving the desired thickness remained challenging due to the constrained supply of fireproofing material available in the laboratory. Preferably, the deviations observed in the fireproofing process should accurately reflect the challenges of fire protection repair and maintenance in real-world conditions.

This fireproofing material required 3.5 to 4 gallons of water per 50 lb bag and took 3 minutes to mix. The fireproofing manufacturer recommends the use of a calibrated water meter for mixing the material, but this was not used in our testing. Water was gradually applied to the mix to achieve the desired consistency within the recommended water content. All fireproofing batches were mixed in a 1 ft^3 mortar mixer capable of 34 revolutions per minute.

The fireproofing manufacturer specifies letting the fireproofing sit 5 days for 50% strength, 12 days for 75% strength, and 28 days for 98% strength. Due to time constraints, the fireproofing was not allowed to set for the recommended amount of time. The first scenario beam sat for 3 days before testing, the second scenario sat for 5 days, the third scenario for 7 days, and the fourth scenario beam sat for 21 days prior to testing.

In fireproofing scenarios, as elaborated upon in a subsequent section of this chapter, where certain segments of the web or flange were not covered, the temperature of the exposed steel was recorded. This method yields the most precise measurement for assessing the reduction in the steel's strength. Moreover, in scenarios where beams were either fully or predominantly fireproofed (scenarios 1 and 2), the recorded temperatures pertain to the fireproofing material atop the steel, rather than the underlying structural steel itself.

It is essential to highlight that, during the entirety of the test, the lower surfaces of the beam (located beneath the top flange) were adequately insulated from the heat source, thereby aligning with in-situ conditions. The fireproofed beams are depicted in Figure 2-15 to Figure 2-18.

Figure 2-15: Fully fireproofed scenario 1 beam

Figure 2-16: Scenario 2 beam

Figure 2-17: Scenario 3 beam

Figure 2-18: Scenario 4 beam

2.5 Fire Curves

Standard fire curves serve as analytical tools for modeling events and facilitating the design of fire resistance systems [29]. A representation of these curves is provided in Figure 2-19.

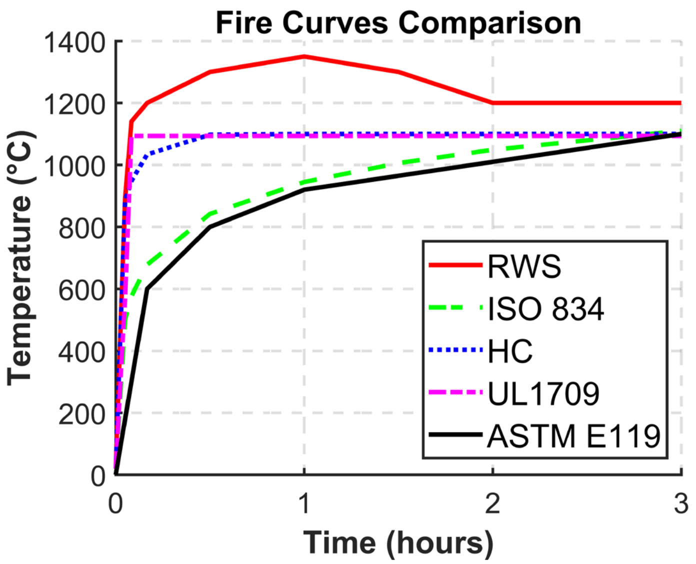

Figure 2-19: Standard fire curves for tunnel safety

All tests in this report are carried out in accordance with the ASTM E119 fire curve. The ASTM curve was selected as the most suitable fire curve for our testing setup. The Watlow heaters are limited to 1100°C, which is the maximum temperature reached in the ASTM curve. The time required for our testing setup to reach the maximum temperature is also most in line with the ASTM curve. The rate of temperature increase in our setup can only be set to a linear model, so an idealized ASTM curve was developed for this study (Figure 2-20).

Not all tests conducted in this study achieved the desired 1100°C peak temperature. The temperature the heaters can achieve in a test is dependent on many variables, such as quality of the insulation, amount of fireproofing on the beam, ambient temperature, and airspace conditions. Some tests exceeded the 1100°C mark, and others struggled to break 950°C. This will be accounted for in the results and discussion.

The ASTM E119 fire curve is based on cellulose fire modeling. Cellulose fires are modeled after the combustion of building materials [30]. This contrasts with hydrocarbon fires, which are modeled after the combustion of petroleum products [29]. Although a hydrocarbon fire would be a better model for a tunnel fire, as previously mentioned, equipment limitations prevent testing of hydrocarbon fire curves such as the RWS curve.

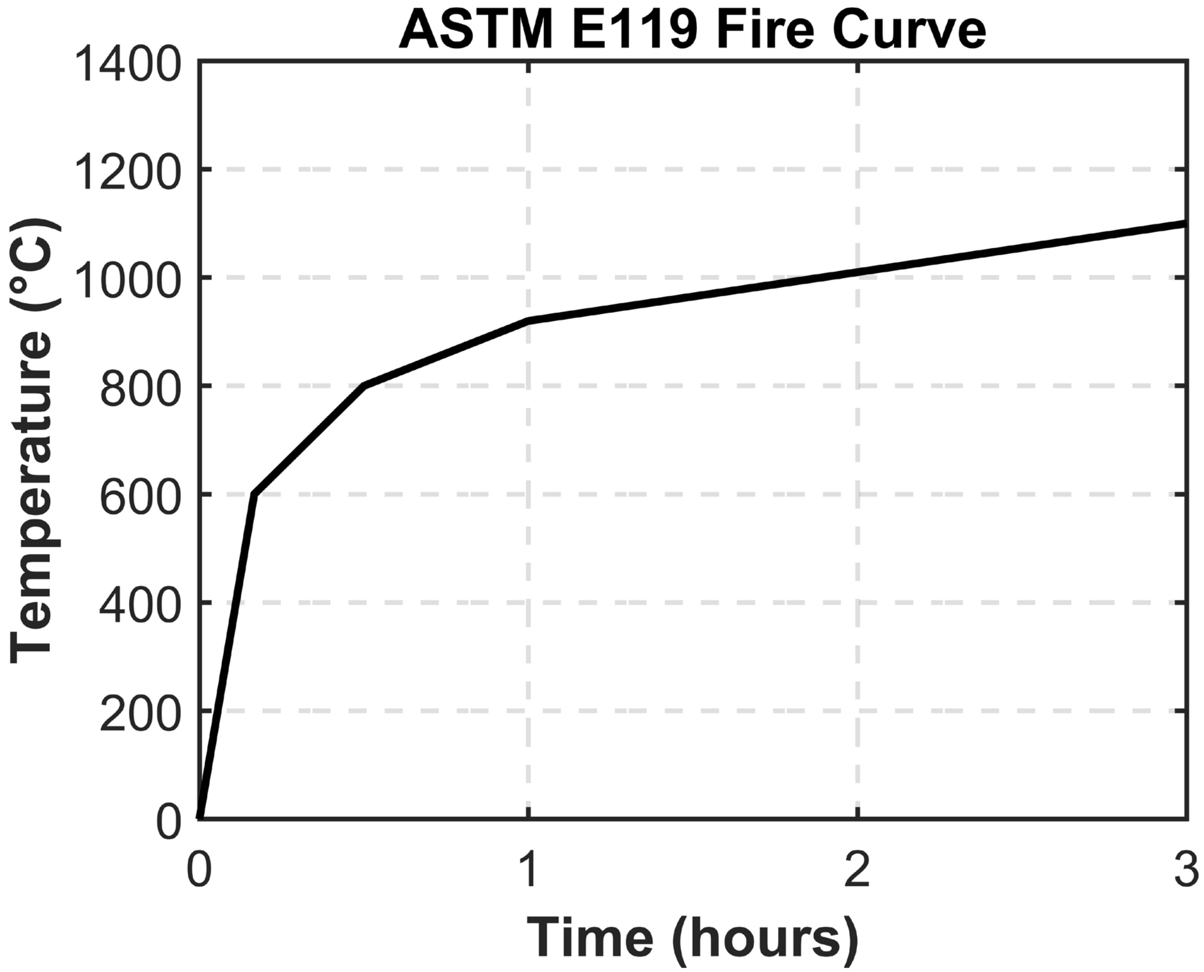

Figure 2-20: Idealized fire curve for the testing setup

2.6 Testing Procedure

The overall testing procedure was conducted as follows. First, a beam was placed on a cardboard sheet in the lab and the wire was brushed thoroughly until all dirt and debris was removed. Then, the L-shaped decking was installed as close to the edge of the top flange as possible to ensure that adequate spacing was provided in the testing setup. Fireproofing was applied by hand and with a trowel. After the fireproofing was installed, the beams were left in a well-ventilated environment for 3 to 4 hours, after which they were placed in the laboratory for 3 to 21 days and allowed to set.

Testing started by lowering the beams into the firebrick setup. This was done by using an overhead crane and lifting straps. The beam was placed in the center of the heating spaces, and the gaps on the sides between the beam and the firebricks were filled in with extra firebricks (see Figure 2-21). The heaters were lowered onto the firebricks until the galvanized decking came into contact with the metal grate over the heaters.

Figure 2-21: Placement of the beam in the testing setup

2.7 Tension Coupon Testing

The residual strength of the steel beams after being exposed to a fire event was also of interest. Following testing, the top flange of the control beam, the beam of scenario 1 and an untested beam were cut out. Two tension coupons were cut from the top flange of each beam using a water jet and tested to fracture. The tension coupon was dimensioned according to ASTM E8 (Figure 2-22) [39]. The coupons are highly elongated on the ends to ensure a secure grip in the tension testing machine (Figure 2-23).

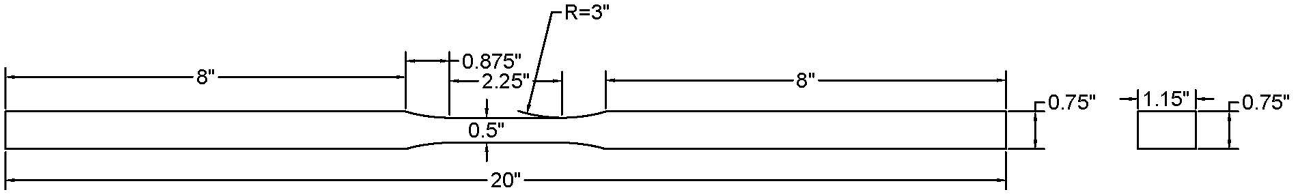

Figure 2-22: Tension coupon dimensions in accordance with ASTM E8

Figure 2-23: Tension coupons

The Tinius Olsen 400 kip machine was used to conduct tension testing. All tests were run at 500 mm/min. The yield strength was determined from the 0.2% offset method.

2.8 Durability Testing

The resilience of the fireproofing material after a significant fire incident was assessed. The evaluation involved the application of force using a screwdriver hammer and sledgehammer to detach the fireproofing from the beam. This experiment aimed to replicate the impact of a vehicular collision within the tunnel environment and to assess the adhesion strength of the fireproofing material to the beams.

2.9 Simulation Procedure

Phase – I: Without Fireproofing

The simulation was designed to replicate the thermal behavior of a W21 × 147 wide flange beam under fire exposure conditions, with the primary goal of establishing a baseline model for heat transfer prior to the application of any fireproof material. This basis is essential to understand the intrinsic thermal properties of the steel beam when exposed to controlled heating that reflects laboratory conditions. The simulation was carried out in Abaqus, and all dimensions and material properties were defined in SI units to ensure consistency and accuracy throughout the analysis. The focus of the model is to capture the spatial and temporal evolution of the temperature within the beam structure as it is exposed to a thermal source placed under the beam.

The W21 × 147 wide flange beam was modeled according to its actual geometric specifications, ensuring coherence with laboratory experiments. This beam consists of different structural components: the bottom flange, the web, and the top flange, each of which plays a crucial role in the behavior of heat transfer. The use of shell elements was selected because they can efficiently represent thin-wall structures without the computational overhead of modeling volumetric elements. Shell elements are particularly advantageous in scenarios where the interaction between conduction, convection, and radiation must be captured with precision while maintaining computational efficiency.

In this context, the beam was discretized using DS4 elements, a 4-node heat transfer quadrilateral shell element that excels at modeling temperature gradients in thin structures under transient conditions. These elements were used to represent the bottom and top flanges, as well as the web, where heat conduction and radiative heat transfer must be captured accurately over time. The DS4 elements were chosen for their suitability to handle complex heat transfer scenarios in wide flange beams, ensuring that the model could accurately replicate the heat transfer characteristics observed in the experimental setup.

The heating source in the experiment was a ceramic heater positioned underneath the wide flange beam, which delivered direct heat to the bottom flange. To mirror this in the simulation, a heater plate was modeled below the beam, designed with thermal properties that closely match the ceramic heater. The placement and size of the heater plate were carefully calibrated to ensure that its thermal impact on the bottom of the beam flange mirrored the experimental setup. The heater plate's emissivity was set to 0.95, reflecting the highly efficient radiative properties of ceramic materials, which enable the plate to emit a significant portion of its heat toward the steel surface. The bottom surface of the bottom flange was assigned an emissivity value of 0.75, corresponding to the lower radiative efficiency of the structural steel. This differentiation in emissivity was critical for accurately modeling the radiative exchange between the heater plate and the surface of the beam.

An important aspect of the experimental configuration was the air gap between the heater plate and the bottom of the wide-face beam. This gap of 25.4 mm (equivalent to 1 inch) provides significant barriers to direct thermal transmission and requires focusing on radiation and convection as the main modes of thermal transmission. The air gap was explicitly modeled in Abaqus to ensure that its thermal influence was accurately captured. The transfer of radiation heat is the dominant mechanism in the gap, whereas convective currents make a secondary contribution. This gap introduces a thermal resistance layer, reduces direct heat flow between the heating plate and the bottom flange, and requires accurate calibration to match the experimental results.

The interaction between the heater plate and the bottom flange was defined using the Abaqus interaction module, with a focus on capturing heat transfer across the 25.4 mm gap. Thermal conductance across the air gap was set at 0.002 W/m²·K, representing the limited conductive heat transfer properties of air over this distance. This low conductance value reflects the minimal role of conduction and emphasizes radiation as the primary mechanism of heat transfer. The view factor for radiative transfer between the heater plate and the bottom flange was set to 0.8, which accounts for the geometric arrangement and distance between the two surfaces. The view factor models the portion of radiative energy leaving the heater plate that successfully reaches the bottom surface of the flange. Together, the conductance and the view factor define the thermal interaction between the heater plate and the wide flange beam, providing a comprehensive representation of how heat is transferred across the gap during simulation.

The thermal load on the heater plate was defined by the ASTM E119 fire curve, a standard temperature-time relationship used to simulate fire exposure in structural components. This fire curve was applied as a surface heat flux to the heater plate, ensuring that the thermal conditions in the simulation accurately reflected those observed in the experimental tests. The ASTM E119 fire curve dictates a rapid increase in temperature during the initial stages of exposure, followed by a leveling period as the fire reaches a sustained phase. The heater plate absorbed heat flux over time and radiated energy toward the bottom flange, which absorbed the radiated heat and began to conduct it throughout the beam structure. The time-dependent nature of the fire curve was essential to replicate the transient conditions of fire exposure, allowing the simulation to capture the dynamic thermal response of the wide flange beam over a three-hour heating period.

Heat transfer was modeled across the various surfaces of the wide flange beam to accurately reflect the interaction of conduction, convection, and radiation. The bottom surface of the bottom flange, located closest to the heater plate, was modeled to transfer heat predominantly through radiation. Radiant heat from the heater plate was absorbed by this surface, with the rate of heat transfer being governed by the previously defined emissivity values and view factor. The top surface of the bottom flange experienced both convection and radiation, as it dissipated heat upward into the surrounding air while also conducting some heat into the web of the beam. This dual mode of heat transfer was critical to capture the interactions between the heated bottom flange and the adjacent components of the wide flange beam.

The beam web acted as the primary conduit to conduct heat from the bottom flange to the top flange. Both sides of the web were modeled to transfer heat through radiation and convection, reflecting its role in radiating heat outward while conducting thermal energy upward to the top flange. Heat conduction through the web is a key factor in determining how quickly the top flange heats up during fire exposure, making it essential that the thermal behavior of the web is captured accurately. The bottom surface of the top flange experienced a similar combination of radiation and convection, as it absorbed heat conducted through the web and interacted thermally with the surrounding air. In contrast, the upper surface of the top flange was modeled to transfer heat exclusively through convection, reflecting its contact with the tunnel walls in the experimental setup. Since the top surface was shielded by the tunnel walls, the radiative heat loss from this surface was minimized and convective heat dissipation became the dominant mode of heat transfer.

Natural convective cooling was modeled using a surface film coefficient of 1 W/m²·K, a value chosen to reflect typical convection conditions in fire-exposed structures. This coefficient was applied to all beam surfaces exposed to the surrounding air, ensuring that the convective heat loss was accurately captured. In addition to convection, radiative heat transfer was modeled using the Stefan-Boltzmann law, with emissivity values ranging from 0.75 to 0.95 depending on the surface material. The interaction between radiation and convection on the beam surfaces was essential to represent the complex heat transfer processes that occur during exposure to fire, where the surfaces radiate energy while simultaneously losing heat through convective air currents.

A structured mesh was generated for the wide flange beam to ensure high-resolution thermal analysis. The mesh was refined in regions where steep temperature gradients were expected, such as the bottom flange and the web flange junctions, which were likely to experience rapid changes in temperature due to their proximity to the heat source and their role in conducting heat throughout the beam. The seeding size was established at 40 mm for the beam to ensure that local temperature variations were accurately resolved.

The simulation was configured to run for 10800 seconds (3 hours) to match the duration of the ASTM E119 fire test. The time increment was automatically controlled to ensure stability and accuracy throughout the simulation. The initial time increment was set to 0.2 seconds, with minimum and maximum increments of 0.05 seconds and 2 seconds, respectively.

Phase – II: Fireproofing Scenario 1

In Phase II, the fireproof material was represented as a shell element with a consistent thickness of 19.05 mm (¾”), mirroring the settings used in the related laboratory experiment. The thermal properties of the fireproofing were specified according to the manufacturer's details, possessing a thermal conductivity of 0.19 W/mK at 20°C and a specific heat capacity of 970 J/kgK between 25°C and 35°C. To accurately capture the dynamics of heat transfer, the fireproof layer was modeled using a DS4 heat transfer shell element.

In Scenario 1, fireproofing was applied selectively to essential surfaces, notably the underside of the bottom flange, leaving other surfaces exposed to ambient conditions. The effect of fireproofing was represented by modifying the radiation and surface film coefficients on the web and exposed flange surfaces. Fireproofing was tested against the ASTM E119 fire exposure standard, mimicking direct fire exposure. A perfect bond was assumed between the fireproofing and the bottom flange to ensure precise modeling of heat transfer processes, including radiation, convection, and conduction. This facilitated an effective simulation of heat transfer from the fireproofing layer to the steel of the bottom flange. In this simulation stage, the heater plate from the experimental set-up was excluded, and the fireproofing-steel interaction was adjusted to incorporate all pertinent heat transfer mechanisms.

Phase – III: Fireproofing Scenario 2

During this stage of the simulation, the fireproof material was delineated as a shell element with a uniform thickness of 19.05 mm (¾”) to replicate the conditions observed in the associated laboratory experiment. The thermal properties of the fireproof material were determined based on the manufacturer's data, exhibiting a thermal conductivity of 0.19 W/mK at 20°C and a specific heat capacity of 970 J/kgK within a temperature range of 25°C to 35°C. A DS4 heat transfer shell element was used to effectively capture the phenomenon of heat transfer through the fireproofing layer. The properties of the steel in this simulation were based on the equations from the ASCE Manual (1992) and Eurocode 3 (2005), with the thermal conductivity of the steel calculated as 54 W/mK at 20°C, extended for temperatures up to 1100°C. Furthermore, the specific heat was established at 439 J/kgK at 20°C.

In Scenario 2, fireproofing was applied to critical surfaces, including the upper side of the bottom flange and the underside of the top flange, while other surfaces were left exposed to ambient conditions. The thermal influence of the fireproofing was represented by modifying the radiative properties, such as the emissivity and surface film coefficients, on both the web and the flanges. In Approach 1, the surface film coefficient for the web and the bottom surface of the upper flange was set at 7.5 $W/m^2 \cdot K$, simulating conditions characterized by low heat dissipation from the surface. This lower value depicts a scenario with minimal convective heat loss, which allows the structure to retain more heat, a condition typical of enclosed environments or when surfaces are insulated with fireproofing.

In Approach 2, the coefficient of the surface film was increased to 10 $W/m^2 \cdot K$, representing a scenario with increased airflow or ventilation, which enhances convective heat transfer and is more closely aligned with the exposure to fire in open environments. The higher value permits more realistic heat loss, thus capturing the impact of external cooling or ventilation during fire exposure. The top flange was assigned a fixed surface film coefficient of approximately 7.5 $W/m^2 \cdot K$, as it is generally more distant from the primary heat source. This fixed value accounts for efficient heat dissipation from the top flange due to convective heat transfer, thereby preventing excessive temperature accumulation in this region. By maintaining this coefficient, the heat transfer process at the top flange remains consistent with expectations for a surface exposed to less direct heat and greater natural cooling.

Emissivity values were chosen to range between 0.7 and 0.9, reflecting the varying surface conditions. The ceramic heater and steel surfaces exposed to fire were modeled with higher emissivity values (up to 0.9) to account for substantial radiative heat transfer, as these surfaces radiate more heat when exposed to high temperatures. Lower emissivity values (0.7~0.8) were employed for the web, flanges, and fireproofed surfaces reflecting their diminished capacity to radiate heat, a feature typical of the insulating nature of fireproofing materials. In this case, an important modeling assumption involved accounting for heat losses to the surrounding environment, estimated to be approximately 15%, primarily due to the heating of the surrounding air. This was implemented in Abaqus through the ambient temperature coefficient, incorporating radiation to model these environmental losses effectively.

Phase III: Fireproofing Scenario 3

In this phase of the simulation, the fireproofing material was defined as a shell element with a uniform thickness of 19.05 mm (¾") to replicate the conditions of the corresponding laboratory test. The thermal characteristics of the fireproofing were determined based on the manufacturer's data, with a thermal conductivity of 0.19 W/mK at 20°C and a specific heat capacity of 970 J/kgK within a temperature range of 25°C to 35°C. A DS4 heat transfer shell element was used to effectively capture heat transfer dynamics through the fireproofing layer.

In Scenario 3, fireproofing was specifically applied to essential surfaces, including the upper side of the bottom flange, the underside of the top flange and one side of the web, while other surfaces were left exposed to ambient conditions. The thermal effect of the fireproofing was represented by adjusting radiative properties such as emissivity and surface film coefficients on both the web and flanges. The surface film coefficient for the web and underside of the top flange was set at 7.5 W/m^2·K, simulating conditions characterized by low heat dissipation from the surface. The top surface of the top flange was assigned a fixed surface film coefficient of approximately 5 W/m^2·K, as it is generally more distant from the primary heat source. This fixed value accounts for efficient heat dissipation from the top flange due to convective heat transfer, thereby preventing excessive temperature accumulation in this region.

The fireproofing was adhered to steel with interaction properties that assumed no gaps between the layers, ensuring continuous heat transfer. Fireproofing was tested according to the ASTM E119 fire exposure standard, simulating direct fire exposure. Heat flux was introduced to the underside of the bottom flange using a simulated ceramic heater. A perfect bond was assumed between the fireproofing and the bottom flange, allowing for precise modeling of the heat transfer mechanisms, namely radiation, convection and conduction, from the fireproofing layer to the steel. In this case, an important modeling assumption involved accounting for heat losses to the surrounding environment, estimated to be approximately 17.5%, primarily due to the heating of the surrounding air. This was implemented in Abaqus through the ambient temperature coefficient, incorporating radiation to effectively to effectively model these environmental losses.

Phase – V: Fireproofing Scenario 4

The fireproof material was modeled as a shell element with a thickness of 19.05 mm (¾ in.), consistent with the laboratory experimental configuration. Thermal properties, including a thermal conductivity of 0.19 W/mK at 20°C and a specific heat capacity of 970 J/kgK within the temperature range of 25°C to 35°C, were implemented based on manufacturer-provided data. Fireproofing was represented using a DS4 heat transfer shell element to accurately capture thermal dynamics in response to fire exposure.

In Scenario 4, fireproofing was applied selectively to half of the underside of the bottom flange, while the other half was modeled as an exposed heater plate surface, the remaining surfaces subject to environmental conditions. To simulate the interaction between fireproofing and steel, the surface film coefficient for the web, underside, and upper side of the top flange was set to 1 W/m^2·K. This decision reflects the anticipated reduction in convective losses in bonded interfaces, where heat transfer occurs predominantly through conduction. It accounts for the insulating properties of fireproofing, which creates a controlled heat transfer scenario by minimizing heat dissipation into the surrounding environment.

The underside of the bottom flange was assigned a radiation emissivity value of 0.85, reflecting the steel's radiative heat transfer characteristics under direct fire exposure, thus accurately capturing the thermal behavior in high-temperature conditions. Furthermore, heat losses to the surrounding environment were estimated to be approximately 15%, primarily resulting from the heating of the airspace. This was modeled using the ambient temperature coefficient in Abaqus via radiation effects, simulating the impact of environmental heat loss. A perfect bond was assumed between the fireproofing and the bottom flange to ensure accurate modeling of radiation, convection, and conduction. This approach facilitated a precise simulation of heat transfer from the fireproofing layer to the steel, replicating the conditions observed in the fire exposure experiments.

3.0 Results

The following section contains the results of the fire testing. This includes the temperature of the heaters, airspace between the heating element and the beam, and the various locations on the beam.

3.1 Laboratory Test Results

Throughout the experimentation process, it was observed that the thermal conductivity of the test specimen significantly influences the maximum temperatures attainable by the heaters. Materials with lower thermal conductivity, such as cementitious fireproofing, reflect heat back towards the heaters, enabling them to achieve elevated temperatures. Conversely, the bare steel, which absorbs considerable heat and conducts it along the length of the beam, limits the maximum temperature achievable by the heaters. In the control test, depicted in Figure 3-1, the unprotected steel beam was subjected to temperatures exceeding 935°C. Despite this, the temperature did not reach the benchmarks set by the ASTM E119 fire curve standard, further emphasizing the effect of heat conduction in bare steel on limiting temperature rise. The highest temperature line in Figure 3-1 represents the heating element temperature, the second highest temperature line represents the airspace temperature, the third highest temperature line represents the top flange (exposed surface) temperature, the fourth highest temperature line represents the middle of the web temperature, and the lowest temperature line represents the bottom flange temperature.

The airspace temperature peaked at 719°C. This presents losses of 23.1% from the heating element. The most likely cause of these losses is heat escaping from the top of the testing setup. The top of the heaters was not insulated because the wiring and circuitry present cannot resist significant temperatures and begin to melt around 500°C. Additionally, there was about 2 inches of airspace between the control beam and the heating coils, which were separated by a metal grate that remained in contact with the top flange of the beam. Air can escape along the sides of the heating setup in the airspace. These losses were limited by layers of insulation that were focused on the top half of the testing setup. Another important note is that the heating element curve is not from the same test as the rest of the data. While moving the heaters, the thermocouple attached to the heating element was knocked loose, and so an accurate reading of the coils was not available during the control test. The heating element temperature curve presented in Figure 3-1 is from another control test in which nearly identical beam temperatures were achieved. This explains why the airspace temperature is higher than the heating element temperature 5 minutes into the test.

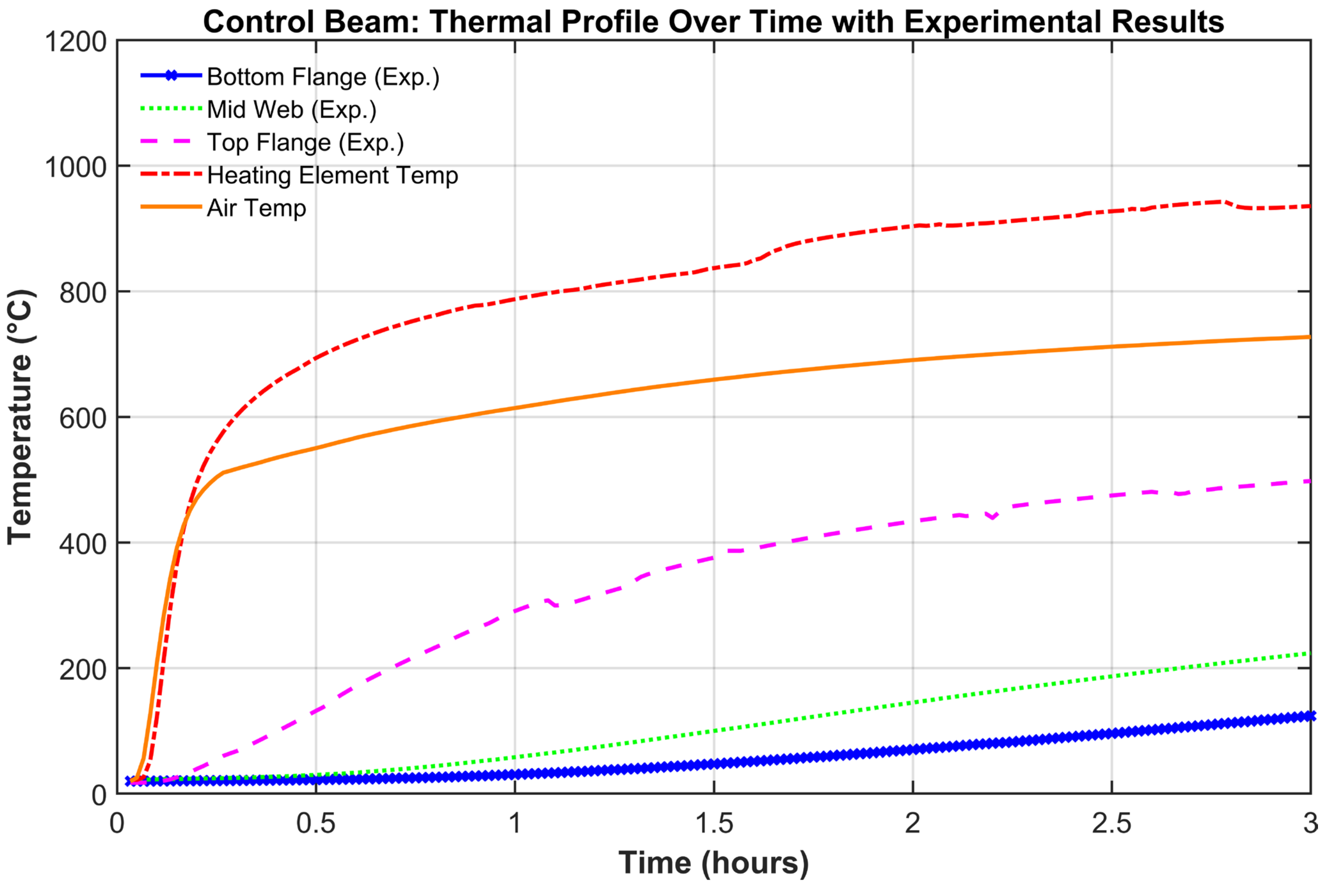

Figure 3-1: Temperature distribution of the control test (no fireproofing)

As mentioned previously, the exposed top flange surface temperature is absent. It is reasonable to assume that the temperature of this surface is between the temperature of the bottom surface of the top flange, which peaks at 499°C, and the airspace temperature, which peaks at 719°C. This places the exposed surface temperature in the range of 499–719°C. The temperature of the middle of the web peaks at 225°C and the temperature of the bottom flange peaks at 125°C. This presents a 44.4% reduction in the temperature from the middle of the web to the bottom flange and a 54% reduction from the top flange to the middle of the web.

Figure 3-2 presents the cooldown data for the control beam, with temperatures measured using a Fluke Ti400 infrared (IR) thermal camera [50]. The cooldown process focused on the exposed top flange surface, as data for the non-exposed surface was unavailable. The cooldown occurred entirely in ambient air, with the top flange ventilated by outside air at a temperature of 69°F (20.6°C). While the IR thermal camera was employed for the control test, thermocouples were used in subsequent tests for greater accuracy and efficiency in tracking temperature changes. As described in the methodology section, the top flange surface rapidly lost heat after the heaters were turned off, insulation was removed, and the heaters were lifted. This sharp temperature drop highlights the rapid initial cooldown phase. In Figure 3-2, the exposed surface (red) is the surface being considered. Time elapsed is measured from the time the heaters are shut off.

The fireproofing present in the test contributed to a more pronounced initial cooldown, as it radiated heat into the surrounding air more efficiently than unprotected steel. This is why the cooldown began at a relatively high temperature of >450°C. The cooldown followed an approximately exponential pattern, with temperatures dropping from 462°C to 305°C within the first 20 min. These data show that fireproofing accelerates the heat dissipation process, allowing the beam to cool down more quickly than unprotected steel. The rapid reduction in temperature in fireproofed beams during cooldown suggests its effectiveness in mitigating post-fire thermal effects and protecting tunnel structures during fire exposure.

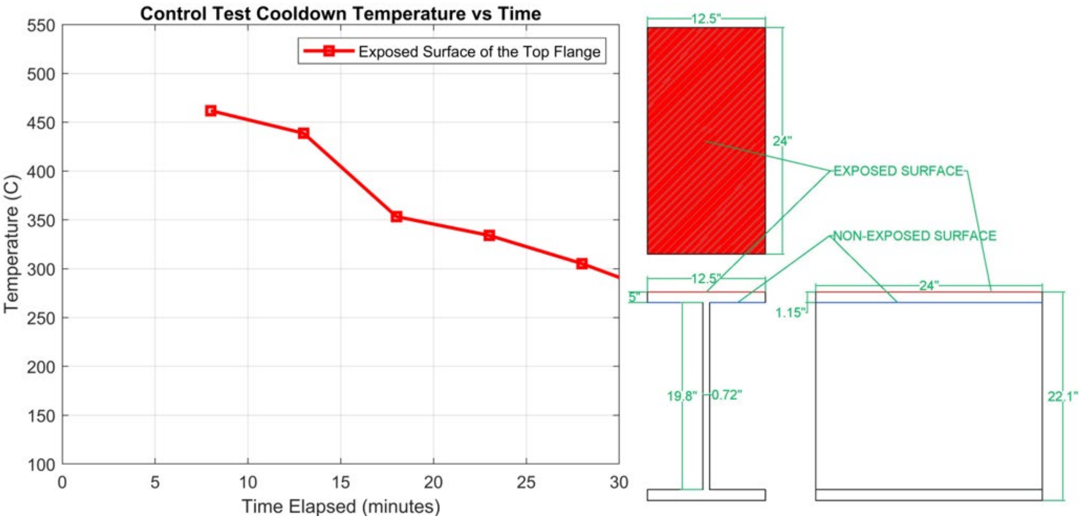

Figure 3-2 Cooldown temperature vs. time for the control test

The control beam displayed significant visual and structural changes following testing, as shown in Figure 3-3. The most evident alteration was the darkening of the exposed surface of the top flange, likely resulting from oxidation caused by prolonged exposure to high temperatures. This discoloration underscores the intensity of heat experienced by the beam, as the steel surface was directly impacted by thermal exposure. Over time, oxidation layers form on steel surfaces subjected to high heat, which not only affects the appearance of the beam but also signals the potential for long-term material degradation.

In addition to the visual changes, the galvanized steel showed considerable warping, a deformation attributed to thermal expansion under elevated temperatures. This deformation was particularly pronounced in areas where self-drilling screws were used to secure the decking to the beam. These screws acted as mechanical restraints, restricting the natural lateral expansion of the galvanized steel, causing it to warp upward under the stress of thermal expansion. The localized stress created by the fasteners intensified the warping effect, resulting in upward buckling (Figure 3-4). The interaction between the thermal expansion of the steel and the mechanical restraint of the fasteners led to this pronounced deformation. These observations show the direct impact of thermal stress on structural steel components and highlight the critical role structural connections play in exacerbating deformation during fire exposure, where mechanical constraints can lead to more severe localized damage.

Figure 3-3: Condition of the top flange and decking before (left) and after (right) testing

Figure 3-4 illustrates the findings from the heater testing for the initial fireproofing scenario, wherein the entire beam was enveloped in fireproofing material. The depicted temperature originates from the exposed top surface of the top flange.

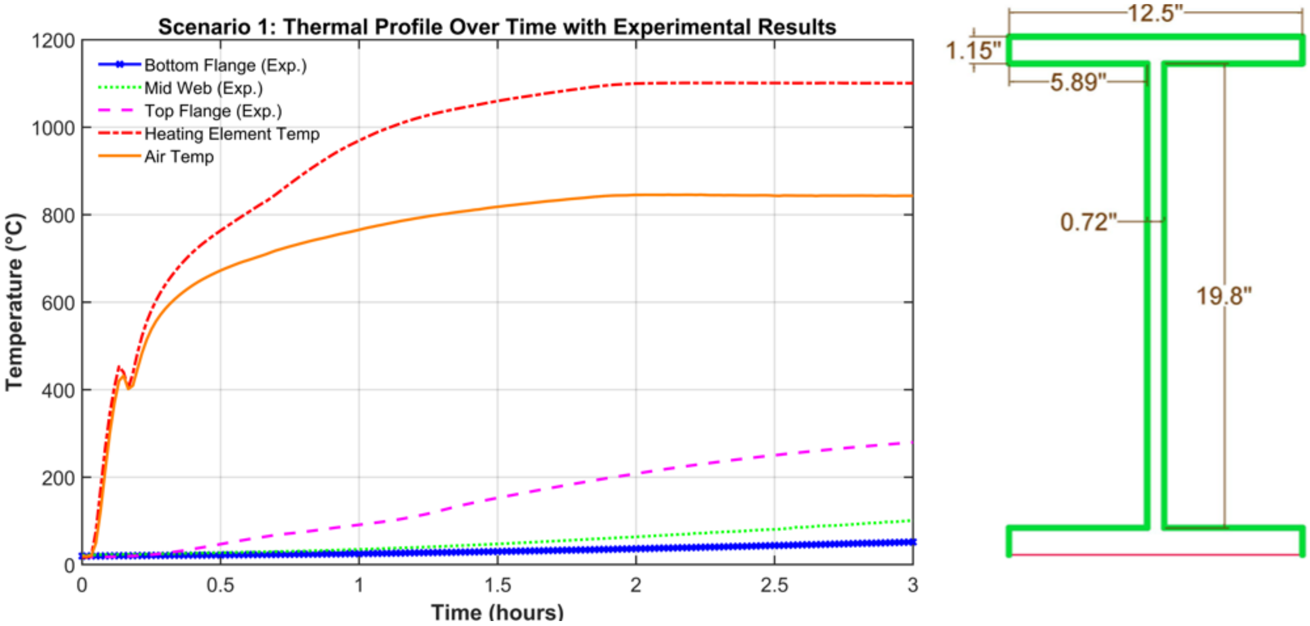

Figure 3-4: Scenario 1 test data

The highest temperature line in Figure 3-4 represents the heating element temperature, the second highest temperature line represents the airspace temperature, the third highest temperature line represents the top flange (exposed surface) temperature, the fourth highest temperature line represents the middle of the web temperature, and the lowest temperature line represents the bottom flange temperature. In the scenario 1 test, the temperature curve from the heaters outpaced that of the ASTM E119 fire curve, reaching 1100°C in less than 2 hours. This occurred because the fireproofing on the beam radiates heat back at the heaters instead of conducting it into the rest of the beam like the bare steel in the control test. The airspace temperature peaked at 843°C, which presents 23.4% in losses between the heater and the airspace. In this test, the airspace was reduced in comparison to the control test due to the added height of the beam from the ¾" fireproofing on the top flange. This is another factor in the increased testing temperatures for this scenario.

The non-exposed surface top flange temperature peaked at 281°C in this test, which is a 43.7% reduction compared to the control beam testing despite being exposed to higher temperatures (1100°C vs 935°C, a 17.6% increase). The middle of the web and the bottom flange peaked at 101°C and 52°C respectively, presenting a 55.1% and 58.4% reduction for the top flange and web respectively compared to the control test. The drop off in temperature throughout the height of the beam (48.5% from web to bottom flange) is consistent with the results of the control test, which had a 44.4% reduction along the height of the beam. The drop off from top flange to middle of the web was 64.1%, which is about 10% higher than the control test.

An important note from the test procedure is that during the test of scenario 1 beam, smoke arose from the heaters around 425°C. The heaters were shut off to investigate the situation, which explains the dip in temperature at the 10-minute mark of testing. The smoke had no odor and went away after about 10 minutes. It was likely the remaining moisture in the fireproofing evaporating out of the testing setup as the temperature of the fireproofing increased.

The cooldown data for scenario 1 is presented in Figure 3-5. This data includes both the top and bottom surface of the top flange. The exposed surface of the beam starts at 278°C and cooling follows an approximately linear model. As with the control beam, the flange was cooled in air and allowed to exchange heat with the open atmosphere freely. The outside temperature on the day of the test was 23.9°C (75°F). The cooling of the top flange was measured by placing a thermocouple in between the fireproofing and the beam itself. The exposed surface of the beam only cools about 60°C in the 20 minutes of monitored cooling. This is because the strong thermal insulation properties of the cementitious fireproofing also trap heat on the beam once the heat source is removed. This must be considered when determining the strength of the beam shortly after a fire event. The non-exposed surface starts at approximately 300°C and cools at a much slower rate than the exposed surface due to the lack of ventilation. This cooling process also follows an approximately linear model, and the beam cools about 35°C the 25 minutes of monitored cooling.

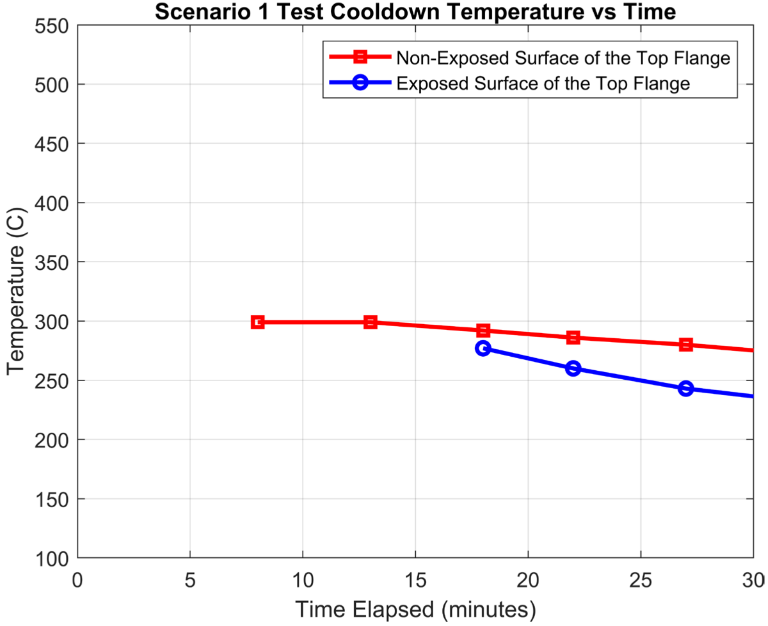

Figure 3-5: Cooldown data for scenario 1

The control beam and the fully fireproofed scenario are of particular importance as they represent the two extremes in fire protection performance. Consequently, a comparison between these two cases is essential. Figure 3-6 presents the temperatures of the non-exposed surface of the top flange for both the control test and the initial fireproofing scenario, highlighting the differences between these extremes. The heating temperature achieved is also presented on this graph. The highest temperature line represents the heating element temperature from the scenario 1 test, the second highest temperature line represents the heating element temperature from the control test, the second lowest temperature line represents the top flange temperature from the control test, and the lowest temperature line represents the top flange temperature from the first fireproofing configuration test.

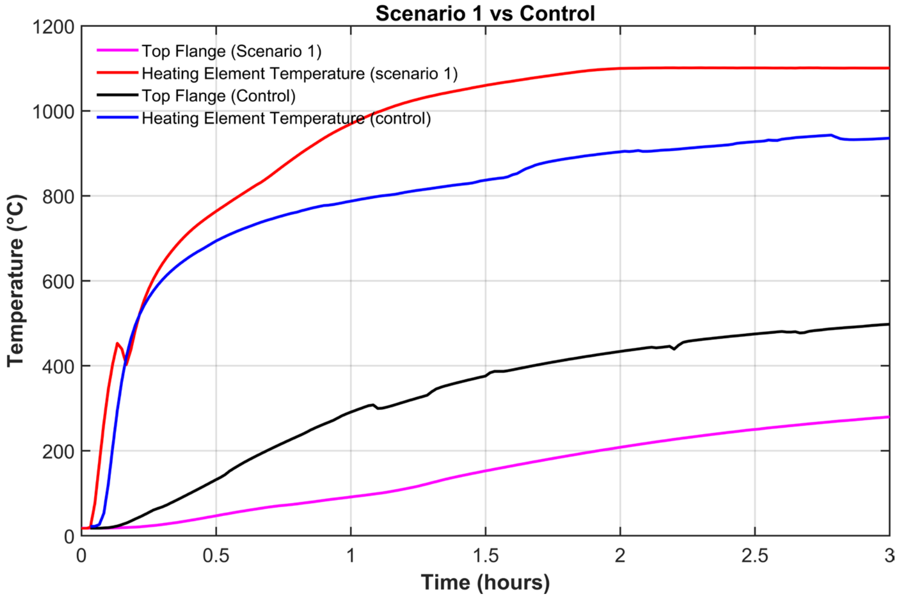

Figure 3-6: Control vs. Scenario 1 top flange temperature vs. time

The fireproofing applied to the beam demonstrated a substantial impact on reducing the temperature, resulting in approximately a 50% reduction across key areas, including the top flange, mid-web, and bottom flange. This significant decrease in temperature highlights the effectiveness of the fireproofing in mitigating thermal exposure during testing, particularly in protecting the critical sections of the beam from excessive heat.

In addition to the thermal effects observed on the heated beams, there were noticeable physical changes, particularly in the fireproofing layer itself. During testing, the fireproofing on the top flange experienced a visible color change, which indicated the material's response to sustained high temperatures. This discoloration, as shown in Figure 3-7, suggests that the fireproofing underwent thermal stress during the fire exposure. Such color changes often serve as early indicators of material fatigue or alteration due to extreme heat, highlighting the impact of fire conditions on the protective layer.

This color shift may point to surface oxidation or thermal degradation, revealing that while the fireproofing successfully insulated the beam from excessive temperatures, it also experienced transformation under fire exposure. These physical alterations are critical to note, as they may affect the long-term performance and resilience of the fireproofing in real-world applications.

Figure 3-7: Fireproofing on the scenario 1 beam before and after testing

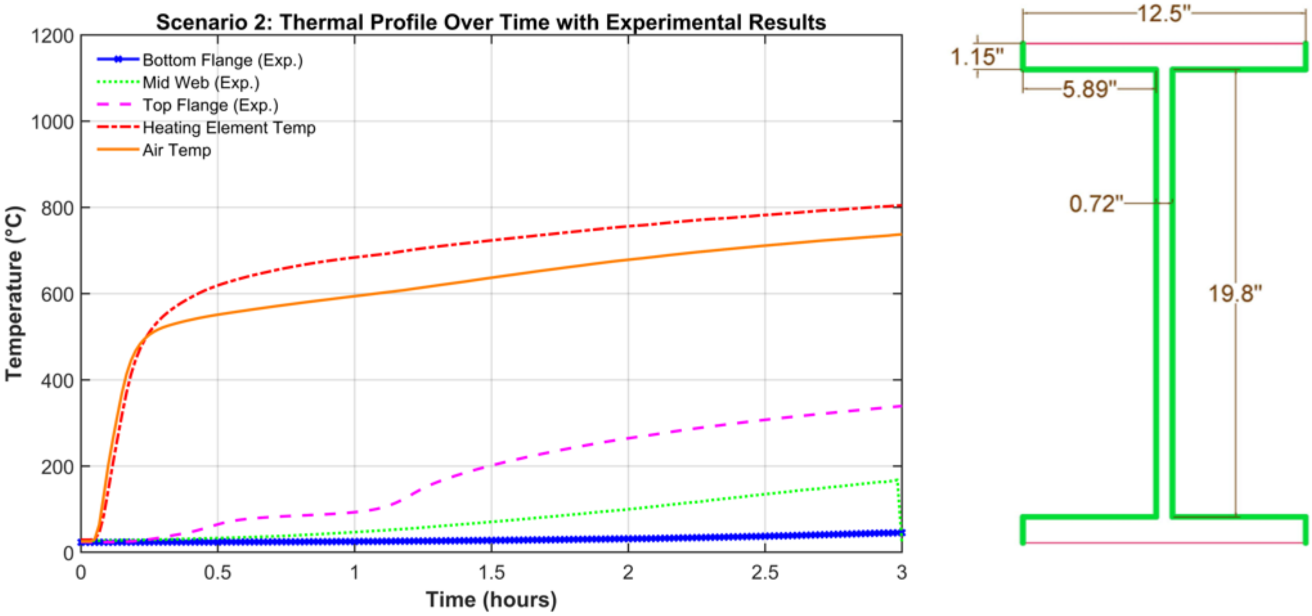

Figure 3-8: Scenario 2 test data.

The highest temperature line in Figure 3-8 represents the heating element temperature, the second highest temperature line represents the airspace temperature, the third highest temperature line represents the top flange (exposed surface) temperature, the fourth highest temperature line represents the middle of the web temperature, and the lowest temperature line represents the bottom flange temperature. The experimental procedure was conducted five days subsequent to the application of the fireproofing treatment, suggesting that the material retained merely 50% of its total strength at the time of evaluation. Figure 3-8 illustrates that the maximum temperature registered for the heating element was 804°C; however, the precision of this measurement is subject to a certain degree of uncertainty. Upon comparing the peak temperature observed within the airspace, measured at 737°C, to that of the control test at 727°C, it appears probable that there was a disconnection between the thermocouple and the heating coils during the current test. The actual peak temperature of the heating element is more likely proximate to the control test's measurement of 935°C. This discrepancy would signify approximately a 21% transfer loss from the heating element to the surrounding airspace, aligning closely with the findings from other tests executed within this study.

The top flange peaked at 339°C, a 32% reduction from the control test. This indicates that the fireproofing on the non-exposed surface helped reduce temperatures throughout the beam by limiting the increase in temperature of the airspace below the top flange.

The midpoint of the web attained a peak temperature of 169°C, while the lowest flange reached a peak temperature of 46°C. In comparison to the control test, which recorded 224°C for the web and 124°C for the bottom flange, the application of fireproofing results in a temperature reduction of 24.6% for the web and 63% for the flange, respectively. Furthermore, this indicates a temperature decrease from the web to the bottom flange of 72.8%, surpassing the control test's 44.4%. The temperature diminution from the top flange to the middle of the web is 50.1%, aligning with the results observed in other tests.

There were notable adherence issues with the fireproofing in this configuration. Although the material initially appeared well-bonded during testing, upon removal from the setup, the fireproofing peeled away from the underside of the top flange, as shown in Figure 3-9. This detachment likely resulted from a combination of factors, including prolonged heat exposure, thermal expansion, and possible flaws in the bonding process. The peeling raises concerns about the fireproofing's ability to provide long-term protection, as any loss of adhesion could expose the steel to higher temperatures, potentially compromising its structural integrity during a fire.

Figure 3-9: Fireproofing chipped off the top flange of the scenario 2 beam

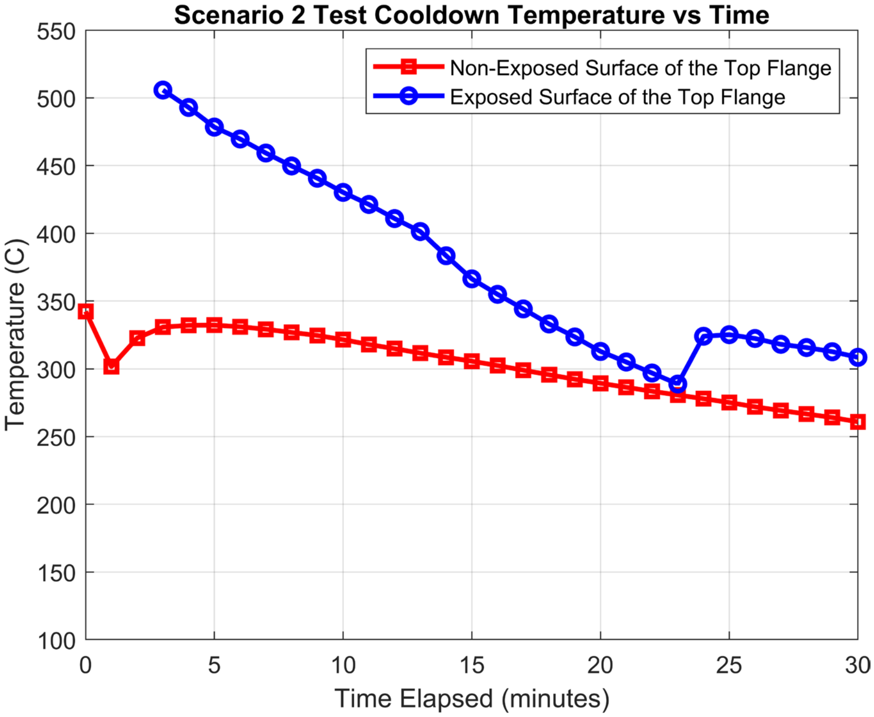

Figure 3-10: Cooldown data for the scenario 2 test

The exposed surface of the top flange started at 506°C and the non-exposed surface started at 342°C. It is important to consider the exposed surface was not fireproofed, while the non-exposed surface was. The exposed surface experienced a linear decrease in temperature for the initial 23 minutes, after which there was an abrupt increase in temperature at the 23-minute mark. This may be attributed to the potential displacement of the thermocouple within the testing apparatus, causing it to come into contact with a surface of higher temperature. The non-exposed surface exhibited an approximately linear cooling pattern over the 30-minute duration. The dip in temperature at the beginning of the cooling process is the result of temporarily shifting the thermocouple while removing the insulation. Similar to the observations in scenario 1, the rate of cooling for the exposed surface surpasses that of the non-exposed surface. This is the result of increased ventilation and a lack of thermal insulation from the fireproofing on the exposed surface. Unlike the first test, the exposed surface begins at a higher temperature than the non-exposed surface.

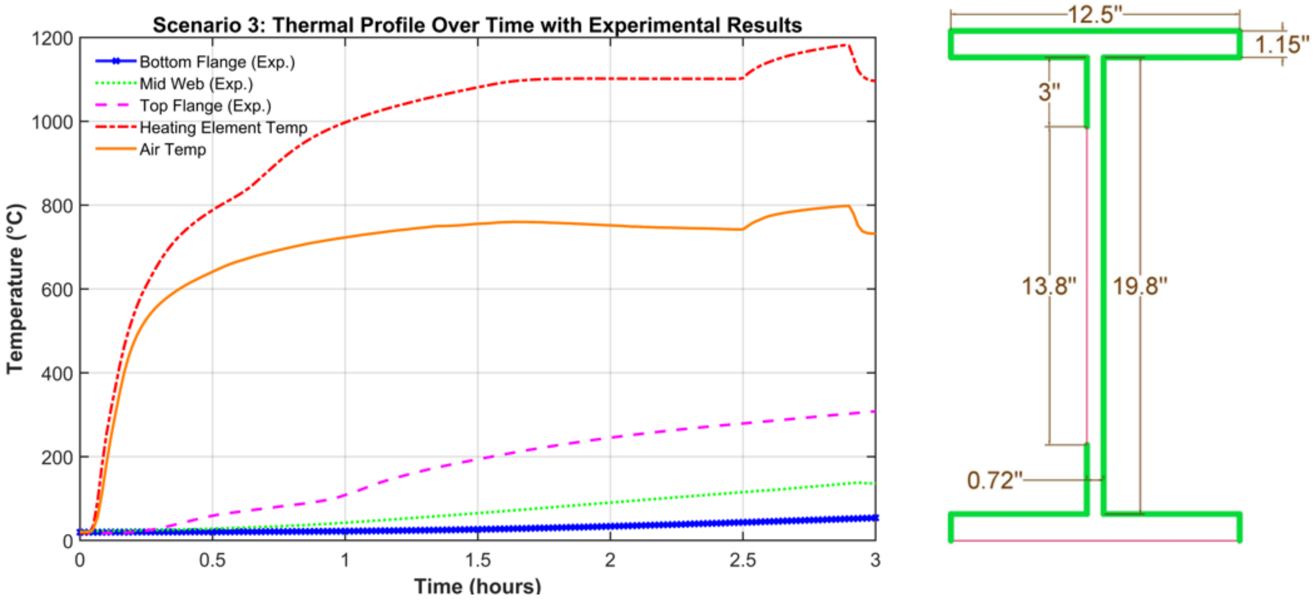

Figure 3-11: Scenario 3 test data

The highest temperature line in Figure 3-11 represents the heating element temperature, the second highest temperature line represents the airspace temperature, the third highest temperature line represents the top flange (exposed surface) temperature, the fourth highest temperature line represents the middle of the web temperature, and the lowest temperature line represents the bottom flange temperature. The temperature of the heating element reached a maximum of 1181°C, representing the highest value recorded among all tests conducted within this study. The airspace temperature attained a peak of 798°C, indicating a 32.4% reduction, which is the most significant loss observed in any test. The peak temperature at the top flange was 310°C, which signifies a 37.9% decrease in comparison to the control test, notwithstanding the peak temperature being 26.3% higher.

The maximum temperatures attained at the midsection of the web and the bottom flange were 137°C and 54°C, respectively. These figures represent reductions of 39.1% and 56.8% from the control test results for the web and bottom flange, respectively. The observed temperature decrease from the web to the bottom flange was 60.6%, which exceeds the reduction noted in the control test (44.4%). Furthermore, the temperature decrease from the top flange to the midsection of the web was 55.8%, a value consistent with those observed in other tests.

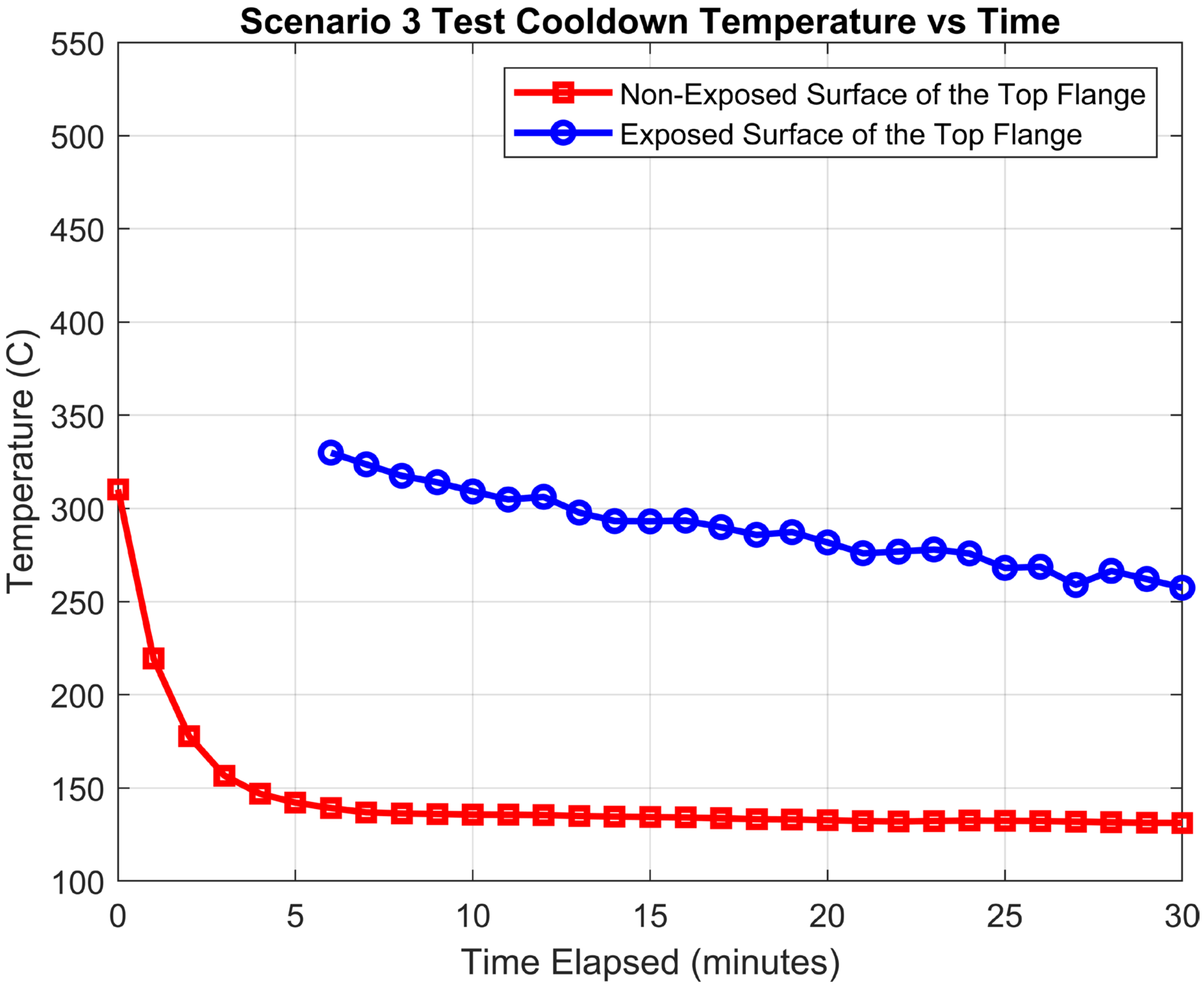

Figure 3-12: Cooldown data for scenario 3

Initial temperatures for the exposed and non-exposed surfaces were measured at 329°C and 310°C, respectively. The cooling process took place in open air with constant ventilation, while the ambient temperature was recorded at 23.3°C (74°F). A marked decrease in temperature was observed on the non-exposed surface immediately following the deactivation of the heaters, which is presumed to be inaccurate. This discrepancy is likely attributable to the repositioning of the thermocouple when the insulation was removed, resulting in this abrupt temperature drop. The validity of this particular measurement is uncertain, as it recorded lower temperatures than any other test conducted in the study. Furthermore, the subsequent portion of the cooling curve exhibited negligible temperature variation, presumably due to heat retention beneath the fireproofing layer. In contrast, the cooling trajectory of the exposed surface adhered to a nearly linear pattern, characterized by a gradual temperature reduction of 84°C over a span of 24 minutes, reflecting the cooling behavior observed in scenario 1.

The third fireproofing configuration also displayed a significant color change on the top flange exposed surface fireproofing during the testing. In addition to the color change, the fireproofing experienced a significant crack running along the length of the beam, right where the galvanized steel decking meets the structural steel. This observation aligns with previous experiments, where the fireproofing exhibited strong adhesion to the structural steel but encountered difficulties in bonding to the galvanized surface. This is illustrated in Figures 3-13. In a vertical application analogous to the orientation of beams in the case study tunnel, the fireproofing would have detached from the flange, leaving the surface exposed.

Figure 3-13: Fireproofing on the scenario 3 beam before (left) and after (right) testing

Figure 3-14: Fireproofing damage on the underside of the top flange for scenario 3.

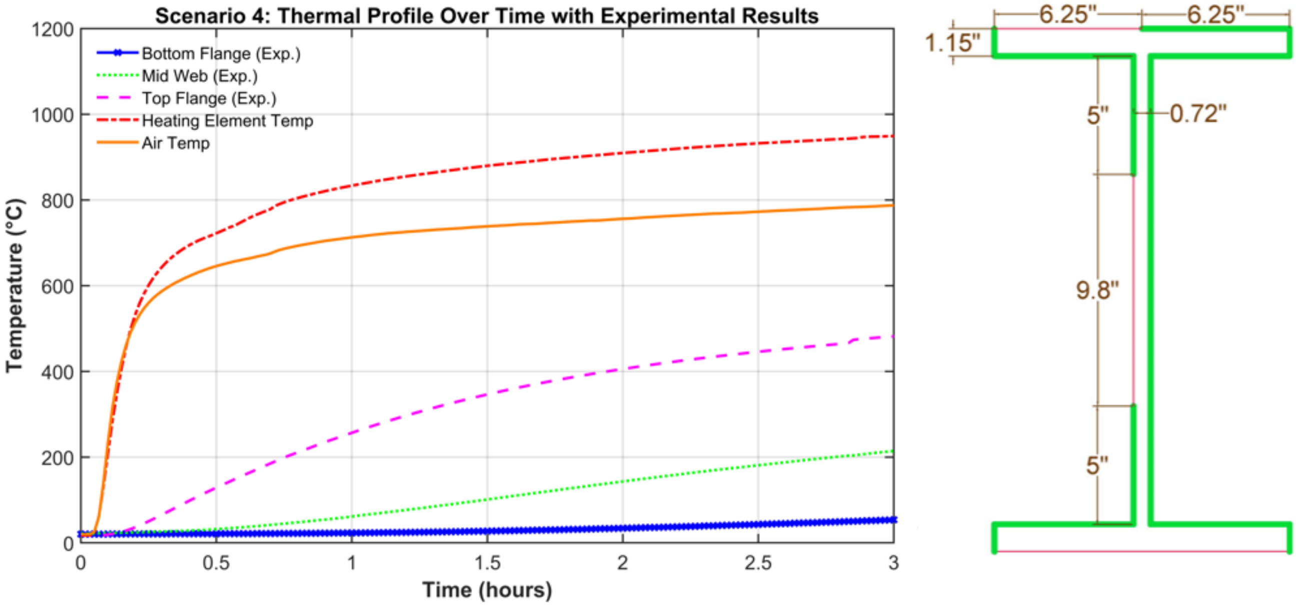

Figure 3-15: Temperature vs. time elapsed for the fourth fireproofing scenario

The highest temperature line in Figure 3-15 represents the heating element temperature, the second highest temperature line represents the airspace temperature, the third highest temperature line represents the top flange (exposed surface) temperature, the fourth highest temperature line represents the middle of the web temperature, and the lowest temperature line represents the bottom flange temperature. Figure 3-15 showed that the maximum temperature of the heating element during the test was recorded at 949°C, which remained below the E119 fire curve. This variance can be attributed to the configuration, wherein half of the top flange consisted of exposed steel. The exposed steel facilitated increased heat dissipation, thereby mitigating the heat radiation that had led to elevated temperatures in the scenario 1 test. The ambient air temperature achieved a peak of 787°C, indicating a 17.1% heat loss from the heating element. The surface of the top flange that was not exposed attained a peak temperature of 481°C, which is in close agreement with the control beam's temperature of 499°C. This minor difference signifies a 3.7% decrease in temperature, with the peak test temperature being merely 1.5% higher than that of the control beam.

In the more distal areas of the beam, the temperature at the midpoint of the web reached a maximum of 214°C, while the bottom flange exhibited a markedly lower peak temperature of 55°C. In comparison to the control test, this signifies a 4.9% reduction in temperature for the middle of the web and an extensive 56% decrease for the bottom flange. Although the middle of the web exhibited temperature trends comparable to the control test, the bottom flange underwent a significant reduction, analogous to the fully fireproofed beam observed in scenario 1. This pronounced temperature decrease from the middle of the web to the bottom flange, calculated at 74.3%, substantially exceeded the 44.4% recorded in the control test. Concurrently, the temperature drop from the top flange (481°C) to the middle of the web (214°C) was 55.6%, a steady trend observed throughout all tests. This suggests that, notwithstanding some variations, the global heat transfer patterns across distinct beam regions followed similar gradients, with the bottom flange displaying the most effective temperature reduction when fireproofing was implemented. These findings emphasize the critical role of fireproofing in curbing heat transmission, particularly in the lower sections of the beam, where notable temperature reductions were documented.

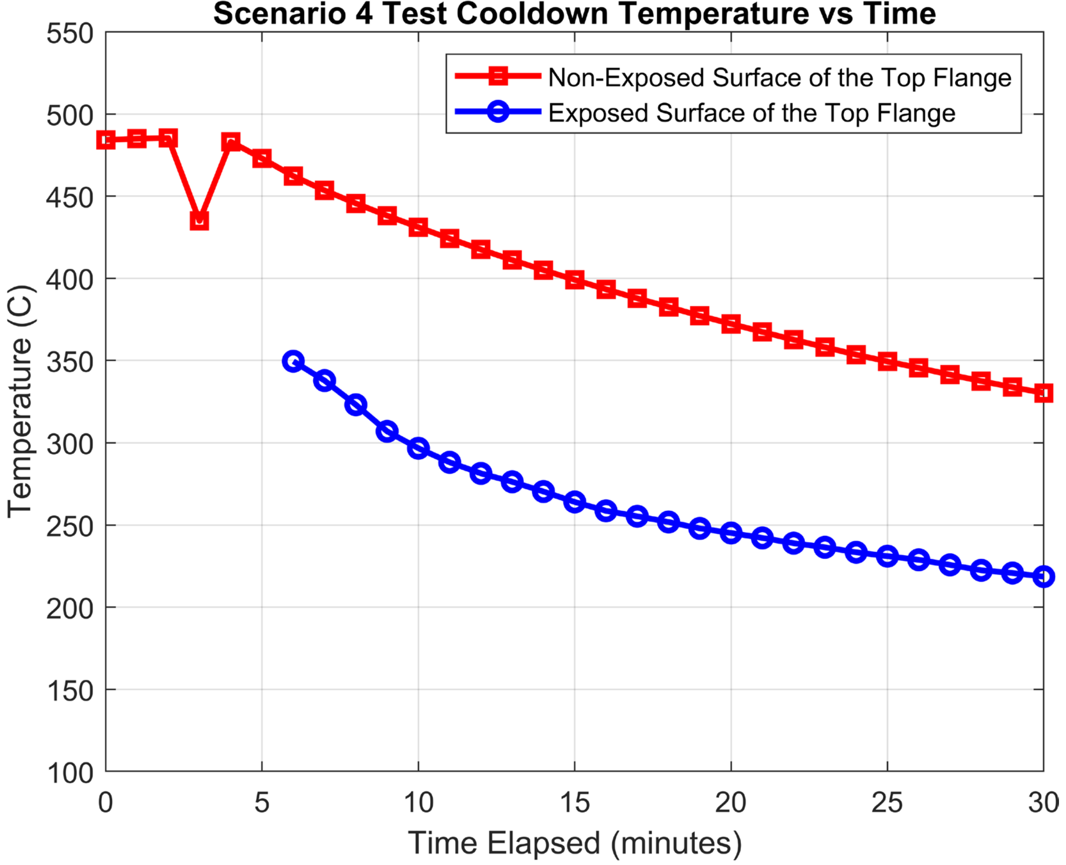

Figure 3-16: Cooldown data for scenario 4

The beam underwent cooling facilitated by consistent ventilation with external air, recorded at 22.2°C (72°F) during the cooldown phase, as shown in Figure 3-16. Similar to what was observed in the first scenario, the non-exposed surface began at a higher temperature than the exposed surface, due to the increased airflow and the higher thermal reflectivity of the fireproofing. The fireproofing material allowed the non-exposed surface to radiate heat more quickly into the surrounding air once the heaters were turned off, highlighting its effectiveness in managing heat dissipation.

Both the exposed and non-exposed surfaces cooled at relatively similar rates, but with a slight difference in their temperature decline. The non-exposed surface, protected by the fireproofing, cooled from 485°C to 330°C over the course of 30 minutes, while the exposed surface, in direct contact with ventilated air, dropped from 350°C to 219°C in just 24 minutes. The faster cooling rate of the exposed surface is indicative of the direct airflow exposure, while the fireproofed surface retained heat slightly longer, showcasing the material's insulating properties. Detailed data and a comprehensive overview of the test results, including the cooldown rates and temperatures at various intervals, are presented in Table 3-1, offering critical insights into the thermal behavior of the beam in this configuration.

Table 3-1: Summary of test data

Fireproofing Configuration	Peak Heater Temperature (°C)	Peak Top Flange Temperature (°C)	Top Flange Temperature Reduction vs. Control Test (%)	Peak Middle Web Temperature (°C)	Middle Web Temperature Reduction vs. Control (%)	Peak Bottom Flange Temperature (°C)	Bottom Flange Temperature Reduction vs. Control (%)
Control Test	935	499	NA	225	NA	125	NA
Scenario 1	1,100	281	43.7	101	55.1	52	58.4
Scenario 2	935*	339	32.1	169	24.9	46	63.2
Scenario 3	1182	308	38.3	137	39.1	54	56.8
Scenario 4	949	482	3.4	214	4.9	54	56.8

3.1.1 Durability Test

The durability test was conducted to evaluate the resiliency of fireproofing following significant heat exposure. This test involved using a screwdriver to attempt to remove fireproofing from the beam forcefully. The fireproofing showed impressive adherence to the structural steel but had trouble sticking to the galvanized decking. Screwdriver impacts easily broke up chunks of fireproofing on the galvanized steel, but only made minor indentations in the structural steel sections. Hammer hits followed the same trend. Larger impacts from a sledgehammer removed chunks of fireproofing from the beam, particularly in the applications against gravity such as on the web and top flange underside.

3.2 Tension Coupon Testing

In this study, tensile tests were conducted on steel coupons extracted from the fully fireproofed beam classified under Scenario 1, following its exposure to a standardized fire event. The pre-fire mechanical properties of the steel, obtained from the steel manufacturer under ambient conditions, documented an initial yield strength of 55 ksi and an ultimate tensile strength of 75 ksi. These baseline values served as a reference point for assessing the post-fire performance of the steel. After the fire exposure, tensile tests on the coupons demonstrated a slight but notable shift in the material's mechanical response. The post-fire yield strength was found to average 59.5 ksi, reflecting an increase over the pre-fire value. This increment in yield strength is indicative of strain hardening, likely resulting from the high-temperature environment, where thermal effects such as recrystallization and residual stress relief may have contributed to enhancing the material’s yield point.

In contrast, the ultimate tensile strength of the steel showed minimal deviation, with a post-fire average of 74.7 ksi, aligning closely with the initial 75 ksi measurement. The stability in ultimate strength suggests that the fireproofing system effectively mitigated the severe thermal degradation typically associated with high-temperature exposure. This result implies that the fireproofing provided a protective thermal barrier, preventing significant metallurgical deterioration that would normally reduce the material’s yield or ultimate strength in unprotected conditions. The combined findings highlight the efficacy of the fireproofing in preserving the steel's structural integrity, particularly by limiting thermal weakening mechanisms, thereby maintaining both its yield and ultimate strength under post-fire conditions.

3.3 Fire Event Simulation

Figure 3-17 illustrates the simulation of fire events by depicting the temperature distribution of a non-fireproofed beam, highlighting the variation of temperature across the web in addition to the top and bottom flanges. Furthermore, Figure 3-18 provides a comprehensive comparison of the thermal profiles of a steel beam without fireproofing, detailing the heat distribution across the bottom flange, mid-web, and top flange over a duration of three hours. Both the FEA and the experimental results exhibit non-linear behavior in temperature escalation, with each section of the beam displaying distinct thermal responses. Specifically, the temperature at the bottom flange escalates rapidly within the first hour, as evidenced by both the FEA (solid blue line on the top) and experimental data (dashed blue line on top), suggesting that heat transfer is most intense during the initial phase. The FEA anticipates a peak temperature of 557°C, surpassing the experimental result of 499°C by approximately 11.6%. This overestimation implies that the FEA model may overstate conductive heat transfer or fail to adequately consider factors such as air gaps or thermal resistance. As the heating process advances, the bottom flange curve begins to stabilize, indicating a non-linear pattern where the rate of temperature increase diminishes, potentially due to a reduction in the heat absorption rate and possibly convective heat losses.

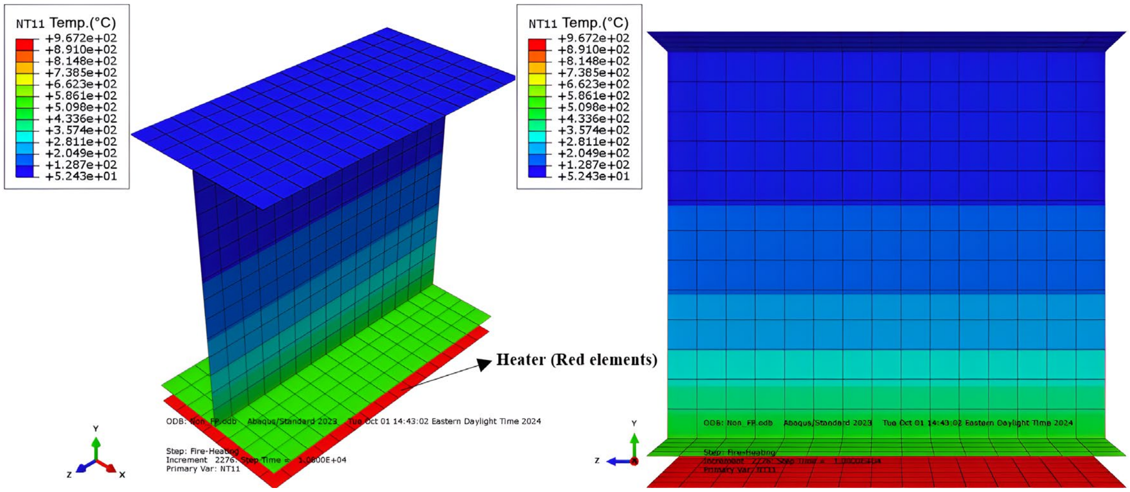

Figure 3-17: Temperature distribution for steel beam without fireproofing

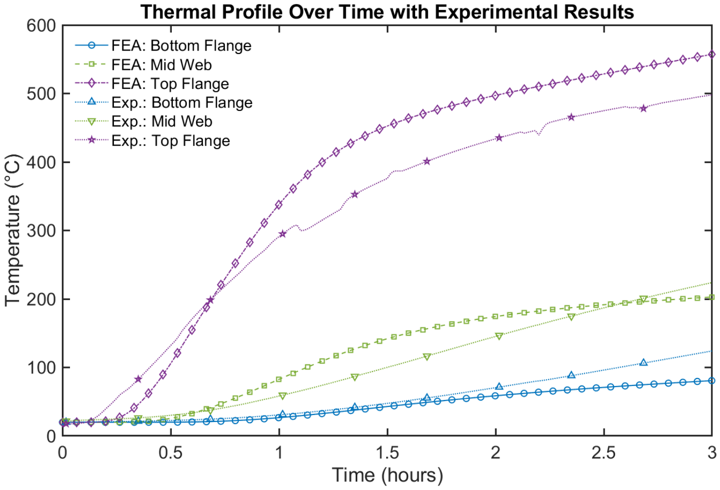

Figure 3-18: Comparison of thermal profiles: FEA predictions and experimental results (no fireproofing)

Figure 3-18 shows the thermal profile for the simulated (solid) and experimental (dashed) tests for the control beam. The bottom two lines (blue) represent the bottom flange or the exposed surface, the middle two lines represent the middle of the web, and the top two lines represent the temperature of the top flange or non-exposed surface. For the mid-web, the temperature increases gradually, showing a less steep curve in both the FEA and experimental data. The experimental data peaks at 225°C, while the FEA predicts a slightly lower peak of 202°C, resulting in a deviation of 10.2%. The relatively consistent rise suggests that heat transfer in the mid-web is slower but steady, following a non-linear trajectory similar to that of the bottom flange, though at a slower rate. In contrast, the top flange demonstrates the slowest temperature increase. The FEA predicts a peak temperature of 81°C, significantly lower than the experimental peak of 125°C. The top flange experiences a slower rate of heat transfer throughout the entire heating period, with both the FEA and experimental data showing relatively shallow curves. This indicates that convective and radiative heat losses play a greater role in this region, which may not have been fully captured by the FEA. Overall, while the FEA models the general thermal behavior of the beam, the discrepancies in temperature rise, particularly in the top flange, highlight the need for more precise calibration of boundary conditions and heat transfer mechanisms, such as radiation and convection, to better reflect real-world conditions.

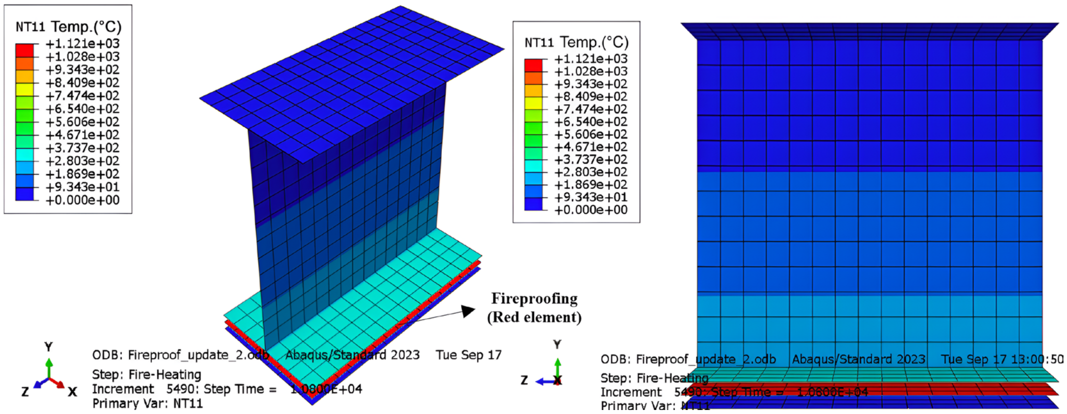

Figure 3-19: Fireproofing scenario 1

Figure 3-19 depicts the temperature distribution within a fireproofed beam for Scenario 1, emphasizing the temperature variations across the web, top flange, and bottom flange. The findings indicate that the bottom flange incurs the most significant temperature increase, which can be directly attributed to its proximity to the principal heat source. This results in efficient conductive heat transfer through the steel, leading the bottom flange to accumulate more thermal energy relative to other sections of the beam. Furthermore, Figure 3-20 provides a detailed comparison between experimental data and FEA predictions, demonstrating a strong correlation between the two. The experimental measurements report a peak temperature of 280.70°C, closely aligned with the FEA prediction of 279.30°C, thereby underscoring the accuracy of the simulation. Despite the effectiveness of the fireproofing in mitigating heat transfer, the FEA illustrates that the bottom flange, owing to its direct or near-direct exposure to the heat source, still experiences substantial conductive heat transfer. This is a critical observation, as it signifies that while fireproofing alleviates heat transfer, it cannot entirely eliminate the thermal load on the steel in areas with direct contact with the heat source.

Furthermore, the fireproofing material, designed to serve as an insulating barrier, reveals its limitations when subjected to prolonged exposure to elevated temperatures. The FEA model precisely captures these dynamics, illustrating the gradual penetration of heat through the fireproofed layer and its conduction through the steel, especially in regions experiencing continuous thermal stress.

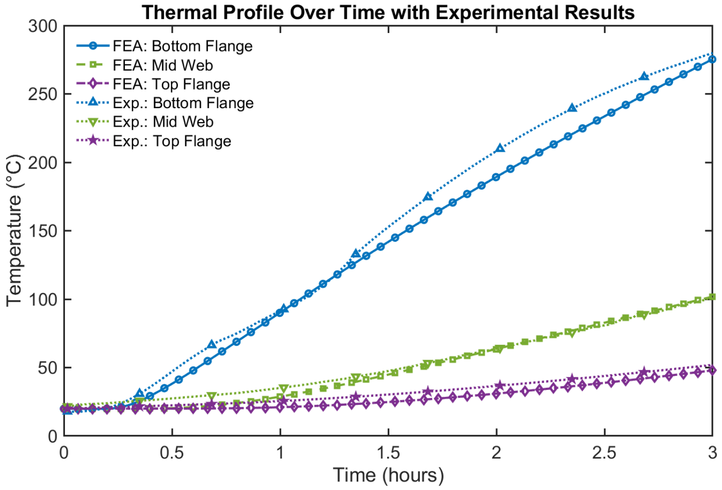

Figure 3-20: Comparison of thermal profiles: Scenario 1

Figure 3-20 shows the thermal profile for the simulated (solid) and experimental (dashed) tests for the first fireproofing scenario. The top two lines (blue) represent the bottom flange or the exposed surface, the middle two lines represent the middle of the web, and the bottom two lines represent the temperature of the top flange or non-exposed surface. In contrast, the mid-web and top flange experience significantly lower temperatures due to their distance from the heat source and the insulating effect of the fireproofing material. The mid-web reaches 101.40°C experimentally and 103.70°C in the FEA, suggesting that heat conduction through the steel is less effective in this region, where the fireproofing insulates more effectively. The reduced thermal conductivity of the fireproofing material traps heat, limiting how much can be transferred to the steel core. The top flange, with the least thermal load, shows even lower temperatures (52.3°C experimentally and 48.90°C in the FEA), which can be attributed to the combined effects of heat loss through convection and radiation from the surface, as well as the fireproofing's ability to reflect or absorb heat. However, the slight underprediction in the FEA suggests that the model may not fully capture the complex interactions of radiative heat loss and convective cooling, which are more significant at the exposed surfaces like the top flange. These differences in thermal behavior across the beam highlight the role of fireproofing in delaying heat transfer, but also point to the complexities of accurately modeling the combination of conductive, convective, and radiative heat transfer in structural components under fire exposure.

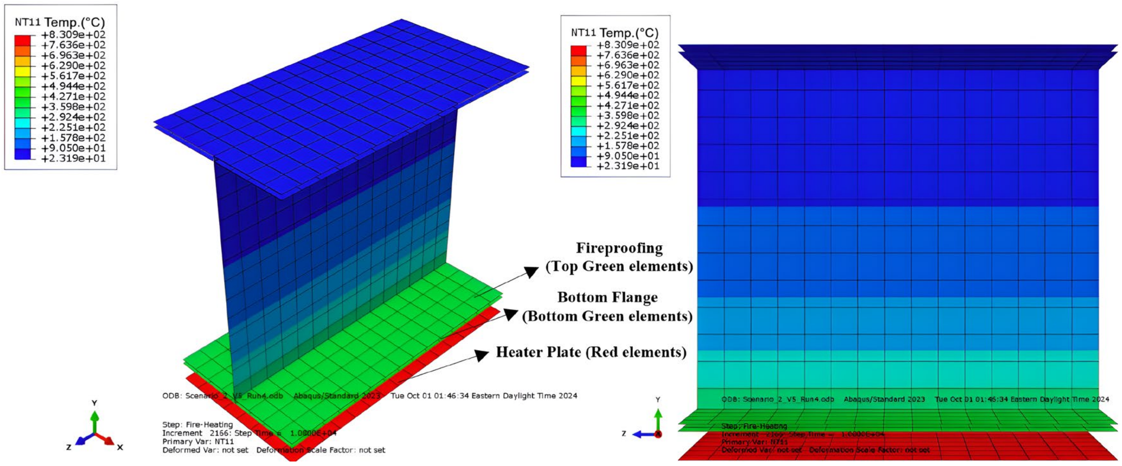

Figure 3-21: Fireproofing Scenario 2

Figure 3-21 presents the temperature distribution for fireproofing scenario 2 across the web, as well as the top and bottom flanges. Furthermore, Figure 3-22 (Approach 1) indicates that the bottom flange attains a temperature of 373°C in the FEA results, in contrast to 339.34°C observed in the experimental data. This suggests that the FEA overpredicts the temperature increase, particularly during the initial hour, when the heating rate is substantially higher. The mid-web exhibits a temperature of 146°C in the FEA, as opposed to 168°C experimentally, further suggesting that the FEA underestimates heat transfer in the web region. Conversely, the top flange demonstrates a close correlation, with temperatures of 44.54°C in the FEA and 45.60°C in the experimental findings, indicating that the FEA more accurately reflects heat transfer to the top flange.

In Figure 3-23 (Approach 2), a similar trend is observed, with the bottom flange showing a temperature difference between the FEA (approximately 373°C) and experimental data (339.34°C). The mid-web experiences slightly less temperature in the FEA model (147°C) compared to 168°C in the experiment, while the top flange again remains closely aligned with both FEA and experimental results. The primary difference between the two approaches is the consideration of different surface film coefficients, such as using values 7.5 or 10 W/m²·K, affecting how heat is transferred, especially in the bottom flange. This change impacts the initial heating rates and overall temperature distributions, as seen in the figures.

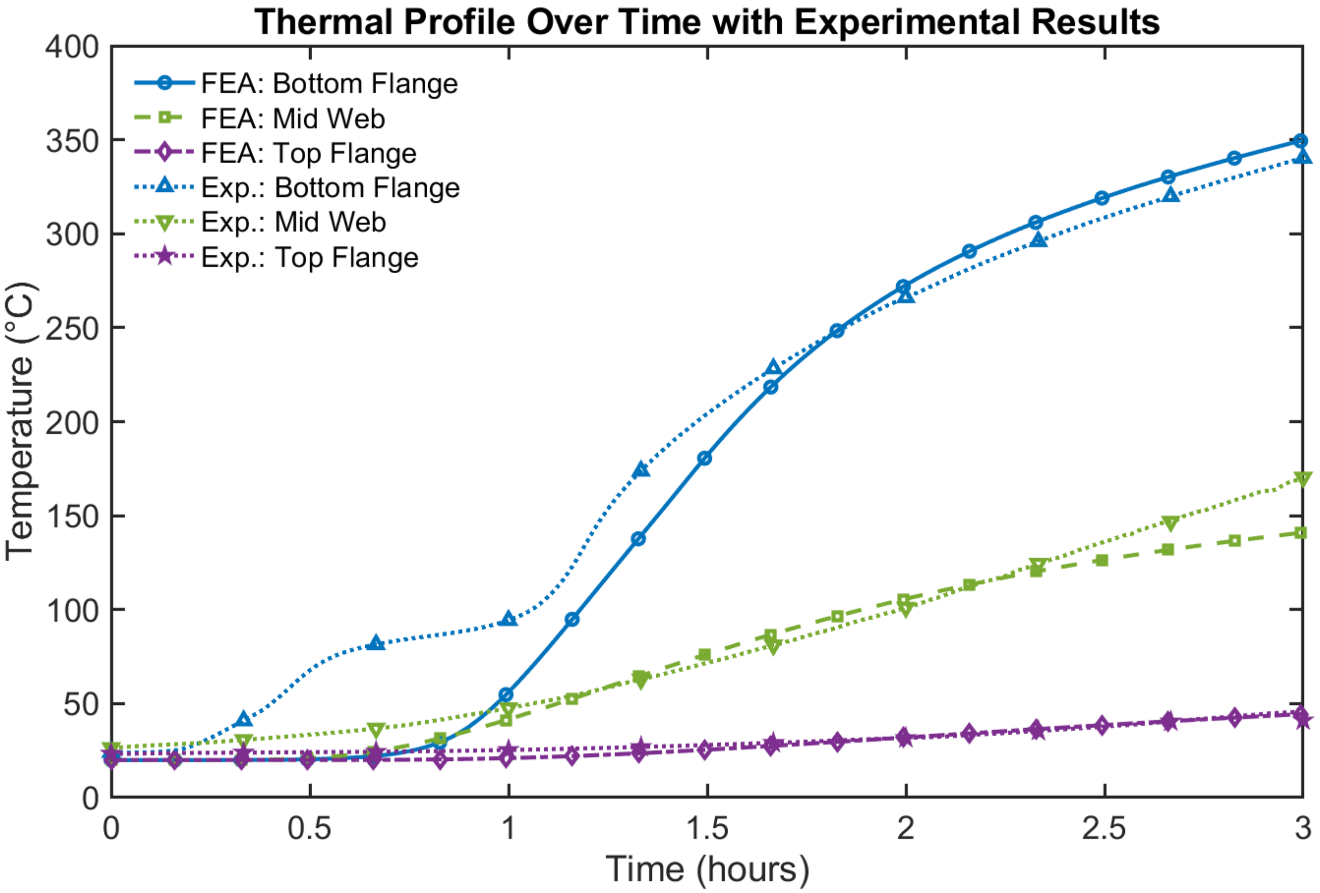

Figure 3-22: Comparison of thermal profiles: Scenario 2, Approach 1

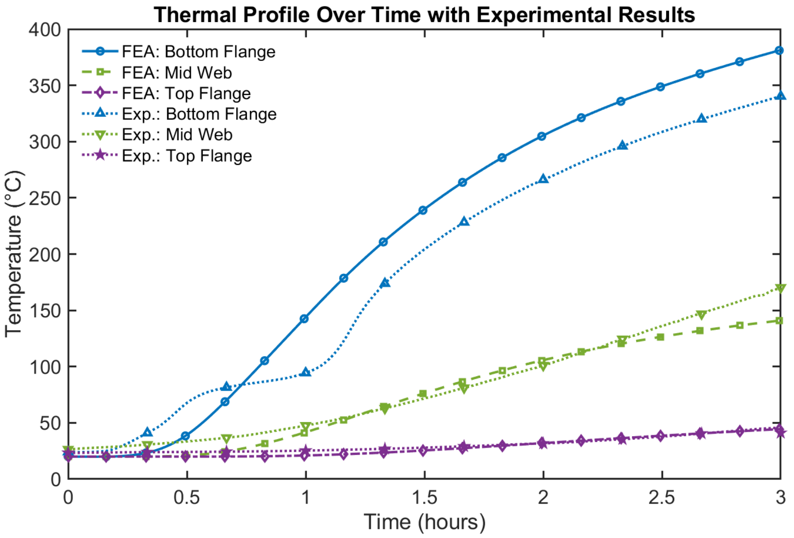

Figure 3-23: Comparison of thermal profiles: Scenario 2, Approach 2

Figures 3-22 and 3-23 show the thermal profile for the simulated (solid) and experimental (dashed) tests for the second fireproofing configuration under the two different approaches. The top two lines (blue) represent the bottom flange or the exposed surface, the middle two lines represent the middle of the web, and the bottom two lines represent the temperature of the top flange or non-exposed surface. The key difference between the two figures lies in the FEA curve for the bottom flange. The discrepancy is likely due to variations in the surface film coefficient used in the simulations. In the figure with a higher bottom flange FEA curve, the surface film coefficient might be set lower, resulting in reduced convective heat loss and a more rapid increase in temperature. A lower coefficient slows heat dissipation, leading to higher internal temperatures. In contrast, the figure with a closer alignment between FEA and experimental results might have employed a higher surface film coefficient, which promotes more efficient heat dissipation, thereby producing a temperature profile that more closely matches the experimental data. This emphasizes the importance of adjusting the surface film coefficient to ensure accurate heat transfer predictions, particularly in fire-heating simulations.

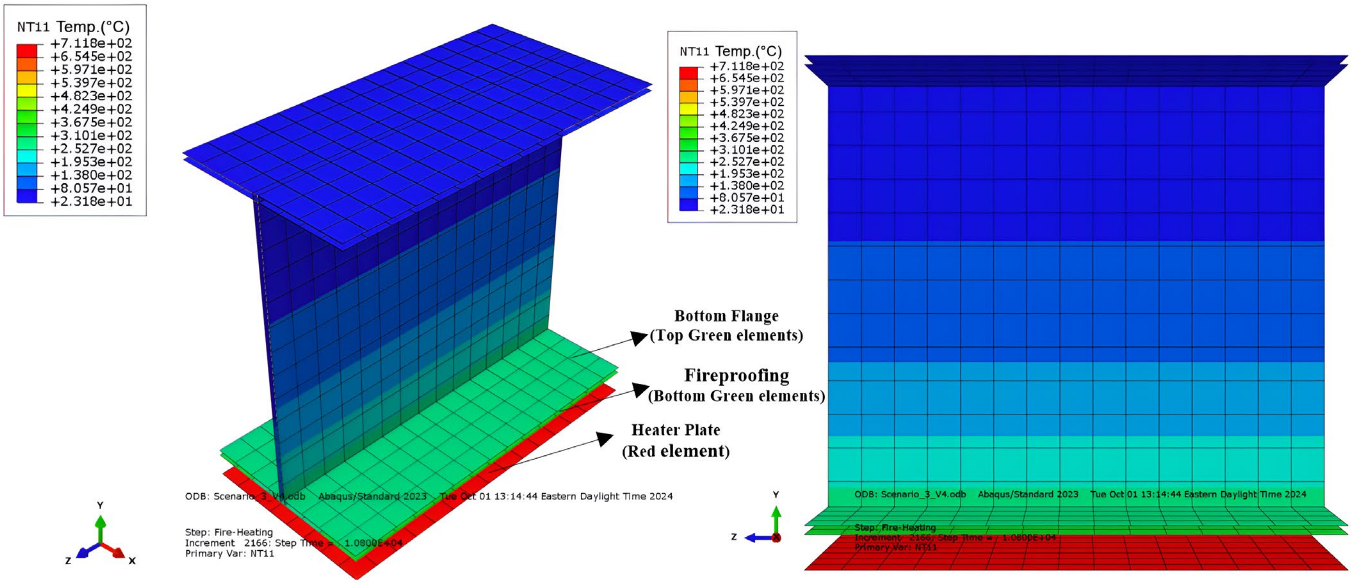

Figure 3-24: Temperature distribution: Fireproofing Scenario 3

Figure 3-24 presents the temperature distribution for fireproofing scenario 3 across the web, as well as the top and bottom flanges. Furthermore, Figure 3-25 compares the thermal profiles of the bottom flange, mid-web, and top flange over a 3-hour period, showing FEA results alongside experimental data. In the bottom flange, both FEA and experimental curves exhibit a rapid temperature rise in the first hour, with the FEA predicting 310°C and the experimental data showing 308°C. This rapid increase reflects the bottom flange's proximity to the heat source, allowing efficient conductive heat transfer. After the initial steep rise, the curve flattens, indicating a reduction in heating rate as heat redistributes across the beam and heat losses through convection and radiation become more pronounced.

The mid-web follows a slower, more gradual temperature rise. The FEA predicts 129°C, while the experiment records 136.7°C, indicating slightly less heat conduction in the FEA model. The mid-web's distance from the heat source results in a delayed heat transfer, and the profile remains nonlinear, reflecting steady heat absorption and redistribution over time. While the temperature increase is significant, it occurs at a slower rate compared to the bottom flange. For the top flange, the temperature rise is minimal, with the FEA showing 45°C and the experiment 54°C. The nearly linear behavior in this region suggests limited heat transfer due to its distance from the heat source, with heat losses like radiation and convection dominating. The overall trend in the FEA closely follows the experimental data, but the FEA slightly underestimates heat transfer to both the mid-web and top flange.

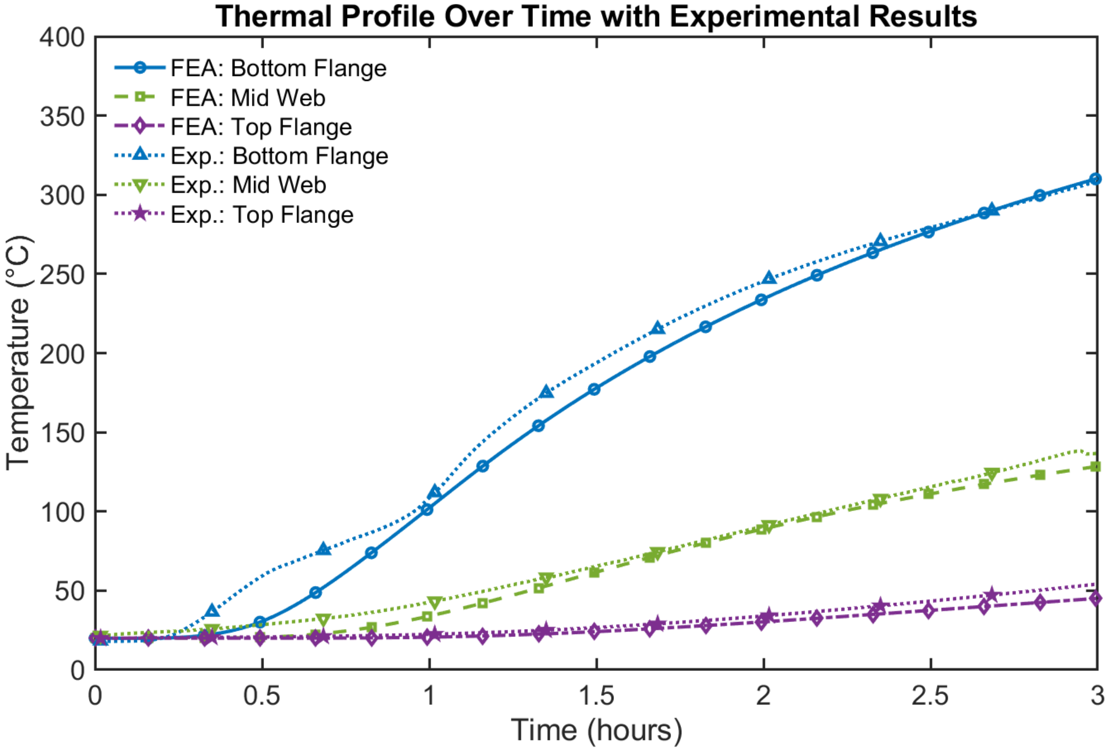

Figure 3-25: Comparison of thermal profiles: Scenario 3

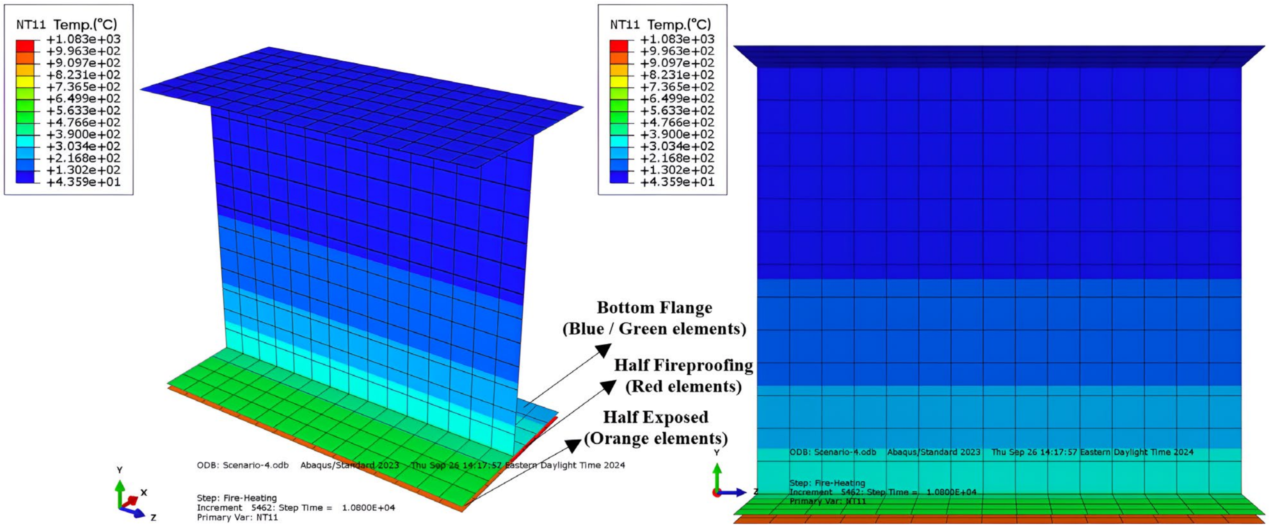

Figure 3-26: Temperature distribution: Fireproofing Scenario 4

Figure 3-25 shows the thermal profile for the simulated (solid) and experimental (dashed) tests for the third fireproofing configuration. The top two lines (blue) represent the bottom flange or the exposed surface, the middle two lines represent the middle of the web, and the bottom two lines represent the temperature of the top flange or non-exposed surface. Figure 3-26 presents the temperature distribution for fireproofing scenario 4, spanning the web in addition to the top and bottom flanges. Additionally, Figure 3-27 demonstrates the thermal profiles of a steel beam within Scenario 4 over a duration of 3 hours, juxtaposing FEA predictions with experimental results for the bottom flange, mid-web, and top flange. Both sets of data exhibit non-linear temperature rise behavior, with the FEA results represented by solid lines and the experimental data by dashed lines. In the bottom flange, the temperature rises rapidly during the first hour, peaking at around 450°C in the FEA and 475°C in the experimental results. This initial sharp increase is due to the bottom flange's proximity to the heat source, allowing for rapid conductive heat transfer. However, the temperature rise slows after the first hour, with the curve flattening, indicating a reduction in the heating rate as heat is redistributed within the beam and convective and radiative heat losses become more significant.

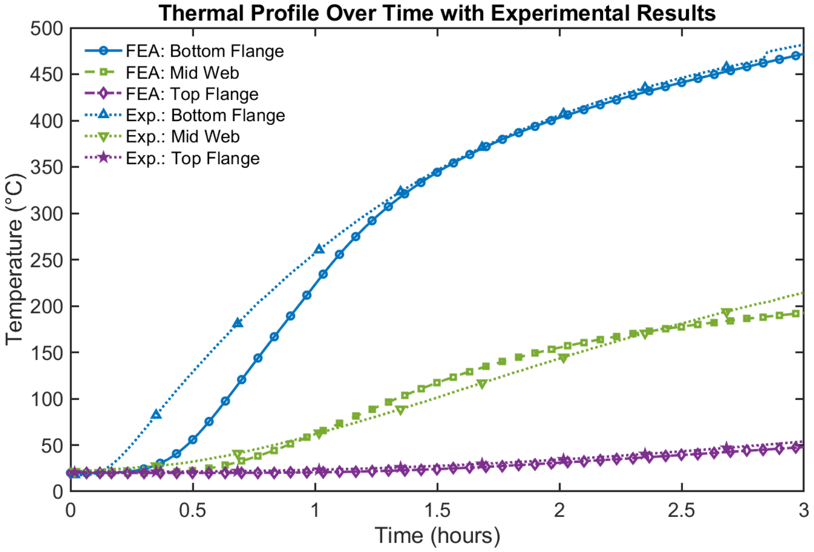

Figure 3-27: Comparison of thermal profiles: Scenario 4

Figure 3-27 shows the thermal profile for the simulated (solid) and experimental (dashed) tests for the fourth fireproofing scenario. The top two lines (blue) represent the bottom flange or the exposed surface, the middle two lines represent the middle of the web, and the bottom two lines represent the temperature of the top flange or non-exposed surface. The mid-web experiences a more gradual temperature increase, with the FEA predicting a peak of around 150°C, and the experimental data showing a slightly higher peak of approximately 175°C. The slower temperature rise is a result of the mid-web's greater distance from the heat source, leading to less direct heat transfer. The curve here remains non-linear, though less pronounced, as the heat absorption continues steadily over the 3-hour period. The top flange shows the slowest temperature increase, with both FEA and experimental curves closely aligned. The FEA predicts a peak of about 50°C, slightly lower than the experimental results. The near-linear behavior in the top flange suggests limited heat transfer due to its distance from the heat source, where heat loss mechanisms such as radiation and convection dominate, preventing significant temperature buildup.

Figure 3-27 shows that while the FEA captures the general thermal behavior of the steel beam, it slightly underestimates the heat transfer to the mid-web and bottom flange compared to experimental data. However, the trends are well aligned, indicating that the FEA model reasonably predicts the overall heat distribution, especially in regions like the top flange where heat transfer is minimal. The non-linear nature of the temperature rise, particularly in the bottom flange and mid-web, reflects the complex interplay between conductive heat transfer, heat redistribution, and heat losses that affect the thermal performance of the beam in Scenario 4.

This page left blank intentionally.

4.0 Conclusions

This chapter presents conclusive reflections on the efficacy of the fireproofing and the congruence of computational methodologies with experimental laboratory outcomes.

4.1 Fireproofing Effectiveness

The application of cementitious fireproofing has demonstrated efficacy in mitigating the peak temperatures encountered by a beam during a substantial fire event. This efficiency is contingent upon the provision of adequate coverage. When compared to an unprotected beam, comprehensive fireproofing resulted in a temperature reduction of 43.7%, 55.1%, and 58.4% for the top flange, the middle of the web, and the bottom flange, respectively, under a more stringent heating scenario. This was observed even though the fireproofing was operating at less than 50% efficacy during the testing phase. In the context of scenario 1, the top flange of the beam attained a peak temperature of 281°C, while the middle of the web and the bottom flange did not exceed temperatures of 101°C and 52°C, respectively. Research indicates that beam temperatures reaching 300°C can diminish the strength of steel by approximately 20%, whereas temperatures below 150°C exert minimal influence on the yield strength of structural steel [1]. Moreover, the residual strength of structural steel subjected to temperatures as high as 500°C exhibits no irreversible alterations in either behavior or strength [17, 18]. These findings suggest that, irrespective of professional application, the fireproofing material can substantially mitigate the reduction in structural integrity during tunnel fire scenarios. Furthermore, the fireproofing exhibited a strong bond to the structural steel post-exposure to elevated temperatures, effectively preserving its bond even under minor mechanical impacts.

Nevertheless, beams installed in situ are vulnerable to substantial damage from vehicular collisions, which may lead to the detachment of fireproofing material from the exposed flange and other sections of the beam. Variability was observed in the results of fireproofing configurations designed to emulate this partial protection. In scenario 2, wherein the beam was entirely fireproofed excluding the exposed flange, there was a recorded decrease in temperatures by 32.1%, 24.9%, and 63.2% for the top flange, the middle of the web, and the bottom flange respectively, under testing conditions that closely resembled those of the control beam. These results indicate that the absence of fireproofing on the exposed flange results in an increase in beam temperature compared to a fully fireproofed flange, but the peak temperature of 339°C does not present a significant risk to the structural safety of the tunnel. Research indicates that temperatures in this range would result in a 20–25% reduction in yield strength and a 15–20% reduction in stiffness for the top flange of the beam [1]. The middle web and bottom flange temperatures of 169°C and 46°C present minimal reduction in strength and stiffness [1]. For a tunnel designed with the level of conservatism as the one in question, the findings suggest minimal risk to structural integrity. Permanent alterations in strength and stiffness are expected to be negligible.

It is imperative to acknowledge that the evaluation of structural components must be conducted on an individual basis, given that aspects such as material properties, design tolerances, and specific loading conditions could potentially affect the overall reaction to elevated temperatures.

A further investigation into a partially protected configuration was conducted utilizing Scenario 3 within the series of tests. In this third scenario, the fireproofing application was uniformly applied except for a substantial unprotected section in the web on one side of the beam. Notwithstanding the exposure to the highest recorded temperatures among all tests, this particular beam demonstrated temperature reductions of 38.3%, 39.1%, and 56.8% in the exposed flange, middle of the web, and bottom flange, respectively, compared to the control test. This was achieved even with a peak temperature that was 26.4% higher. The attained peak temperatures—308°C for the top flange, 137°C for the middle of the web, and 54°C for the bottom flange—do not present any significant hazard to the structural integrity of the system.

The final partially protected configuration was scenario 4, which had half of the exposed flange and most of the middle of the web of the same side unprotected. In testing, this beam experienced temperatures that were only 1% higher than the control test, yet the top flange temperature was only reduced by 3.4% in comparison to a completely unprotected beam (482°C vs. 499°C). The middle of the web showed similarly poor results, peaking at 214°C, a 4.9% reduction in temperature compared to the control test. Research indicates temperatures around 500°C experience a 40–45% reduction in yield strength and 35–40% reduction in stiffness [1]. This could be a problem, particularly for flexural members, where the extreme fiber (the bottom of the exposed flange in-situ) experiences the highest bending stress across the cross section.

From the results of scenario 4, we can conclude that having gaps in fireproofing along the same face of a member may result in a path for conductive heat transfer throughout a beam. This may not have led to any permanent strength reductions in our laboratory testing, but a fire event induced by alternative fuels exceeding the ASTM E119 curve could create unsafe conditions in a tunnel.

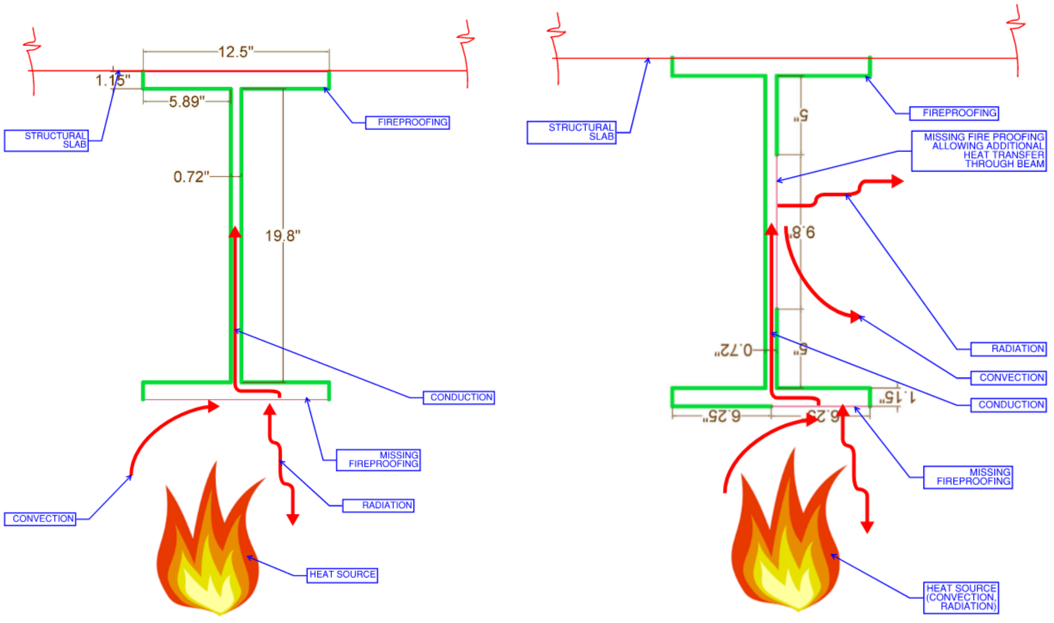

Figure 4-1: Primary heat transfer mechanisms: (left) Scenario 2, (right) Scenario 4

Figure 4-1 illustrates the primary heat transfer mechanisms observed during fire testing for Scenarios 2 (left) and 4 (right), respectively. These figures illustrate the pathways for radiation, conduction, and convection within the beam and the adjacent fireproofing layers.

In Figure 4-1 (left), the heat transfer mechanisms for Scenario 2 are shown, where the beam is partially fireproofed, leaving the top flange exposed. This configuration demonstrates how the exposed top flange experiences radiative heating, with conduction transferring heat through the beam and convection occurring in the surrounding air. Despite the lack of fireproofing on the top flange, the middle of the web and the bottom flange are partially protected, reducing their temperatures.

Conversely, Figure 4-1 (right) illustrates the more severe circumstances presented in Scenario 4, in which the fireproofing is absent from both the bottom flange (partially) and the web. This lack of fireproofing establishes a critical thermal pathway, markedly enhancing heat transfer via conduction and convection, which results in elevated temperatures throughout the beam. This situation exemplifies the compounded risk linked to the absence of fireproofing in multiple areas of the beam and emphasizes the necessity for thorough fireproofing coverage to ensure structural safety in the event of a fire.

Based on the results presented in Table 3-1, it is evident that:

- Beams missing fireproofing at the bottom flange only still exhibit moderate protection against fire events when comparing scenarios 1 and 2.

- Beams missing fireproofing at the bottom flange and web greatly compromise the function of the fireproofing when comparing scenarios 1 and 4.

Table 4-1 summarizes these results, ranking the criticality of fireproofing damage cases, highlights these key findings to assist in making fireproofing recommendations to MassDOT:

Table 4-1: Fireproofing configurations and their relative fire protection ratings.

Fireproofing configuration	**Bottom flange Fireproofing**	**Web Fireproofing**	**Relative fire protection**
Scenario 1	✓	✓	High
Scenario 2	X	✓	Moderate
Scenario 3	✓	X	Moderate
Scenario 4	X	X	Low

The primary mechanisms of heat transfer are contingent upon the segment of the beam in question. The top flange, being in direct exposure to the heat source, undergoes heating predominantly via radiation. Furthermore, thermal conduction occurs at the interface between the metal grate and the top flange; however, this is likely marginal in comparison to radiative transfer owing to the limited surface area of the beam enveloped by the decking. In addition, convection might transpire within the air gap between the beam and the heaters; nevertheless, the constrained space available for air circulation consequently mitigates the extent of heat transfer.

The heat is applied to the top flange of the beam using a heater in the laboratory setting, while the middle of the web and the bottom flange are thermally insulated and not directly exposed to the heat source. This significantly reduces the radiative heat transfer. These parts of the beam are primarily heated by conduction from the top flange and upper half of the web, which are at a higher temperature as demonstrated by the testing. The rate of conductive heat transfer is dependent on the temperature of the surfaces in contact, the surface area of contact, and the thermal conductivity of the sources in contact. The application of fireproofing on the beam serves to lower its temperature by establishing a thermal barrier between the source of heat and the beam, albeit without altering the inherent thermal characteristics of the steel material. As a result, the fireproofing reduces conduction throughout the beam by reducing the temperature of the surface in contact. The other form of heat transfer present in the middle of the web and bottom flange is convection. The large air space underneath the top flange contained in the firebricks allows for the movement of fluid that is necessary for convective heat transfer. Convective heat transfer is dependent on the fluid and surface temperature, surface area, and speed of flow across the surface. Analogous to conductive heat transfer, the application of fireproofing leads to a reduction in the temperature of the top flange, thereby diminishing the surface temperature and consequently lowering the air temperature of the bottom flange and the surrounding airspace. This explains the reduction in temperature of the bottom flange. Even when fireproofing was only partially protective or completely absent from the top flange, the temperature of the bottom flange still showed significant reduction in comparison to the control test. This indicates that the fireproofing was able to reduce temperatures induced by convective heat transfer in the bottom flange.

Specifically comparing the Scenario 4 beam to the control test, the temperatures of the top flange and the middle of the web were extremely close to the control test (3.4% and 4.9% reduction in temperature for the top flange and middle of the web from the fireproofing respectively). Despite this, the temperature of the bottom flange, which was fully covered by fireproofing, was 56.8% lower than the control test. This confirms that convective heat transfer makes up a significant portion of heat transfer to the middle of the web and bottom flange.

The heat transfer mechanisms observed in scenario 2 are of particular interest. Scenario 2 has full protection with the exception of the exposed surface of the top flange. As a result, scenario 2 allows for an examination of the conductive heat transfer throughout the beam because the top flange allows full radiative heat transfer with the heaters, but the rest of the beam is protected from convective heat transfer. As expected, the non-exposed surface for scenario 2 experiences increased temperatures in comparison to the fully fireproofed scenario (339°C vs. 289°C for scenario 2 and 1, respectively). Although it was shielded from direct exposure to the heating source, the middle of the web experiences a 67.3% increase in temperature in comparison to the fully fireproofed configuration (scenario 1). This indicates that conduction from the higher top flange temperatures is significant in the case study tunnel. In addition, the increased web temperature is likely also the result of convection from the increased air temperatures within the heating space below the top flange. Notably, this configuration exhibited the lowest recorded temperature for the bottom flange at 46°C among all tests, with a slight difference of 6°C below the next lowest temperature. This is likely the result of increased fireproofing thickness on the bottom flange in comparison to other tests or a bad temperature reading. Despite the potential error, the consistency of the bottom flange temperatures over different fireproofing configurations suggests that conductive heat transfer to the bottom flange is minimal, and that the main method of heat transfer in the lower half of the beam is convection. This convective heat transfer is limited by the fireproofing, which covered the bottom flange in all scenarios with the exception of the control test.

It is imperative to further examine Scenario 3. Scenario 3 protects the entire beam with the exception of the middle of the web. This configuration experienced the highest temperatures of any test and produced a top flange temperature that was 10% higher than the fully protected configuration. This resulted in a middle of the web temperature that was 35.6% higher than the fully protected scenario, and a bottom flange temperature 3.8% higher than scenario 1. The combined effects of increased convective heat transfer to the web and increased conduction due to the higher top flange temperature resulted in a considerable increase in web temperature, but almost no increase in bottom flange temperature. This confirms the examination of the second and fourth scenarios, which came to the same conclusion that the bottom flange is primarily heated by convection. The slight increase in bottom flange temperature is likely the result of higher air temperature, which occurs as a result of the radiative heat transfer from the exposed middle of the web.

In addition to the thermal transfer within the steel beams, it is essential to consider the heat transfer to the supported concrete slab. The extent of this heat transfer is influenced by the connection between the steel and concrete. Typically, steel girders employ shear studs welded to the top flange before the concrete is poured, subsequently embedding the studs within the concrete slab. These studs establish a thermal pathway for heat to conduct into the concrete slab. As the temperature of the bottom flange (or top flange in situ) elevates during a fire event, the thermal differential between the shear studs and the top flange will instigate heat transfer that elevates the temperature of the shear studs. Given that the shear studs are embedded within the concrete slab, the slab will also be subjected to heat transfer via the same process. Despite the potential risk associated with increased slab temperatures, the temperatures of the bottom flange observed during experimental testing (typically ranging from 40 to 55 degrees Celsius) are unlikely to inflict significant damage upon the concrete.

4.2 Fireproofing Practicality

Despite the general effectiveness of the fireproofing in reducing temperatures, its applicability remains an issue. The trowel application presents challenges as discussed previously. Minor imperfections in the protective coating of the steel beams are not an issue, but there is concern that vertical applications against gravity, as would be necessary in a tunnel, would be difficult and result in fireproofing that is too thin. Although the trowel grade fireproofing is convenient and quick to apply and set, even when using the low end of the water content during mixing, the weight of the material made it unable to stick to upside down surfaces. For this reason, spray application is recommended for repairs in the tunnel.

4.3 Fireproofing Durability

The hammer, screwdriver, and sledgehammer tests revealed mixed outcomes regarding the performance of the fireproofing. While the bond between the fireproofing material and the structural steel was robust, the adhesion to the galvanized steel decking proved to be notably weaker. This poses a potential risk in real-world applications, where the beams are connected by 1.5-inch galvanized steel decking coated with fireproofing. Light cleaning that does not compromise the galvanizing layer would benefit the bond between the fireproofing and the beam.

4.4 Fireproofing Effectiveness in Preventing Permanent Strength Reduction

Tensile tests on the fully fireproofed beam confirmed no significant reduction in steel strength after exposure to a peak temperature of 281°C. Notably, the post-fire specimens exhibited a 5 ksi increase in tensile strength compared to the pre-fire condition, consistent with findings from previous research [19]. The ultimate tensile strength remained unchanged between pre-fire and post-fire scenarios, indicating that the fireproofing effectively safeguarded the steel from heat-induced degradation. These results affirm the effectiveness of the fireproofing in preventing permanent strength reduction in A992 structural steel under elevated temperature conditions.

4.5 Computational Model Alignment with Laboratory Testing

The computational model demonstrates a strong correlation with the experimental data, particularly in capturing the thermal behavior of the bottom flange, where direct heat exposure leads to rapid temperature increases. In both the FEA and experimental results, the initial steep temperature rise in the bottom flange is well-predicted, as seen in Figures 3-17 and 3-18. This alignment suggests that the model is effective in simulating the early stages of conductive heat transfer in fire-exposed steel, particularly where the heat source directly influences the structure. However, the FEA consistently overestimates the peak temperature in certain scenarios, likely due to the model's handling of convective heat losses and minor thermal resistances that exist in real-world conditions but are difficult to account for in simplified simulations.

For the mid-web and top flange, the FEA underestimates the temperature rise compared to experimental results, particularly in the later stages of heating, as highlighted in Figures 3-22 and 3-25. These regions experience slower heat transfer due to their distance from the heat source and are influenced by more complex convective and radiative losses, which are challenging to model with complete accuracy. The lower temperatures predicted by the FEA suggest that surface film coefficients and emissivity values may need further refinement to capture the full extent of heat transfer dynamics in these areas. The model's approach to simulating radiative and convective heat losses is likely oversimplified, leading to discrepancies in regions where these mechanisms dominate.

The variations in temperature predictions across the different beam regions indicate that while the FEA model excels in direct heat transfer scenarios, as seen in the bottom flange, it struggles to fully account for the combined effects of radiation, convection, and the insulating properties of fireproofing in more remote regions like the mid-web and top flange. The difference in the mid-web temperatures between the FEA and experimental data, particularly in Figures 3-22 and 3-23, underscores the need to adjust the surface film coefficients and emissivity settings to better capture the heat transfer dynamics in these less exposed areas, where convective and radiative mechanisms are more significant.

This page left blank intentionally.

5.0 Future Testing and Recommendations

Subsequent to these experiments, there remain several unresolved questions warranting further investigation. These issues are examined in this section.

5.1 Further Fireproofing Testing

The fireproofing tested in these experiments was a readily available cementitious product. In addition to cementitious fireproofing, epoxy-based formulations are also used in fireproofing applications. These materials were not used for this experiment because of their more complicated application process. They require blast cleaning of the steel and primer before the application of the fireproofing. The mechanism by which epoxy materials reduce the impacts of high heat events is also completely different than that of cementitious materials. During a fire event, epoxy fireproofing undergoes a chemical reaction and expands. This reaction begins between 180-200°C. After a high temperature event, the fireproofing that underwent the reaction must be removed and replaced.

Despite the complications with the application process, the effectiveness of epoxy-based fireproofing should be evaluated. Professional application eliminates the imperfections that were present in our application of the cementitious fireproofing.

Further testing of fireproofing materials should include an evaluation of their long-term durability. While immediate fire resistance is critical, fireproofing materials must also maintain their protective qualities over time, especially in harsh tunnel environments. Cementitious and epoxy-based fireproofing are both susceptible to environmental degradation from moisture, corrosion, and freeze-thaw cycles. Long-term durability testing is necessary to ensure that these materials can withstand such conditions and continue to protect tunnel structures effectively over years of service.

Another crucial aspect of fireproofing performance is its behavior under varying fire scenarios. While standard fire curves, such as ASTM E119, provide valuable benchmarks, tunnel fires can differ significantly from typical building fires, often involving hydrocarbon-based fuels and resulting in higher temperatures and faster heat rates. Testing fireproofing materials under different fire scenarios would provide a more comprehensive assessment of their fire resistance and ensure that they can protect tunnel structures under various fire conditions.

Finally, the effect of temperature cycling on fireproofing materials must be examined. Tunnels experience regular fluctuations in temperature due to seasonal changes, vehicle heat, and other environmental factors. These cycles of heating and cooling can weaken fireproofing materials over time, potentially compromising their ability to protect the underlying steel. Testing for the impact of temperature cycling would help identify which materials are best suited for long-term fire protection in tunnel environments.

In addition to epoxy alternatives, there are several cementitious fireproofing materials on the market that were not tested. Finding the most effective and applicable fireproofing material is in the best interest of effective tunnel maintenance. We recommend further evaluation of multiple cementitious fireproofing materials.

The comparison between spray-applied and trowel applied cementitious fireproofing is of interest. In these experiments, fireproofing was applied by hand and trowel and as a result there were several imperfections in the coverage of the beam. It was difficult to apply the fireproofing against gravity because of the liquidity of the mix. This is a concern for many tunnels, where frequent patch-up maintenance against gravity is required. If hand application is selected, the lower end of the required water content should be used to create a more viscous mix, which makes the material easier to cake on by hand. The spray application should remedy these imperfections, but the feasibility of using the spray equipment in a tunnel environment must be determined.

5.2 Temperature Monitoring

Future research should focus on quantifying the heat transfer between the steel beam and the concrete slab through shear connectors during fire exposure. Temperature monitoring should target the regions near the shear connectors, which serve as critical thermal pathways between the non-exposed flange of the steel girder and the concrete slab it supports. Specific attention should be given to the temperature gradients across the interface and the subsequent impact on the slab's performance, particularly under high-temperature conditions that could lead to spalling, cracking, or other degradation phenomena. Experimental setups should replicate realistic in situ conditions to capture these interactions accurately and evaluate their implications for the thermal and structural response of composite systems during fire events.

5.3 Further Strength Testing

Tensile testing was performed solely on the fully fireproofed configuration, which offered valuable insights into how effectively fireproofing can preserve the mechanical properties, especially yield and tensile strength of steel after being exposed to high temperatures during fire events. However, to develop a more comprehensive understanding of the effects of fire on structural steel, it is imperative to expand the scope of testing to include partially fireproofed and unprotected configurations, such as those represented in Scenarios 2 to 4. These additional tests would enable researchers to evaluate how different levels of fireproofing affect the steel's residual strength, providing a more nuanced picture of the material's behavior under various fire conditions. Each configuration may exhibit distinct patterns of strength loss, which will better inform the overall effectiveness of fireproofing strategies, especially in fire-prone environments like tunnels.

Furthermore, testing steel in an unprotected condition—without any fireproofing—should be considered as a critical baseline. This would allow for a clear comparison of how much strength reduction occurs in steel that has no fire protection, offering a contrast to fireproofed scenarios. Understanding this baseline is critical for assessing the full extent of damage fire can inflict on unprotected steel and for establishing how much protection is truly provided by various fireproofing methods. Testing across all configurations will allow for a more precise quantification of the relative benefits of each fireproofing strategy, helping to identify which solutions provide the greatest resilience during fire events. This expanded data will be crucial for refining fire protection strategies, enabling the development of solutions tailored to the specific challenges faced in tunnels and other fire-prone environments, where maintaining structural integrity is paramount. By incorporating tensile testing across various fireproofing configurations, a more accurate understanding of steel's performance under fire exposure can be achieved. This will ensure that fireproofing practices are based on solid, empirical evidence, leading to improvements in fire protection protocols and contributing to more resilient design and construction standards for critical infrastructure.

This page left blank intentionally.

6.0 References

1. Kodur, V., Dwaikat, M., & Fike, R. (2010*). High-temperature properties of steel for fire resistance modeling of structures*. Journal of Materials in Civil Engineering, 22(5), 423–434. https://doi.org/10.1061/(asce)mt.1943-5533.0000041FHWA, National bridge inventory database, (2017). https://www.fhwa.dot.gov/bridge/nbi/no10/defbr17.cfm. (Accessed 27 January 2020).
2. G. A. Khoury, "Effect of fire on concrete and concrete structures," *Progress in Structural Engineering and Materials, vol. 2, no. 4, pp. 429-447, 2000.*
3. Menz, N., S. Gerasimidis, S. Civjan, J. Czach, and J. Rigney. Review of Post-Fire Inspection Procedures for Concrete Tunnels. In *Transportation Research Record: Journal of the Transportation Research Board,* No. 2675(9), Transportation Research Board of the National Academies, Washington, D.C., 2021, pp.1304–1315.EN 1992 1-2. (2004). *European Committee for Standardization*.
4. Tao, Z., Wang, X.-Q., & Uy, B. (2013b). Stress-strain curves of structural and reinforcing steels after exposure to elevated temperatures. *Journal of Materials in Civil Engineering*, *25*(9), 1306–1316. https://doi.org/10.1061/(asce)mt.1943-5533.0000676
5. Rempe, J. L., and Knudson, D. L. _2008_. “High temperature thermal properties for metals used in LWR vessels.” *J. Nucl. Mater.*, 372_2–
6. Bentz, D. P., and Prasad, K. R. (2007). “Thermal performance of fire resistive materials I. Characterization with respect to thermal performance models.” Rep. No. *BFRL-NIST 7401*, NIST, Gaithersburg, Md.
7. Touloukian, Y. (1972). “Thermal radiative properties for non metallic solids.” *Thermal Physical Properties*, 8, 142–151.
8. Yawata Iron and Steel Co. (1969). “WEL-TEN 80 material datasheet.” Tokyo, 22.
9. Powell, R. W., and Tye, R. P. (1960). “High alloy steels for use as a thermal conductivity standard.” *Br. J. Appl. Phys*., 11, 195–198.
10. ASCE. (1992). “Structural fire protection.” *ASCE committee on fire protection, Manual No. 78*, ASCE, Reston, Va.
11. European Committee for Standardization. (2005). “General rules—Structural fire design, EN1993-1-2.” *Eurocode 3*, Brussels.
12. Outinen, J., and Mäkeläinen, P. (2004). “Mechanical properties of structural steel at elevated temperatures and after cooling down.” *Fire Mater*., 28, 237–251.
13. Mäkeläinen, P., Outinen, J., and Kesti, J. (1998). “Fire design model for structural steel S420M based upon transient-state tensile test results.” *J. Constr. Steel Res*., 481, 47–57.
14. Outinen, J., Kesti, J., and Mäkeläinen, P. _1997_. “Fire design model for structural steel S355 based upon transient state tensile test results.” *J. Constr. Steel Res.*, 42_3_, 161–169.
15. Chen, J., Young, B., and Uy, B. (2006). “Behavior of high strength structural steel at elevated temperatures*.” J. Struct. Eng*., 132(12), 1948–1954.
16. Smith, C. I., Kirby, B. R., Lapwood, D. G., Cole, K. J., Cunningham, A. P., and Preston, R. R. (1981). “The reinstatement of fire damaged steel framed structures*.” Fire Saf. J., 4(1), 21–62*

17. Tao, Z., Wang, X.-Q., & Uy, B. (2013b). Stress-strain curves of structural and reinforcing steels after exposure to elevated temperatures. *Journal of Materials in Civil Engineering*, *25*(9), 1306–1316. https://doi.org/10.1061/(asce)mt.1943-5533.0000676
18. Qiang, X., Bijlaard, F. S. K., and Kolstein, H. (2012). "Post-fire mechanical properties of high strength structural steels S460 and S690." *Eng. Struct., 35, 1–10.*
19. L. Jinwoo, M. D. Engelhardt and E. M. Taleff, "Mechanical Properties of ASTM A992 Steel After Fire," *Engineering Journal*, vol. 49, pp. 33-44, 2012.
20. Anderberg, Y. (1988). "Modeling steel behavior." *Fire Saf. J.*, 13, 17–26.
21. Cooke, G. M. E. (1988). "An introduction to the mechanical properties of structural steel at elevated temperatures." *Fire Saf. J.*, 13_1_, 45–54.
22. Stirland, C. (1980). "Steel properties at elevated temperatures for use in fire engineering calculations." *Rep. No. ISO/TC92/WG15*, No. 14, Teeside Laboratories, British Steel Corporation, Rotherham, U.K.
23. Huang, Z.-F., Tan, K.-H., and Ting, S.-K. 2006. "Heating rate and boundary restraint effects on fire resistance of steel columns with creep." *Eng. Struct., 28, 805–817.*
24. C. Maraveas and A. A. Vrakas, "Design of concrete tunnel linings for fire safety," *Structural Engineering International, pp. 1-11, 2014.*
25. Naus, D. J. (2006). *The Effect of Elevated Temperature on Concrete Materials and Structures - a Literature Review.* https://doi.org/10.2172/974590
26. T. Z. Harmathy and J. E. Berndt, "Hydrated Portland Cement and Lightweight Concrete at Elevated Temperatures," *J. American Concrete Institute 63, 93–112 (1966).*
27. Menz, N., S. Gerasimidis, S. Civjan, J. Czach, and J. Rigney. Review of Post-Fire Inspection Procedures for Concrete Tunnels. In *Transportation Research Record: Journal of the Transportation Research Board,* No. 2675(9), Transportation Research Board of the National Academies, Washington, D.C., 2021, pp.1304–1315.EN 1992 1-2. (2004). *European Committee for Standardization*.
28. J. Ingham, "Forensic engineering of fire-damaged structures," in *Civil Engineering*, 2009.
29. Knaack, A. M., Kurama, Y. C., & Kirkner, D. J. (2010). Compressive strength relationships for concrete under elevated temperatures. *ACI Materials Journal*, *107*(2). https://doi.org/10.14359/51663580
30. L. T. Phan, "Fire Performance of High-Strength Concrete: A Report of the State-of-the-Art," National Institute of Standards and Technology, Gaithersburg, 1996.
31. American Concrete Institute, "Code Requirements for Determining Fire Resistance of Concrete and Masonry Construction Assemblies," American Concrete Institute, Farmington Hills, 2014.
32. LaFleur, C., Bran Anleu, G., Muna, A., Ehrhart, B., Blaylock, M., & Houf, W. (2017). *Hydrogen Fuel Cell Electric Vehicle Tunnel Safety Study*. https://doi.org/10.2172/1761273
33. H. M. Elsanadedy, "Residual compressive strength of high-strength concrete exposed to elevated temperatures," Advances in Materials Science and Engineering, vol. 2019, 152 no. 4, pp. 1-22, 2019.
34. G. A. Khoury and Y. Anderberg, "Concrete spalling review," Fire Safety Design, 2000.
35. Z. Tao, "Mechanical properties of prestressing steel after fire exposure," *Materials and Structures*, vol. 48, pp. 3037-3047, 2015.
36. U. Schneider and D. Drysdale, "Repairability of fire-damaged structures," *Fire Safety Journal*, vol. 16, pp. 251-336, 1990.

37. J. C. Liu, K. H. Tan and Y. Yao, "A new perspective on nature of fire-induced spalling in concrete," *Construction and Building Materials*, vol. 184, pp. 581-590, 2018.
38. J. C. Liu, K. H. Tan and Y. Yao, "A new perspective on nature of fire-induced spalling in concrete," *Construction and Building Materials*, vol. 184, pp. 581-590, 2018.
39. K. D. Hertz, "Limits of spalling of fire-exposed concrete," *Fire Safety Journal*, vol. 38, no. 2, pp. 103-116, 2003.
40. Kodur, V. K. R., Dwaikat, M., & Fike, R. (2010). High-Temperature Properties of Steel for Fire Resistance Modeling of Structures. *Journal of Materials in Civil Engineering*, 22(5), 423-434.
41. Dassault Systèmes. *Abaqus 2024 Documentation*. Dassault Systèmes. Retrieved from https://www.3ds.com/products-services/simulia/products/abaqus
42. Ma, G., Young, B., & Uy, B. (2019). Finite Element Model Validation and Advanced Analyses of Steel Members with Steel Claddings at Elevated Temperatures. *Journal of Structural Engineering*, 145(9), 04019096.
43. Ma, G., Young, B., & Uy, B. (2020). Temperature Analysis of Steel Structures Protected by Intumescent Paint. *Fire and Materials*, 44(2), 165-182.
44. Usmani, A. S., Rotter, J. M., Lamont, S., Sanad, A. M., & Gillie, M. (2001). Fundamental principles of structural behavior under thermal effects. *Fire Safety Journal*, 36(8), 721-744.
45. Huang, Z., Zhang, Y., Yang, H., & Wang, X. (2023). Thermomechanical Coupling and Fire Resistance Performance of Fabricated Frame Tunnel Joints. *Fire*, 6(1), 3. https://doi.org/10.3390/fire6010003
46. Bentz, D. P., & Prasad, K. R. (2007). *Thermal Performance of Fire Resistive Materials: I. Characterization with Respect to Thermal Performance Models* (NISTIR 7401). National Institute of Standards and Technology.
47. Jeffers, A. E. (2013). Heat transfer element for modeling the thermal response of non-uniformly heated plates. *Finite Elements in Analysis and Design*, 63, 62-68. https://doi.org/10.1016/j.finel.2012.08.009
48. Kardak, A. A., Bilich, L. A., & Sinclair, G. B. (2017). Stress concentration factors for ASTM E8/E8M-15A plate-type specimens for tension testing. *Journal of Testing and Evaluation*, *45*(6), 20160385. https://doi.org/10.1520/jte20160385
49. Watlow. “Thermocouples.” Global Supplier of Industrial Electric Thermal Solutions, https://www.watlow.com/.
50. UL Product IQ. (2019). *BXUV.X790 - Fire Resistance Ratings - ANSI/UL 263*.